Accepted Manuscript

Geological Society, London, Special Publications

Lower Cretaceous holostratigraphy in Svalbard: the Arctic key piece of the Boreal basin puzzle

Mads E. Jelby, Sten-Andreas Grundvåg, Kasia K. Śliwińska, Peter Alsen, Madeleine L. Vickers, Snorre Olaussen & Lars Stemmerik

DOI: https://doi.org/10.1144/SP545-2023-177

To access the most recent version of this article, please click the DOI URL in the line above. When citing this article please include the above DOI.

Received 20 October 2023
Revised 15 February 2024
Accepted 27 February 2024

Lower Cretaceous holostratigraphy in Svalbard: the Arctic key piece of the Boreal basin puzzle

Mads E. Jelby[1]*, Sten-Andreas Grundvåg[2], Kasia K. Śliwińska[3], Peter Alsen[3], Madeleine L. Vickers[4], Snorre Olaussen[5] & Lars Stemmerik[3,5]

[1]Department of Earth Science, University of Bergen, Allégaten 41, P.O. Box 7803, N-5020 Bergen, Norway

[2]Department of Geosciences, UiT The Arctic University of Norway, P.O. Box 6050, Langnes, N-9037 Tromsø, Norway

[3]Geological Survey of Denmark and Greenland (GEUS), Øster Voldgade 10, DK-1350 Copenhagen K, Denmark

[4]Centre for Planetary Habitability (PHAB), University of Oslo, P.O. Box 1028, Blindern, N-0315 Oslo, Norway

[5]Department of Arctic Geology, The University Centre in Svalbard (UNIS), P.O. Box 156, N-9171 Longyearbyen, Norway

ORCID: MEJ, https://orcid.org/0000-0002-1096-1820

*Correspondence: madsjelby@gmail.com

Abstract

Lower Cretaceous stratigraphy of the high palaeo-latitude Arctic-Boreal Realm is generally more poorly understood than its lower-latitude Tethyan counterpart, prohibiting regional correlations and evaluation of global climate dynamics during this important high-pCO_2 period. In this paper, a holostratigraphic scheme and lithostratigraphic revision are presented for the Valanginian–lower Barremian, siliciclastic ramp succession of the Rurikfjellet Formation in Svalbard, drawn from synthesis of the latest published sedimentological, biostratigraphic, petrophysical, sequence stratigraphic, chemostratigraphic and chronostratigraphic results, supplemented by new measured sections from five localities. The offshore mudstone-dominated Wimanfjellet Member (Valanginian–lower Barremian) is retained, whereas three new members are defined according to their distinct geographic, sedimentological and stratigraphic characteristics: The Adventpynten Member (upper(?) Valanginian–lowermost upper Hauterivian) constitutes a thick, relatively localized succession of mass-transport deposits. The Kikutodden Member (Hauterivian–lower Barremian) is discarded and replaced by the northern Bohemanneset Member and southern Fotografryggen Member, representing respectively: heterogeneous prodelta to delta front deposits; and sandy offshore transition to shoreface deposits. The Rurikfjellet Formation records Valanginian–earliest late Hauterivian shoreline progradation followed by late Hauterivian–early Barremian shoreline retreat

and flooding across a low-gradient ramp, which never experienced full regression into continental deposits within the extent of the present-day outcrop belt.

Following the break-up of the super-continent Pangaea, the Early Cretaceous was characterised by major plate-tectonic reconfigurations and sea-level oscillations, while concomitant climate fluctuations and episodes of increased volcanic activity led to marked perturbations in the carbon cycle (e.g. Gröcke *et al.* 2003; Weissert and Erba 2004; Föllmi 2012; Haq 2014; Bodin *et al.* 2015; Price *et al.* 2018; Vickers *et al.* 2023). Global high atmospheric CO_2 levels and long-lived greenhouse conditions prevailed with reduced equatorial to polar temperature gradients (Wang *et al.* 2014). An increasing number of studies, however, suggest that the warm greenhouse trend was episodically punctuated by short-lived 'cold snaps', potentially capable of sustaining small polar ice caps (Price 1999; Price and Nunn 2010; Vickers *et al.* 2019, and references therein). In the Boreal Realm, strikingly contrasting depositional styles developed between lower and higher latitudes; Euro-Boreal basins were characterised by tropical water conditions with prolific blooms of calcareous nannoplankton and deposition of relatively thin (decametric to hectometric) carbonate successions (Jelby *et al.* 2024; this volume), whereas Arctic-Boreal basins were characterized by near-freezing bottom-water temperatures with major influx of detrital sediment and deposition of relatively thick (hectometric to kilometric) siliciclastic successions (e.g. Grundvåg *et al.* 2017; Sømme *et al.* 2018; Midtkandal *et al.* 2020; Embry *et al.* 2023; Olaussen *et al.* 2023). However, while the stratigraphy of lower palaeo-latitude basins is relatively well-constrained, Arctic-Boreal basins are less understood, inevitably prohibiting evaluation of global causes and consequences of this Early Cretaceous high-pCO_2 Earth. Notably, supra-basinal correlation of Lower Cretaceous successions is commonly challenging, due to significant faunal provincialism of biostratigraphically important fossil groups (such as ammonites) across the Jurassic–Cretaceous boundary, and hence chemostratigraphic discrepancies (Zakharov and Rogov 2008; Žák *et al.* 2011; Dzyuba *et al.* 2013; Shurygin and Dzyuba 2015; Jelby *et al.* 2020b). Of importance, therefore, is the development of an integrated stratigraphic framework for Lower Cretaceous strata in the Arctic-Boreal Realm.

In the High-Arctic archipelago of Svalbard, Norway, the Rurikfjellet Formation forms a superbly exposed up to *c.* 350 m thick, siliciclastic ramp succession of offshore–shallow-marine deposits that record Valanginian–early Barremian basin fill in the Arctic-Boreal Realm. The Rurikfjellet Formation has generally been deemed to comprise a relatively simple stratigraphic development across Spitsbergen, the largest island of Svalbard, including: (1) a mudstone-dominated offshore unit in the lower part, named the Wimanfjellet Member (Dypvik *et al.* 1991a); and (2) a sandstone-dominated nearshore unit in the upper part, named the Kikutodden Member (Midtkandal *et al.* 2008). This bipartite member subdivision, however, has recently been challenged by several integrated stratigraphic studies on the Rurikfjellet Formation. These include: (1) the sedimentology, depositional architecture and palaeogeographic evolution (Grundvåg and Olaussen 2017; Grundvåg *et al.* 2019, 2021; Jelby *et al.* 2020a); (2) dinoflagellate cyst (dinocyst) and ammonite biostratigraphy (Alsen *et al.* 2020; Śliwińska *et al.* 2020); (3) carbon cycling and climate (Vickers *et al.* 2019, 2023; Jelby *et al.* 2020b); and (4) a more regional account on seismic stratigraphy and source-to-sink routes of time-equivalent strata across the Barents Shelf (Grundvåg *et al.* 2017). Of particular importance was: (1) the discovery of a muddy mass-transport complex in two cored onshore wells, informally defined as the 'Adventpynten member'; and (2) the demonstration that the Kikutodden Member consists of a northern relatively fine-grained and lithologically heterogeneous (sandstone and mudstone) deltaic tongue and a southern coarser-grained and lithologically homogenous (sandstone) shoreface (i.e. non-deltaic) tongue (Grundvåg *et al.* 2017, 2019; Jelby *et al.* 2020a). These two clastic wedges are geographically distinct, genetically unrelated, and display markedly

different facies and stratigraphic trends; all of which is not sufficiently accounted for by previous lithostratigraphic schemes. Thus, integration of these results provides a new holostratigraphic scheme for the Rurikfjellet Formation that: (1) accounts for the stratigraphic and architectural complexity of the formation; and (2) necessitates a formal revision of the lithostratigraphy of the succession, in line with the recommendations for lithostratigraphic amendments presented by the Norwegian Committee on Stratigraphy (NCS; Nystuen 1989).

This paper therefore presents: (1) implementation of a holistic approach to present a timely review of the sedimentology, stratigraphy and basin configuration of the Rurikfjellet Formation; and (2) a formal lithostratigraphic revision of the succession in light of the provisionally defined clastic wedges. For this purpose, the latest facies-analytical, biostratigraphic, petrophysical, sequence stratigraphic, chemostratigraphic and chronostratigraphic results (Grundvåg and Olaussen 2017; Grundvåg *et al.* 2017, 2019, 2021; Vickers *et al.* 2019, 2023; Alsen *et al.* 2020; Jelby *et al.* 2020a, b; Śliwińska *et al.* 2020) are synthesized and combined with new sedimentological and stratigraphic data from five localities across Spitsbergen and the recording of a new age-diagnostic ammonite at one locality. Collectively, the compiled data set allows for an integrated stratigraphic scheme and depositional model for the Rurikfjellet Formation.

Regional setting and stratigraphy

Early Cretaceous basin configuration

Svalbard represents the uplifted north-western corner of the Barents Shelf (Fig. 1a). Lower Cretaceous strata are primarily exposed along the margins of the NNW–SSE-oriented Central Tertiary Basin on Spitsbergen (Fig. 1b, c). During the Late Jurassic to Early Cretaceous, the Arctic-Boreal Realm occupied the northern margin of Pangaea with Svalbard being situated at approximately 63–66°N (Fig. 2a, b; Torsvik *et al.* 2002; Shephard *et al.* 2013). Arctic-Boreal basins were characterized by dynamic shifts between Late Jurassic decoupling from and Early Cretaceous recoupling to the southern Tethyan Realm, facilitated by water exchange through the relatively narrow seaway of the Viking Corridor in concert with a long-term eustatic sea-level fall and rise, respectively (Fig. 2c; Galloway *et al.* 2020; Jelby *et al.* 2020b; Vickers *et al.* 2022). The Arctic-Boreal basins formed part of a larger epicontinental area that promoted the formation of widespread, relatively shallow epeiric seas (Fig. 2b, c; Midtkandal *et al.* 2007, 2020; Grundvåg *et al.* 2017). As a result, sediment routing systems in the Svalbard area generally did not encounter any abrupt basin deepening associated with shelf–slope breaks but were instead controlled by various shelf processes that distributed sediments vast distances (Fig. 2b, c; Midtkandal and Nystuen 2009; Midtkandal *et al.* 2020). Several accretionary shelf-breaks have been reported from seismic analyses on the Barents Shelf *c.* 300 km south of Svalbard; these, however, are regarded not to have affected sediment partitioning in the Svalbard area, and clinoforms have not been convincingly demonstrated to occur within the Lower Cretaceous outcrop belt of Spitsbergen (Marin *et al.* 2016; Grundvåg *et al.* 2017; Midtkandal *et al.* 2020). Instead, it has been suggested that the Lower Cretaceous strata of Svalbard represent deposition on a large-scale, low-gradient ramp with shelf-like affinities (Midtkandal *et al.* 2020).

Thermal subsidence generally controlled the regional tectonostratigraphic development of the basin. However, opening of the Canada Basin in the Hauterivian–Aptian inflicted southward

tilting of the ramp and igneous activity (Fig. 2c, d; Grantz *et al.* 2011); the latter peaking in the early Aptian with the development of the High Arctic Large Igneous Province (HALIP; Maher 2001; Corfu *et al.* 2013; Senger *et al.* 2014).

Lower Cretaceous lithostratigraphy

The Middle Jurassic–Lower Cretaceous (Bathonian–Albian) succession in Svalbard is included in the Adventdalen Group; a > 1500 m thick first-order megasequence (*sensu* Catuneanu 2019) recording long-term (*c.* 65 Myr) shoreline progradation and back-stepping in response to a full relative sea-level cycle (Fig. 3; Gjelberg and Steel 1995; Mørk *et al.* 1999; Midtkandal *et al.* 2007; Midtkandal and Nystuen 2009; Grundvåg *et al.* 2017; Midtkandal *et al.* 2020). The succession unconformably overlies the Upper Triassic–Middle Jurassic Kapp Toscana Group and is separated from Paleocene strata above by a major Late Cretaceous–earliest Paleocene (Danian) hiatus (Fig. 3). The Adventdalen Group extends onto the Barents Shelf, and collectively comprises: (1) the mudstone-dominated Agardhfjellet Formation (Bathonian–Ryazanian), representing transgressive open-marine conditions, and being time-equivalent to the prolific source-rocks of the Fuglen and Hekkingen formations on the Barents Shelf; (2) the lower mudstone-dominated and upper sandstone-rich Rurikfjellet Formation (Valanginian–lower Barremian), representing highstand open- to shallow-marine conditions, and being time-equivalent to the Klippfisk and Knurr formations on the Barents Shelf; (3) the sandstone-dominated and coal-bearing Helvetiafjellet Formation (Barremian–lower Aptian), representing lowstand fluvial to paralic conditions, and being time-equivalent to the open-marine succession of the Kolje Formation on the Barents Shelf; and (4) the heterolithic Carolinefjellet Formation (Aptian–Albian), representing a return to highstand open- to shallow-marine conditions, and being time-equivalent to the Kolmule Formation on the Barents Shelf (Grundvåg *et al.* 2017, and references therein). The Agardhfjellet and Rurikfjellet formations are included in the Janusfjellet Subgroup (Dypvik *et al.* 1991a). The boundary between the two units forms an important stratigraphic marker, demarcated by a relatively thin (< 10 m), glauconitic clay unit of plastic texture named the Myklegardfjellet Bed (Fig. 3; Birkenmajer 1980). The base of the Myklegardfjellet Bed is generally regarded as hiatal in origin (Dypvik *et al.* 1992; Jelby *et al.* 2020b) and roughly corresponds to the Base Cretaceous Unconformity prevalent in offshore basins of the Norwegian Continental Shelf (e.g. Lundin and Doré 1997). In Kong Karls Land, the easternmost group of islands in the Svalbard archipelago (Fig. 2c), strata being time-equivalent to the Rurikfjellet Formation are included in the *c.* 30 m thick Tordenskjoldberget Member of the Klippfisk Formation, intercalated between underlying Kimmeridgian organic-rich mudstones of the Agardhfjellet Formation and overlying Barremian–Aptian fluvial sandstones of the Helvetiafjellet Formation and extrusive volcanics (Olaussen *et al.* 2018). The Tordenskjoldberget Member consists of a lower calcareous sandstone and sandy limestone unit and an upper mudstone unit with inoceramid bivalve fragments and carbonate concretions, representing highly condensed offshore deposits, which probably reflects tectonic contraction and associated uplift in eastern Svalbard (Olaussen *et al.* 2018, 2023, and references therein).

The cyclic (marine–continental–marine) depositional trend of the Adventdalen Group is generally regarded to largely have been controlled by thermo-tectonic uplift north of Svalbard related to formation of the HALIP, which peaked in the early Barremian, followed by Aptian–Albian quiescence and/or sag-type subsidence (Gjelberg and Steel 1995; Grundvåg *et al.* 2017). The uplift caused vast erosion of the Rurikfjellet Formation ramp, with fluvial incision and progradation of the

fluvio-deltaic Helvetiafjellet Formation shoreline far towards the south to south-east (Gjelberg and Steel 1995; Midtkandal and Nystuen 2009; Grundvåg *et al.* 2017; Midtkandal *et al.* 2020). Consequently, the Rurikfjellet Formation is separated from the Helvetiafjellet Formation by a regionally extensive subaerial unconformity, which forms the base of coarse-grained and conglomeratic fluvial sandstones of the Festningen Member (Fig. 3; Gjelberg and Steel 1995; Midtkandal *et al.* 2008). The basal part of the Festningen Member is locally comprised by the Louiseberget Bed; a laterally tapered, sandstone-dominated unit inferred to represent a bay-head delta succession or infill of incised valleys (Midtkandal *et al.* 2008; Grundvåg and Olaussen 2017).

Material

Sedimentology

Sedimentological observations, facies analyses and stratigraphic correlations of the Rurikfjellet Formation have been abundantly reported. Notably, more than 50 measured sections have recently been retrieved from exposures distributed across the entire outcrop belt and seven cored onshore wells (Grundvåg and Olaussen 2017; Grundvåg *et al.* 2017, 2019, 2021; Jelby *et al.* 2020a), complementing previous studies (e.g. Dypvik *et al.* 1991a, b; Midtkandal *et al.* 2008). Consequently, systematic facies analyses are not presented herein. The seven onshore wells (DH-1 to DH-7) have been drilled near the settlement of Longyearbyen in relation to assessment of the viability of CO_2 sequestration, as part of the 'Longyearbyen CO_2 Lab' pilot project (Figs 1c & 4; Braathen *et al.* 2012; Grundvåg *et al.* 2019). Herein, additional measured sections are incorporated from four localities in the northern basin reaches (Festningen, Oppdalssåta, Romnæstoppen and Slottsmøya) and one locality in the southern basin reaches (Fotografryggen) (Fig. 1b). The measured sections were retrieved from decimetre-scale logging, generally in a scale of 1:50 to 1:20, but intervals exhibiting centimetre-scale facies variations were logged in a scale of 1:10 to 1:2. The logging included recording of body and trace fossil assemblages and the seven-fold (0–6) Bioturbation Index (BI) of Taylor and Goldring (1993).

Biostratigraphy

A detailed dinocyst biostratigraphy has recently been established, based on palynological analysis of outcrop sections (Bohemanneset, Myklegardfjellet and Ullaberget) and onshore wells (DH-1, DH-2 and DH-5) (Figs 1b, c, 4; Śliwińska *et al.* 2020). The dinocyst biostratigraphy is constrained by rare age-diagnostic ammonites in the Rurikfjellet Formation and uppermost Agardhfjellet Formation (Jelby *et al.* 2020b; This study).

Geochemistry

New organic stable carbon-isotope ($\delta^{13}C_{org}$) stratigraphic records for the Rurikfjellet Formation have recently been established, including: (1) a curve from the Festningen section, western Nordenskiöld Land (Vickers *et al.* 2019, 2023); and (2) a Bathonian–lower Barremian curve (Jelby *et al.* 2020b). The Bathonian–lower Barremian curve is based on correlation of previously published curves (Koevoets *et al.* 2016) with two outcrop sections (Bohemanneset and Myklegardfjellet) and two onshore wells (DH-5 and DH-6) through the Agardhfjellet and Rurikfjellet formations (Figs 1b, c, 4). The $\delta^{13}C_{org}$ curves are supplemented by data of: (1) Total Organic Carbon (TOC) and Total Sulphur; and (2)

source-rock characteristics from Rock-Eval pyrolysis (Jelby *et al.* 2020b); and (3) paleo-bottom-water temperatures from the presence of glendonites (an ikaite pseudomorph formed in marine waters with temperatures ≤7 °C) in the sediments (Price and Nunn 2010; Vickers *et al.* 2018, 2019, and references therein).

Petrophysics

Wireline gamma-ray (GR) logs are available from several onshore wells (Grundvåg *et al.* 2019), notably: (1) the historic well 7816/12-1 near Reindalspasset, eastern Nordenskiöld Land, drilled by Norsk Hydro AS in relation to an oil and gas exploration campaign in 1991 (Senger *et al.* 2019); and (2) the DH-1, DH-2, DH-4 and DH-5 wells (Braathen *et al.* 2012) (Figs 1b, c, 4).

Lithostratigraphy

The lithostratigraphy of the Rurikfjellet Formation is herein formally revised according to the guidelines of NCS for naming geological units in Norway (Nystuen 1989). The Wimanfjellet Member is redefined; the Adventpynten Member is formally erected; and the Kikutodden Member is discarded and replaced by two new members. The reason for replacing the Kikutodden Member is two-fold: First, the sandy development of the member is absent in the central part of the basin. Second, the northern and southern parts of the basin exhibit markedly different sedimentological and stratigraphic characteristics. Collectively, this advocates for the presence of two geographically separate and stratigraphically distinct clastic wedges (Grundvåg *et al.* 2017). The two new members, therefore, are defined as: (1) the Bohemanneset Member, which forms a fine-grained, heterogeneous deltaic clastic wedge in the northern basin reaches; and (2) the Fotografryggen Member, which forms a coarser-grained, sandstone-dominated shoreface clastic wedge in the southern basin reaches. The name 'Kikutodden Member' is discontinued, because future usage of this name could potentially lead to confusion as to which part of the Rurikfjellet Formation it refers to. The lithostratigraphic amendment and new nomenclature have been reviewed and accepted by NCS, with the Adventpynten Member, Bohemanneset Member and Fotografryggen Member accepted by NCS into the formal lithostratigraphic subdivision of the Adventdalen Group and the Lower Cretaceous succession of Svalbard per December 19, 2023.

Rurikfjellet Formation

Revised formation (Figs 5–7)

History. In general, the Rurikfjellet Formation has been regarded to constitute a relatively simple stratigraphic development, including a basal glauconitic, plastic clay unit succeeded by a mudstone-dominated part that gradually coarsens upwards into a sandstone-dominated part. The sandstone-dominated upper portion of the Rurikfjellet Formation was originally recognized and referred to as the 'Ullaberget Series' by Rozycki (1959), and Parker (1967) subsequently formally introduced the Rurikfjellet Formation while claiming that the sandstone-dominated upper unit was confined to the western areas of the outcrop belt. The 'Ullaberget Series' (Rozycki 1959) was later formalized as the Ullaberget Member by Birkenmajer (1975), prior to demotion in rank and inclusion in the 'Rurikfjellet Member' as part of the Janusfjellet Formation (Birkenmajer 1980; Dypvik 1980; Birkenmajer *et al.* 1982; Dypvik and Bue 1984; Steel and Worsley 1984; Dypvik 1985). The basal

glauconitic, plastic clay unit of the formation, the Myklegardfjellet Bed, was originally defined by Birkenmajer (1980) and later described in detail by Dypvik *et al.* (1992). Edwards (1976) and Mørk (1978) demonstrated that the sandstone-dominated upper unit was organized in decametre-thick coarsening-upwards successions in Sørkapp Land and south-eastern Wedel Jarlsberg Land, southern Spitsbergen. This stratigraphic architecture was later confirmed in the northern part of the outcrop belt by Dypvik *et al.* (1991a, b) who performed a thorough lithostratigraphic revision of the succession by elevating the Janusfjellet Formation to subgroup rank (i.e. Janusfjellet Subgroup), thus reinstating the Rurikfjellet Formation. Simultaneously, Dypvik *et al.* (1991a) defined the Wimanfjellet Member as the lower mudstone-dominated interval and reinstated the Ullaberget Member for the upper sandstone-dominated interval. Subsequently, the Ullaberget Member was replaced by the Kikutodden Member by Midtkandal *et al.* (2008), who recognized that the Rurikfjellet Formation is barren of sandstone at the locality of Ullaberget, and that the sandstone-dominated section of Keilhaufjellet near Kikutodden in southernmost Spitsbergen therefore constituted a better candidate as type section for the member (Fig. 1b). More recently, mass-transport deposits identified in cored sections of wells DH-1 and DH-2 (Fig. 1c) were initially documented by Braathen *et al.* (2012), subsequently discussed by Grundvåg *et al.* (2017), and later described in detail by Grundvåg *et al.* (2019) who informally referred these deposits to the 'Adventpynten member'. Herein, the definition of the Wimanfjellet Member and Myklegardfjellet Bed (Dypvik *et al.* 1991a, 1992) is followed, with the exception of a redefined type section and introduction of new reference sections; the Adventpynten Member is formally erected; and the Kikutodden Member is discarded and replaced by the northern Bohemanneset and southern Fotografryggen members, due to the recent recognition that these constitute geographically separate and stratigraphically distinct clastic wedges (Grundvåg *et al.* 2017, 2019).

Name. The formation was named after the Rurikfjellet mountain (alternatively spelled 'Rjurikfjellet'), southern Sabine Land (N77°58'32.8"/E18°19'13.0"; Figs 1b & 7a) (Parker 1967).

Type section. The type section of the Rurikfjellet Formation was originally assigned to the Agardhfjellet mountain, southern Sabine Land (N78°04'30.0"/E18°51'15.5"; Fig. 1b). Due to a relatively incomplete and less representative stratigraphic development at this locality, the type locality is reassigned herein to the Janusfjellet mountain, northern Nordenskiöld Land (N78°20'15.2"/E15°51'06.4"), where the lower and upper boundaries are well-exposed, and the typical overall stratigraphic development of the formation is clearly expressed (Figs 1c, 5, 7b, c).

Reference sections. The reference section of the Rurikfjellet Formation was originally defined as the Wimanfjellet mountain, northern Nordenskiöld Land (N78°20'02.6"/E16°01'53.4"; Fig. 1c). Due to a present-day poor exposure at this locality, it is discarded here in favour of four new reference sections (Fig. 1b, c), including: (1) the Festningen coastal cliff exposure, north-western Nordenskiöld Land (N78°05'59.0"/E13°56'36.1"; Fig. 6a); (2) the Keilhaufjellet mountain, southern Sørkapp Land (N76°37'17.0"/E16°54'40.3"; Fig. 6b) (Grundvåg and Olaussen 2017); (3) core retrieved from the 440–214 m depth interval of the DH-1 well, drilled at Adventpynten, northern Nordenskiöld Land (N78°14'09.9"/E15°32'51.4"; Fig. 6c); and (4) core retrieved from the 407–188 m depth interval of the DH-4 well, drilled in Adventdalen, northern Nordenskiöld Land (N78°12'09.0"/E15°49'38.8"), located *c.* 5 km south-east of Longyearbyen.. The DH-1 and DH-4 cores are stored and available for inspection at The University Centre in Svalbard (UNIS), Longyearbyen, Norway.

Thickness. The Rurikfjellet Formation has previously been reported to be 400 m thick at Festningen (e.g. Parker 1967; Vickers *et al.* 2019, 2023); in this study, however, the section has been re-measured to be 353 m thick. At the type locality of Janusfjellet, the formation is 232 m thick, and 237 m of stratigraphy has been recorded at Keilhaufjellet (Grundvåg and Olaussen 2017). The succession thins towards the central and eastern reaches of the basin, being *c.* 118 m thick at Oppdalssåta, southern Sabine Land, and close to 100 m in southern and eastern Wedel Jarlsberg Land, including Strykejernet, Polakkfjellet, Fotografryggen and Skiferkammen (Fig. 7d; Midtkandal *et al.* 2008; This study).

Lithology. The Rurikfjellet Formation predominantly consists of moderately to intensely bioturbated, dark-grey to black mudstone, with subordinate intervals of: (1) interbedded mudstone, siltstone and discrete very fine-grained hummocky cross-stratified (HCS) and ripple cross-laminated sandstone beds; (2) trough to tabular cross-stratified, coarse-grained and gravel-rich sandstone beds; and (3) poorly sorted, sandy mudstone and muddy sandstone diamicts (Figs 5–7). Detailed lithological and sedimentological descriptions are provided under the component members.

Fossils. Macrofossils in the Rurikfjellet Formation occur locally and include: (1) ammonites; (2) belemnites; (3) buchiid and inoceramid bivalves, particularly in the Wimanfjellet Member; (4) crinoids and cheilostome bryozoans; and (5) various plant remains, such as drifted tree branches and lesser trunks (Jelby *et al.* 2020b). Microfossils primarily include dinocysts and foraminifera, which occur relatively frequently throughout the succession (Nagy and Naoroz 2018; Śliwińska *et al.* 2020). The diversity, abundance and preservation of dinocyst assemblages in the Rurikfjellet Formation are highly variable, both spatially and temporally (Śliwińska *et al.* 2020). The formation is commonly pervasively bioturbated by a wide range of marine trace fossils; detailed ichnological descriptions are provided under the component members.

Depositional environment. A range of open- to shallow-marine environments are recognized, including: (1) open-marine offshore; (2) mass-transport complex; (3) prodelta to delta front; and (4) offshore transition to nearshore strandplain (Dypvik *et al.* 1991a, b; Grundvåg and Olaussen 2017; Grundvåg *et al.* 2019, 2021; Jelby *et al.* 2020a). Detailed environmental interpretations are provided under the component members.

Boundaries. The Rurikfjellet Formation unconformably overlies the Agardhfjellet Formation, which is generally demarcated by a relatively abrupt lithological break from black, finely laminated to fissile mudstone (*sensu lato* 'paper shale'; Dypvik *et al.* 1991b) to glauconitic, green to yellow and buff or rusty red, plastic clay of the Myklegardfjellet Bed (Fig. 3; Birkenmajer 1980). The boundary coincides with a marked drop in GR and TOC values, with the latter reaching some of the lowest values through the entirety of the Upper Jurassic–Lower Cretaceous succession of Svalbard (down to 0.1 wt%; Fig. 4; Jelby *et al.* 2020b). In outcrop sections, the Myklegardfjellet Bed is typically associated with a vague topographic flattening that locally forms minor plateaus, and the green to yellow colour of the unit makes it easily recognizable at the surface of weathered and poorly exposed outcrops. In Wedel Jarlsberg Land and core sections of Nordenskiöld Land, however, the lower boundary is less conspicuous due to pervasive structural deformation, most likely due to decollement-related slip along the plastic clay (Figs 1b, 4, 6d, 7d; Midtkandal *et al.* 2008; Braathen *et al.* 2012). The upper boundary of the Rurikfjellet Formation is generally easily recognized, being a regionally extensive

erosional and incised contact between the gently sloping, dark mudstone of the Rurikfjellet Formation (although HCS sandstone beds are locally truncated) and the prominently cliff-forming, white to yellow, coarse-grained to conglomeratic and tabular cross-stratified sandstone of the Festningen Member of the Helvetiafjellet Formation (Fig. 7; Midtkandal *et al.* 2008).

Distribution. The Rurikfjellet Formation is mainly exposed along the margins of the NNW–SSE-oriented Central Tertiary Basin, from southern Oscar II Land through northern, western and eastern Nordenskiöld Land, southern and south-eastern Sabine Land, eastern and south-eastern Heer Land, western and south-western Nathorst Land, eastern and south-eastern Wedel Jarlsberg Land, and northern and southern Sørkapp Land (Fig. 1b, c).

Chronostratigraphy. The Rurikfjellet Formation has been variably dated as Ryazanian–Barremian from dinocyst and foraminiferal assemblages (Bjærke 1978; Birkenmajer *et al.* 1982; Nagy *et al.* 1990; Århus *et al.* 1990; Århus 1991, 1992; Grøsfjeld 1991; Midtkandal *et al.* 2016), ammonites and bivalves (Pchelina 1965a, b; Parker 1967), and belemnites (Nalnyaeva *et al.* 2011). However, Harland (1972) claimed that the Berriasian stage (i.e. upper Volgian–Ryazanian Boreal stages) is missing in Svalbard, thus arguing for a Valanginian age for the basal part of the succession. This notion is supported by the latest chronostratigraphic model of the formation, which is based on correlation and calibration of sedimentary facies, dinocyst and ammonite biostratigraphy, $\delta^{13}C_{org}$ stratigraphy and TOC trends between five sections (the Bohemanflya and Myklegardfjellet outcrop sections, and the DH-2, DH-5 and DH-6 wells; Figs 1b, c, 3, 4) (Jelby *et al.* 2020b). Collectively, the Rurikfjellet Formation is inferred to be of Valanginian–early Barremian age (Jelby *et al.* 2020b; Śliwińska *et al.* 2020), confirming the previous age assessment of Århus (1992) based on dinocyst biostratigraphy.

Key references. Parker (1967); Dypvik *et al.* (1991a, b); Mørk *et al.* (1999); Midtkandal *et al.* (2008); Grundvåg and Olaussen (2017); Grundvåg *et al.* (2017, 2019, 2021); Vickers *et al.* (2019, 2023); Jelby *et al.* (2020a, b); Śliwińska *et al.* (2020).

Superior unit. The Rurikfjellet Formation constitutes the upper part of the Janusfjellet Subgroup, which also contains the Agardhfjellet Formation in the lower part (Fig. 3; Dypvik *et al.* 1991a).

Subdivision. As defined herein, the Rurikfjellet Formation is subdivided into four members; the Wimanfjellet, Adventpynten, Bohemanneset and Fotografryggen members (Fig. 3).

Wimanfjellet Member

Redefined member (Figs 8–10)

Name. The member is named after the Wimanfjellet mountain in northern Nordenskiöld Land (N78°20'02.6"/E16°01'53.4"; Fig. 1c) (Parker 1967). The name is retained herein in accordance with the lithostratigraphic guidelines of NCS (Nystuen 1989).

Type section. The type section was originally defined as the Wimanfjellet mountain (Fig. 1c; Dypvik *et al.* 1991a). Due to a present-day poor exposure at this locality, it is replaced herein by the superbly exposed and stratigraphically complete section of the Myklegardfjellet mountain, south-eastern Sabine Land (N78°03'24.5"/E18°42'25.6"), which also forms the type section for the Myklegardfjellet Bed, in line with the original definition of Birkenmajer (1980) and Dypvik *et al.* (1992) (Figs 1b, 8, 10c).

Reference sections. Two reference sections for the Wimanfjellet Member are introduced here (Fig. 1b), including: (1) the Oppdalssåta mountain, southern Sabine Land (N78°04'27.8" /E17°23'32.2"; Fig. 9a); and (2) the Baronfjella mountain in south-eastern Heer Land (N77°36'11.6"/E18°16'44.4"; Fig. 9b, 10a, b). At Baronfjella, the lower boundary of the member is not exposed, as it is situated below terrain (beach) level (Fig. 10a, b).

Thickness. The thickness of the Wimanfjellet Member generally decreases towards the east, with a thickness of 314 m recorded at Festningen, decreasing to 166 m at the type section of Myklegardfjellet and *c.* 118 and 113 m at the reference sections of Oppdalssåta and Baronfjella, respectively (Figs 6a, 8, 9). The Myklegardfjellet Bed is *c.* 0.5 to 10 m thick (Dypvik *et al.* 1992), with a thickness of 3 m recorded at its type section at Myklegardfjellet (Figs 8 & 10c).

Lithology. The Wimanfjellet Member forms an overall coarsening-upwards succession (Figs 8, 9, 10a). The basal Myklegardfjellet Bed, which consists of glauconitic clay, is primarily green to yellow and buff or rusty red in appearance, and forms a soft and plastic unit that is commonly intersected by a thin (< 30 cm) interbed of dark-grey, more fissile, mudstone (Fig. 10c). The Myklegardfjellet Bed exhibits very few discernible physical sedimentary structures due to an intensively bioturbated fabric (detected by CT scanning; Koevoets *et al.* 2019b) and commonly weathered character. The overlying part of the Wimanfjellet Member is predominantly characterized by black to dark-grey, homogeneously bioturbated mudstone (Fig. 10d) that is intersected by abundant siderite concretions. The siderite concretions form either centimetre to decimetre-scale: (1) nodules that are scattered or strata-bound with spherical, ellipsoid or irregular to ptygmatic shapes; or (2) bands that are laterally persistent and tabular (Figs 8, 9, 10a, b). In outcrop sections, the siderite concretions commonly weather out to form dark-red to burgundy-coloured slopes (Fig. 10c). The homogenously bioturbated mudstone is characterized by sparse to moderate bioturbation (BI 0–3) with a low-diversity, moderate-abundance trace-fossil suite (including *Chondrites*, *Nereites missouriensis*, and lesser *Schaubcylindrichnus*, *Zoophycos* and *Palaeophycus* isp.). The homogeneous mudstone generally coarsens upwards into lenticular to biomottled sandy mudstone, which is reflected by steadily decreasing GR values in well sections (Fig. 4; Grundvåg *et al.* 2019), and accompanied by moderate to intense bioturbation (BI 4–6) with a moderate-diversity, high-abundance trace-fossil suite (including *Nereites missouriensis*, *Chondrites*, *Schaubcylindrichnus*, *Planolites* and lesser *Phycosiphon*, *Palaeophycus* isp., *Palaeophycus heberti*, *Zoophycos* and rare top-down shafts) (Fig. 9). Locally, metre-scale coarsening-upwards units are superimposed on the gross coarsening-upwards trend in the uppermost part of the member (Figs 8 & 9). Rare glendonites, soft-sediment deformation structures (SSDS), dispersed granules and dropstones are locally present in the top of the succession (Jelby *et al.* 2020b).

Fossils. Belemnites, buchiid and inoceramid bivalves, crinoids, allochthonous assemblages of cheilostome bryozoans, plant remains (including drifted tree branches and trunks), and rare ammonites occur locally. In particular, an exceptionally well-preserved assemblage of the belemnite *Arctoteuthis bluethgeni* Doyle has been collected from the upper part of the Wimanfjellet Member at Bohemanneset, southern Oscar II Land (Fig. 1b; Alsen *et al.* 2020). Microfossils include foraminifera (e.g. Dypvik *et al.* 1992; Nagy and Naoroz 2018), and dinocysts (Śliwińska *et al.* 2020).

Depositional environment. The Myklegardfjellet Bed has been variably attributed to bentonites, weathered carbonate beds or dolerites; however, prolonged sediment starvation of the basin and intense bioturbation in combination with a maximum flooding event is generally favoured as interpretation (Dypvik *et al.* 1992; Koevoets *et al.* 2019b; Jelby *et al.* 2020b). The overlying part of the Wimanfjellet Member is interpreted to consist of two facies associations: First, the lower homogeneous mudstone interval represents prolonged deposition of mud well below storm-wave base (SWB), and the sparse to moderation bioturbation facilitated by a low-diversity, moderate-abundance trace-fossil suite is consistent with a depauperate expression of the *Zoophycos* Ichnofacies in a lower offshore setting (MacEachern *et al.* 2007; Grundvåg *et al.* 2019). Second, the upper lenticular to biomottled sandy mudstone interval reflect shoaling to near or immediately above SWB, and the moderate to intense bioturbation facilitated by a moderate-diversity, high-abundance trace-fossil suite is consistent with a distal expression of the archetypal *Cruziana* Ichnofacies in an upper offshore setting (MacEachern *et al.* 2007; Grundvåg *et al.* 2019). Deposition was most likely governed by hemipelagic to suspension fallout of mud in a relatively tranquil setting, although it cannot be ruled out that influx of mud was episodically governed by hyperpycnal flows and/or wave-enhanced sediment gravity flows (MacQuaker *et al.* 2010; Grundvåg and Olaussen 2017). This notion is supported by the abundance of siderite concretions, which may indicate that discharge of riverine freshwater into marine seawater caused dilution of the seawater that led to a concomitant reduction in sulfate activity and formation of low-eH conditions, thereby reflecting depleted substrate oxygenation (Mozely 1989; MacEachern *et al.* 2007).

Boundaries. The lower boundary of the Wimanfjellet Member corresponds to the lower boundary of the Rurikfjellet Formation. The upper boundary of the Wimanfjellet Member is demarcated by the base of the first appearing (i.e. basal), discrete sandstone bed of: (1) the Adventpynten Member in the DH-1 and DH-2 wells and in the north-eastern part of Forkastningsfjellet, northern Nordenskiöld Land; (2) the Bohemanneset Member in sections of Oscar II Land, Nordenskiöld Land (except the DH-1 and DH-2 wells and in the north-eastern part of Forkastningsfjellet where the Adventpynten Member is present) and Heer Land; and (3) the Fotografryggen Member in sections from Sørkapp Land northwards to Langryggsåta in eastern Wedel Jarlsberg Land (Fig. 1b, c). In sections of the eastern (Myklegardfjellet, Oppdalssåta and Slottsmøya in southern Sabine Land) and central (Annaberget, Louiseberget and Ullaberget in southern Nathorst Land) parts of the basin, the Wimanfjellet Member is instead overlain by the Helvetiafjellet Formation, with the contact being noticeably sharp between the gently sloping, dark-grey to black mudstones of the Wimanfjellet Member and the cliff-forming, white to yellow sandstones of the Festningen Member and Louiseberget Bed (Figs 1b & 10d; Midtkandal *et al.* 2008).

Distribution. The Wimanfjellet Member is present across the entire outcrop belt of the Rurikfjellet Formation, from southern Oscar II Land through northern, western and eastern Nordenskiöld Land, southern and south-eastern Sabine Land, eastern and south-eastern Heer Land, western and south-western Nathorst Land, eastern and south-eastern Wedel Jarlsberg Land, and northern and southern Sørkapp Land (Fig. 1b, c).

Chronostratigraphy. The Wimanfjellet Member has a relatively wide chronostratigraphic range, due to its gross stratigraphic and architectural relationship with the other members of the Rurikfjellet Formation. Dinocyst and ammonite biostratigraphy dates the member to a Valanginian–early Hauterivian age in the western basin reaches, with its base coinciding with the Ryazanian–

Valanginian boundary, whereas it is of Valanginian–early Barremian age in the eastern basin reaches (Figs 4, 5, 8; Jelby *et al.* 2020b; Śliwińska *et al.* 2020).

Key references. Dypvik *et al.* (1991a, b; 1992); Grundvåg *et al.* (2019); Alsen *et al.* (2020); Jelby *et al.* (2020b); Śliwińska *et al.* (2020).

Subdivision. The Wimanfjellet Member includes the basal Myklegardfjellet Bed; an up to *c.* 10 m thick, green and yellow to buff or rusty red, glauconitic clay unit of plastic texture (Birkenmajer 1980; Dypvik *et al.* 1992). The Myklegardfjellet Bed is not redefined herein.

Adventpynten Member

New member (Figs 11–13)

Name. The member is named after the Adventpynten coastal point situated *c.* 3 km north-west of Longyearbyen, northern Nordenskiöld Land (Fig. 1c; Grundvåg *et al.* 2019). The name was initially proposed by Grundvåg *et al.* (2019) and is retained herein in accordance with the lithostratigraphic guidelines of NCS (Nystuen 1989).

Type section. The type section is defined in core retrieved from the 413–267 m depth interval of the DH-1 well, drilled at Adventpynten (N78°14'09.9"/E15°32'51.4") (Figs 1c & 11; Braathen *et al.* 2012; Senger *et al.* 2019). The core is stored and available for inspection at The University Centre in Svalbard (UNIS), Longyearbyen, Norway.

Reference section. The reference section is defined in core retrieved from the 417–265 m depth interval of the DH-2 well, drilled at Adventpynten (N78°14'09.6"/E15°32'48.6"), *c.* 20 m west of the type section well (Figs 1c & 12; Braathen *et al.* 2012; Senger *et al.* 2019). The core is stored and available for inspection at The University Centre in Svalbard (UNIS), Longyearbyen, Norway.

Thickness. The Adventpynten Member is 146 m and 152 m thick in the type and reference sections, respectively (Figs 11 & 12).

Lithology. The Adventpynten Member predominantly consists of decimetre- to metre-thick, poorly sorted diamictites (Fig. 13a; Grundvåg *et al.* 2019). The diamictites are composed of matrix-supported sandy mudstone that typically exhibit high GR values (Figs 11 & 12). Granule and mudstone intraclasts are common, and the diamictites are generally organized as relatively discrete beds with sharp, erosive or loaded bases (Fig. 13b, c). The beds display chaotic fabrics with pervasive SSDS and local coarse-tail inverse-to-normal grading (Fig. 13b). Micro-faulted intervals with centimetre-scale offsets, minor injectites, and folded heterolithic units also frequently occur (Fig. 13d). Locally, the diamictites are intersected by cleaner, better sorted sandstone beds that result in comparably lower GR values (Figs 11 & 12), and heterolithic units of laminated or thin-bedded sandstone and mudstone also occur. The cleaner sandstone beds are characterized by planar lamination and current ripple cross-lamination. In both the DH-1 and DH-2 cores, the lower part of the Adventpynten Member is dominated by interbedded lithic conglomerates and bioturbated siltstones, and in the DH-2 core, the succession is intersected by a metre-thick unit of medium-grained sandstone with rootlets capped by coal (Figs 11 & 12). The member is generally devoid of

bioturbation in the sandstone beds; in the mudstone divisions, however, it comprises a low-diversity, low-abundance trace fossils suite, including *Planolites*, *Phycosiphon*, *Schaubcylindrichnus*, *Nereites missouriensis* and *Chondrites* (Grundvåg *et al.* 2019).

Fossils. The Adventpynten Member is generally devoid of fossils, but contains rare belemnites and dinocysts (Grundvåg *et al.* 2019; Śliwińska *et al.* 2020).

Depositional environment. The Adventpynten Member is interpreted to represent a wide range of gravity-flow deposits that accumulated in a mass-transport complex (Grundvåg *et al.* 2019). The general low-intensity bioturbation facilitated by a low-diversity, low-abundance trace fossil suite is consistent with a depauperate expression of the *Zoophycos* Ichnofacies, indicating a relatively deep lower offshore setting (MacEachern *et al.* 2007). The facies association of the diamictites are consistent with deposition from slumps and debris flows, hyperpycnal and hypopycnal feeding of fluid mud from river floods, and post-depositional remobilization and slumping, including mass movement and/or loading in concert with liquefaction (Grundvåg *et al.* 2019). Cleaner sandstone beds are most likely consistent with: (1) surge-type turbidity currents (Bouma 1962); (2) rapid deposition from collapsing high-density turbidity currents (Lowe 1982); (3) aggradation from sustained, depletive turbidity currents (Kneller and Branney 1995); and (4) sandy debris flows (Shanmugam 1996). Collectively, the facies are interpreted to record deposition in front of an advancing deltaic shoreline that commonly experienced over-steepening of the delta front due to rapid progradation. This assertion is consistent with the presence of the metre-thick sandstone unit with rootlets and a coal cap, which is inferred to represent an allochthonous rafted block of delta-plain deposits that was transported into the basin due to slope failure with associated collapse and slumping (Grundvåg *et al.* 2019).

Boundaries. The lower boundary of the Adventpynten Member corresponds to the upper boundary of the Wimanfjellet Member in wells DH-1 and DH-2 and in the north-eastern part of the Forkastningsfjellet section (Fig. 13a). The contact forms a conspicuous lithological and GR drop (Fig. 11). The upper boundary of the member is relatively gradational and demarcated by the base of the first appearing (i.e. basal), comparably clean and discrete sandstone bed of the Bohemanneset Member, which in the DH-2 well corresponds to a marked GR drop (Figs 6c, 11, 12, 13a).

Distribution. The Adventpynten Member has mainly been recorded in the DH-1 and DH-2 wells (Fig. 11 & 12). However, deposits strikingly similar to those described above have been reported from the north-eastern part of Forkastningsfjellet, northern Nordenskiöld Land (Fig. 1c; Kuhn *et al.* 2019), and these are tentatively confirmed herein to form part of the Adventpynten Member (Fig. 13a). The deposits at this locality await further detailed investigations.

Chronostratigraphy. The Adventpynten Member is dated as late(?) Valanginian–earliest late Hauterivian from dinocyst biostratigraphy in the DH-1 and DH-2 wells (Figs 11 & 12; Śliwińska *et al.* 2020). However, dinocyst assemblages are characterized by a predominantly poor preservation and very low diversity (Śliwińska *et al.* 2020).

Key references. Braathen *et al.* (2012); Grundvåg *et al.* (2017, 2019); Śliwińska *et al.* (2020).

Bohemanneset Member

New member (Figs 14–16)

History. The succession included in the new Bohemanneset Member partly corresponds to the northern part of the succession included in the former Kikutodden Member (Midtkandal *et al.* 2008). The Bohemanneset Member eliminates the usage of the Kikutodden Member.

Name. The member is named after the Bohemanneset coastal point at the south-eastern tip of the Bohemanflya lowland, south-eastern Oscar II Land (Fig. 1b).

Type section. The type section is defined as the coastal cliff exposure at Bohemanneset (N78°23'41.8"/E14°43'52.5"; Figs 1b & 14). The Bohemanneset section is located *c.* 11 km sout-east of Sylfjellet, the northernmost outcrop of the Rurikfjellet Formation, and *c.* 18 km north-east of Ramfjellet with both of these localities inferred to represent the most proximal sections of the member (Figs 1b & 16a; Grundvåg *et al.* 2017, 2019, 2021; Jelby *et al.* 2020a). The Bohemanneset section constitutes the stratigraphically most complete, and one of the thickest (82 m), succession of the Bohemanneset Member recorded throughout the outcrop belt (Fig. 14). The succession is exposed in up to *c.* 25 m high cliffs, and dips gently (< 3°) towards the SE, thus disappearing below terrain (beach) level in the south-eastern end of the coastal point. The foot of the cliffs is subject to ongoing alternating wave ravinement and subaerial exposure within the tidal zone, and in combination with scouring from winter-associated pack ice, the sections are generally fresh, clean and easily accessible (Fig. 16b–d; see also Alsen *et al.* 2020).

Reference sections. Four reference sections for the Bohemanneset Member are introduced here in (Fig. 1b, c), including: (1) the Festningen coastal cliff section (Fig. 15a); (2) core retrieved from the 221–188 m depth interval of the DH-4 well (Fig. 15b); (3) the northwards-facing coastal outcrop in the south-western part of the Forkastningsfjellet mountain, northern Nordenskiöld Land (N78°18'48.8"/E15°38'11.6"; Fig. 15c); and (4) the inner Mälardalen outcrop section, exposed at the north-western margin of the terminal moraine of the Mälarbreen glacier, northern Nordenskiöld Land (N78°16'25.1"/E15°57'11.9"; Figs 15d & 16e). The DH-4 core is stored and available for inspection at The University Centre in Svalbard (UNIS), Longyearbyen, Norway.

Thickness. The thickness of the Bohemanneset Member is 97 m at the type section of the Rurikfjellet Formation (Janusfjellet; Fig. 5) but in general it conspicuously decreases towards the E and S, with a thickness of 82 m recorded at Bohemanneset; 39 m at Festningen; *c.* 40 m at Romnæstoppen, western Nordenskiöld Land; and a minimal thickness of 24 m at Baronfjella and 11 m at Kvalhovden (Grundvåg *et al.* 2021), south-eastern Heer Land (Figs 1b, 14, 15a, 16f). The reference sections of Forkastningsfjellet, Mälardalen and the DH-4 core yields member thicknesses of *c.* 56, 46 and 33 m, respectively (Fig. 15b–d).

Lithology. The Bohemanneset Member is dominated by interbedded discrete sandstone beds and bioturbated sandy mudstone beds (Figs 14, 15, 16b–f; Jelby *et al.* 2020a; Grundvåg *et al.* 2021). The sandstone beds are generally medium-bedded (10–30 cm thick), but can reach thicknesses of more than 1 m (Jelby *et al.* 2020a). The beds display a wide range of physical sedimentary structures, notably HCS and wave, combined-flow and climbing current ripple cross-lamination, and local SSDS and trough cross-stratification (Figs 14, 15, 16b–d). The sedimentary structures of the sandstone

beds are commonly stacked in relatively predictable vertical arrangements; for example with a basal planar-laminated or HCS division overlain by wave or combined-flow ripples, which may be capped by homogeneous, black mudstone (Jelby *et al.* 2020a). Alternatively, the sandstone beds are overlain by biomottled mudstone, forming conspicuously fining-upwards bed arrangements. The sandstone beds predominantly comprise diminutive assemblages of top-down shafts, including *Rosselia* (Fig. 16g), *Tisoa habichi* (*sensu* Knaust 2019), *Arenicolites, Cylindrichnus*, and fugichnia (i.e. escape burrows), with rare *Macaronichnus* and *Paleodictyon*. The mudstone beds are generally characterized by moderate to intense bioturbation governed by a high-abundance, high-diversity trace-fossil suite, including *Nereites missouriensis*, *Schaubcylindrichnus*, *Chondrites*, *Helminthopsis*, *Planolites*, *Palaeophycus* isp., *Palaeophycus heberti*, *Phycosiphon*, *Rosselia*, *Tisoa habichi*, *Asterosoma*, *Zoophycos*, fugichnia, *Scolicia*, *Thalassinoides*, *Rhizocorallium*, *Cylindrichnus*, *Teichichnus* and *Skolithos*. Homogeneous, black mudstone divisions typically comprise navichnia (i.e. 'mantle and swirl' biogenic structures; Jelby *et al.* 2020a). In the type section of Bohemanneset and in the core of well DH-5, sandstone and mudstone beds locally form part of metre-thick slumps and water-escape structures (Fig. 4), and glendonites have been reported locally from across the outcrop belt (Figs 5, 15a, d, 16h; Vickers *et al.* 2019, 2023). In the DH-1 and DH-2 wells, the Bohemanneset Member forms a *c.* 50 m thick unit dominated by poorly sorted, sandy mudstones displaying normal grading with inclined and distorted bedding devoid of bioturbation (Grundvåg *et al.* 2019). In general, the sandstone and mudstone beds are typically arranged in several metre-thick coarsening-upwards bed sets, which stack into decametre-thick coarsening- or fining-upwards successions (Figs 14, 15, 16e, f; Dypvik *et al.* 1991b; Jelby *et al.* 2020a; Grundvåg *et al.* 2021). The upper part of these units is typically characterized by complex intercalation of HCS sandstone bed, resulting in amalgamated beds (Dott & Bourgeois 1982) with thicknesses up to *c.* 1.5 m (Jelby *et al.* 2020a). The number and thickness of the coarsening-upwards successions are highly variable across the outcrop belt, although an average of three to four units are recorded in sections of the western and north-western reaches of the outcrop belt (Oscar II Land, and western and northern Nordenskiöld Land). These units overall decrease in thickness towards the E and SE, conforming to the mean sediment transport direction in those directions as inferred from palaeocurrent measurements (Fig. 1b; Dypvik *et al.* 1991b; Grundvåg *et al.* 2019, 2021; Jelby *et al.* 2020a). The coarsening-upwards units are generally overlain by a several metre-thick mudstone-dominated unit, which forms the top of the member (Figs 15b, d, 16a, e; Grundvåg *et al.* 2019). This upper mudstone-dominated unit corresponds regionally to the uppermost mudstone unit of the Rurikfjellet Formation shown in the type and reference section logs of the former Kikutodden Member by Midtkandal *et al.* (2008) (their Figs 8 & 9) who did not include the mudstone unit in their definition of the member. Herein, the mudstone unit is referred to the Bohemanneset Member, because it locally coarsens upwards into sandstone-dominated facies similar to the rest of the member (Figs 14 & 15b; Grundvåg *et al.* 2019). This trend is particularly well-developed in the sections of south-eastern Oscar II Land (Fig. 1b), with the mudstone unit at Bohemanneset coarsening upwards into an unusually coarse-grained, several metre-thick interval characterized by sandstone beds with gravelly trough cross-stratification, sharp-crested wave ripples, bioturbated 'pipe-rocks' facilitated by *Tisoa habichi*, and more rarely compensational stacking and onlap against laterally tapered scours with erosional reliefs up to *c.* 1.5 m (Figs 14, 16b, d; Jelby *et al.* 2020a).

Fossils. Plant remains, such as drifted wood (mainly branches) occur frequently. Belemnites and allochthonous assemblages of cheilostome bryozoans are rare. Microfossils include foraminifera

(Nagy and Naoroz 2018), and the member yields relatively common dinocysts in the Bohemanneset section and DH-1, DH-2 and DH-5 wells (Śliwińska *et al.* 2020).

Depositional environment. The discrete sandstone beds of the Bohemanneset Member represent storm-generated event beds (i.e. tempestites), as indicated by the predominance of HCS and wave and combined-flow ripples, whereas the bioturbated sandy mudstone beds conform to intermittent periods of fair-weather deposition (Jelby *et al.* 2020a). The vertical facies arrangements locally observed in the tempestites are comparable with Bouma-like bed sequences (Bouma 1962), conforming to deposition during waning storms (Myrow and Southard 1996; Myrow *et al.* 2002), and divisions of homogeneous, black mudstone with navichnia that cap the sandstone beds are consistent with fluid-mud deposits that settled from fluvial discharge at the final waning-storm stage (Bhattacharya and MacEachern 2009; Jelby *et al.* 2020a). In comparison, the compensational stacking of sandstones that onlap against laterally tapered, erosional scours is inferred to represent subaqueous channels carved by hyperpycnal flows (Jelby *et al.* 2020a). The trace-fossil assemblages predominantly conform to the archetypal expressions of the *Phycosiphon* and *Rosselia* Ichnofacies, typical of deltaic settings (MacEachern and Bann 2020, 2023). Collectively, the Bohemanneset Member is interpreted to consist of six facies associations, representing an offshore to deltaic depositional environment (Dypvik *et al.* 1991b; Grundvåg *et al.* 2019; 2021; Jelby *et al.* 2020a), including: (1) lower offshore; (2) upper offshore; (3) distal prodelta; (4) proximal prodelta; (5) distal delta front; and (6) possibly the most distal portion of the proximal delta front, recorded in the uppermost coarse-grained coarsening-upwards unit at Bohemanneset (Fig 14; Grundvåg *et al.* 2021). The delta was generally storm-dominated and fluvial-influenced (*sensu* Ainsworth *et al.* 2011). Storm-controlled sediment delivery was predominantly governed by a combination of: (1) downwelling flows and/or rip currents related to coastal setup (Myrow 1992; Héquette and Hill 1993, 1995); and (2) bottom-hugging hyperpycnal flows and surface hypopycnal plumes, including fluid mud, that were fed from distributary channels during coupled storm-floods (Parsons *et al.* 2001; Bhattacharya and MacEachern 2009; Collins *et al.* 2017). The sediment was distributed relatively patchy, partly due to contemporaneous and post-depositional reworking by storm waves (Jelby *et al.* 2020a; Grundvåg *et al.* 2021).

Boundaries. The lower boundary of the Bohemanneset Member corresponds to the upper boundaries of the Wimanfjellet Member and the Adventpynten Member in the DH-1 and DH-2 wells and north-eastern part of Forkastningsfjellet (Figs 1c, 11–13a). The upper boundary of the Bohemanneset Member corresponds to the upper boundary of the Rurikfjellet Formation (Figs 14, 15, 16a, e).

Distribution. The member is restricted to the north-western, western, south-east-central and eastern part of the Rurikfjellet Formation outcrop belt, from the southern reaches of Oscar II Land through western and northern Nordenskiöld Land, to eastern and south-eastern Heer Land (Fig. 1b). The southernmost sections of the member are Romnæstoppen in western Nordenskiöld Land, and Baronfjella and Kvalhovden in south-eastern Heer Land (Figs 1b, 9b, 10a, 16f).

Chronostratigraphy. The Bohemanneset Member is dated as Hauterivian–early Barremian from dinocyst biostratigraphy in the Bohemanneset section and DH-1, DH-2 and DH-5 wells (Figs 4 & 14; Śliwińska *et al.* 2020).

Key references. Dypvik *et al.* (1991a, b); Grundvåg *et al.* (2019, 2021); Jelby *et al.* (2020a, b); Śliwińska *et al.* (2020).

Fotografryggen Member

New member (Figs 17–19)

History. The succession included in the new Fotografryggen Member partly corresponds to the southern part of the succession included in the former Kikutodden Member (Midtkandal *et al.* 2008). The Fotografryggen Member eliminates the usage of the Kikutodden Member.

Name. The member is named after the Fotografryggen nunatak in eastern Wedel Jarlsberg Land (Fig. 1b). This name has been chosen due to the usage of the type section name (Keilhaufjellet) in the informally defined, Triassic 'Keilhaufjellet member' (Mørk *et al.* 1999).

Type section. The type section is defined as the Keilhaufjellet mountain, southern Sørkapp Land (N76°37'17.3"/E16°54'25.7") (Grundvåg and Olaussen 2017), located *c.* 1 km north of the Kikutodden coastal point (Figs 1b, 17, 19a–c). The Keilhaufjellet section, and its southwards continuation along the Kikutodden promontory, constitute the southernmost outcrops of the Rurikfjellet Formation (Fig. 1b).

Reference sections. Two reference sections for the Fotografryggen Member are introduced here (Fig. 1b), including: (1) the Strykejernet mountain, southernmost Wedel Jarlsberg Land (N77°02'43.7"/E16°16'23.3"; Fig. 18a) (adopted from Mørk 1978); and (2) the Fotografryggen nunatak (N77°18'27.2"/E16°00'25.3"; Figs 18b & 19d–f).

Thickness. The thickness of the Fotografryggen Member conspicuously decreases towards the north, with a thickness of 209 m at Keilhaufjellet (Edwards 1976; Grundvåg and Olaussen 2017) thinning to 79 m at Strykejernet (Mørk 1978) and down to 13 m at Fotografryggen, which is the northernmost section of the member logged in this study (Figs 1b, 17, 18). However, the unit has also been reported 9.5 km further north at Langryggsåta (Fig. 1b), where it is *c.* 9 m thick (Gjelberg and Steel 1995).

Lithology. The Fotografryggen Member forms an overall coarsening-upwards succession (Figs 17 and 18). In the lower part, it is dominated by thin-bedded heterolithic units of alternating intensely bioturbated (BI 4–6), lenticular mudstone and HCS sandstone, with the bioturbation governed by a high-abundance, high-diversity trace-fossil suite, dominated by *Asterosoma*, *Chondrites*, *Helminthopsis*, *Nereites missouriensis*, *Ophiomorpha*, *Palaeophycus* and *Planolites* Fig. 18b). The upper part of the Fotografryggen Member is dominated by flaser- and wavy-bedded sandstone units overlain by relatively tabular or wedge-shaped sets of planar-laminated, wave ripple cross-laminated and low-angle to tabular and trough cross-stratified sandstone (Figs 1b, 17, 18, 19e, f). The cross-stratified sandstone units are generally medium to coarse-grained, commonly gravel-rich, and display a wide range of palaeocurrent directions with a mean southward trend (Fig. 1b; Grundvåg and Olaussen 2017). In some cases, the cross-stratified sandstones comprise 'pipe rock' horizons of *Skolithos* (Fig. 19c). The facies are arranged into several metre-scale coarsening- and thickening-upwards bed-sets, which stack into decametre-thick coarsening- and thickening-upwards

successions (Fig. 17). In the southern sections of Keilhaufjellet and Strykejernet, four of these larger coarsening-upwards units are recorded, and they are capped by a decametre-thick mudstone-dominated unit in the top of the succession (Figs 17, 18a, 19b). This upper mudstone-dominated unit corresponds regionally to the uppermost mudstone unit of the Rurikfjellet Formation shown in the type and reference section logs of the former Kikutodden Member by Midtkandal *et al.* (2008) (their Figs 8 & 9) who did not include the mudstone unit in their definition of the member. Herein, the mudstone unit is referred to the Fotografryggen Member, because it locally coarsens upwards into sandstone-dominated facies similar to the rest of the member (Figs 17 & 18a; Grundvåg and Olaussen 2017). A more complete development of this upper mudstone-dominated unit may be present at Smalegga, northern Sørkapp Land (Fig. 1b; Gjelberg and Steel 1995), although a re-visit to this highly remote locality is necessary in order to confirm this assertion. The thickness and number of the coarsening-upwards successions decrease markedly towards the north, with the Polakkfjellet, Fotografryggen and Langryggsåta sections only comprising one or two coarsening-upwards successions, each less than 10 m thick (Figs 1b, 7d, 18b, 19d; Gjelberg and Steel 1995; cf. Midtkandal *et al.* 2008). At these sections, the upper mudstone-dominated unit is not present (Fig. 18b, 19d, e), possibly indicating a regional southwards dip of the member in combination with differential erosion associated with the basal unconformity of the overlying Helvetiafjellet Formation.

Fossils. Plant remains (such as leaves) and rare belemnites occur locally (Midtkandal *et al.* 2008; Grundvåg and Olaussen 2017).

Depositional environment. The lower intensely bioturbated and lenticular mudstone interval of the Fotografryggen Member is probably consistent with the archetypal *Cruziana* Ichnofacies of an upper offshore to offshore transition zone setting (MacEachern *et al.* 2007; Grundvåg and Olaussen 2017). In comparison, the tabular and trough cross-stratified medium to coarse-grained sandstone displaying southwards progradation parallel to the inferred shoreline is consistent with migrating subaqueous dunes forming longshore bars in a wave-refractory surf zone, and the *Skolithos* 'pipe rocks' conform to the archetypal *Skolithos* Ichnofacies typical of non-deltaic nearshore settings (MacEachern *et al.* 2007; Grundvåg and Olaussen 2017). Collectively, the Fotografryggen Member consists of four facies associations, interpreted to represent an offshore to strandplain shoreface depositional environment, including: (1) upper offshore; (2) offshore transition; (3) lower shoreface; and (4) upper shoreface (Grundvåg and Olaussen 2017).

Boundaries. The lower boundary of the Fotografryggen Member corresponds to the upper boundary the Wimanfjellet Member (Fig. 6b). The upper boundary of the Fotografryggen Member corresponds to the upper boundary of the Rurikfjellet Formation (Figs 6b, 17, 18, 19a, b, d, e).

Distribution. The Fotografryggen Member is restricted to the south-western and southern part of the Rurikfjellet Formation outcrop belt, from eastern Wedel Jarlsberg Land to northern and southern Sørkapp Land (Fig. 1b), with a series of small skerries that extend up to 6 km off the coast to the south of Kikutodden offering some dubious and inaccessible outcrops. However, the exact northwards extent of the member is still unclear. Midtkandal *et al.* (2008) claimed that the Skiferkammen section, located *c.* 3 km north-west of Fotografryggen (Figs 1b & 19d) is virtually barren of sandstone, and thus, only the Wimanfjellet Member is preserved in that locality. However, the log from Skiferkammen presented by Midtkandal *et al.* (2008) clearly constitutes an upper *c.* 8 m thick sandstone unit, and their log and photograph of the section (Figs 10 and 11 in Midtkandal *et al.*

2008) display a stratigraphic development that is strikingly similar to that of Fotografryggen (Fig. 18b in this study). In addition, a similar *c.* 9 m thick sandstone unit immediately below the Festningen Member has been reported from Langryggsåta (Gjelberg and Steel 1995) and can be seen at Einvola (Figs 1b, 19d). This sandstone unit, therefore, is referred herein to the Fotografryggen Member. Preliminary investigations in this highly remote region of the outcrop belt suggests that the unit pinches out before reaching Zillerberget, located *c.* 7 km further north of Langryggsåta (Fig. 1b), where only mudstones of the Wimanfjellet Member have been observed. Consequently, the northern pinch-out of the Fotografryggen Member is considered to be located somewhere between Langryggsåta and Zillerberget.

Chronostratigraphy. The Fotografryggen Member is of Hauterivian–early Barremian age, based on the bracketing ages of the Wimanfjellet Member below (Valanginian–early Hauterivian) and Festningen Member of the Helvetiafjellet Formation above (early Barremian) (Grøsfjeld 1991; Śliwińska *et al.* 2020).

Key references. Edwards (1976); Mørk (1978); Midtkandal *et al.* (2008); Grundvåg and Olaussen (2017); Grundvåg *et al.* (2017).

Sequence stratigraphy

The overarching facies development recorded through the Rurikfjellet Formation is a coarsening-upwards to fining-upwards trend, which conforms to a second-order regressive–transgressive (R–T) supersequence (*sensu* Catuneanu 2019) (Figs. 3). Superimposed on this trend are two to three third-order R–T sequences (*sensu* Catuneanu 2019), that are demarcated by associated maximum flooding (MFS) and maximum regressive surfaces (MRS), which are generally regionally persistent (Figs 4–6, 8, 9, 11, 12, 14, 18; Grundvåg *et al.* 2019). In the Bohemanneset and Fotografryggen members, the decametre-thick coarsening- and fining-upwards successions conform to fourth-order high-frequency sequences (*sensu* Catuneanu 2019) or parasequences capped by flooding surfaces (*sensu* van Wagoner *et al.* 1990; Figs 4–6, 7c, 9b, 14, 15, 16e, 17, 18, 19), which consist of minor fifth-order and sixth-order cycles (i.e. bed-sets) (Figs 7c, 15, 17; Grundvåg and Olaussen 2017; Jelby *et al.* 2020a; Grundvåg *et al.* 2021). The Bohemanneset and Fotografryggen members are clearly geographically distinct (both are pinching out towards and absent in Nathorst Land; Fig. 20a, b), and exhibit facies-architectural differences on the fourth-order to sixth-order sequence scale that conform to relatively local, autogenic controls on the stratigraphic development. In particular, the Bohemanneset Member is characterized by locally variable parasequence stacking patterns in the sections of northern and western Nordenskiöld Land (Figs 15 & 20c). Nevertheless, correlation of the third-order sequences identified in the four members of the Rurikfjellet Formation allow identification of semi-regional to regional sequence stratigraphic trends of allogenic significance (Catuneanu 2019). These include: (1) a long-lived regressive trend through the Wimanfjellet Member, followed by a relatively abrupt transgression that terminates in a MFS immediately before the initiation of progradation of the Bohemanneset and Fotografryggen members; (2) a progradational stacking of the lower parasequences in the Bohemanneset and Fotografryggen members that terminates in a MRS; (3) a retrogradational stacking of the upper parasequences in the Bohemanneset Member; (4) a unit of offshore mudstone that caps the parasequences in the Bohemanneset and Fotografryggen members; and (5) a local development (particularly in the Bohemanneset, Ramfjellet and Sylfjellet sections of south-eastern Oscar II Land; Fig. 1b) of the upper offshore mudstone unit into an

unusually coarse-grained parasequence in the top of the Bohemanneset Member (Figs 1b, 4, 5, 6a, b, d, 7c, 9b, 14, 15, 17, 18a, 20). Collectively, the Rurikfjellet Formation forms a second-order R–T supersequence, superimposed by two to three third-order R–T sequences that constitute up to 10 fourth-order high-frequency sequences and parasequences with various numbers of lower-order fifth-order and sixth-order bed-sets (Fig. 20; Nagy and Naoroz 2018; Grundvåg *et al.* 2019; This study).

The top of the Rurikfjellet Formation is demarcated by the erosive base of the fluvial Festningen Member of the Helvetiafjellet Formation, which forms a regionally persistent subaerial unconformity (e.g. Gjelberg and Steel 1995; Midtkandal *et al.* 2008). Locally, however, the succession is instead capped by inferred incised valley fill of the Louiseberget Bed (or genetically equivalent units) below the regional unconformity; at Annaberget, Louiseberget, Ullaberget and Oppdalssåta in the Wimanfjellet Member, at Forkastningsfjellet, Hanaskogdalen, Louisdalen and Mälardalen in the Bohemanneset Member, and at Keilhaufjellet in the Fotografryggen Member (Figs 1b, c, 6b, 9a, 10d, 15c, d, 16e). At these localities, the formation boundary instead reflects erosion by several relatively small, partly coalescing incised valleys of semi-regional extent that were filled in during stepwise transgression prior to final subaerial exposure and erosion of the ramp (Grundvåg and Olaussen 2017). Hitherto, the stratigraphic depth of the regional subaerial unconformity has been inferred to increase towards the NW and become insignificant towards the SE (Gjelberg and Steel 1995). However, the upper part of the Bohemanneset Member is complete in north-western sections, whereas it is incomplete and significantly eroded in south-eastern sections (Fig. 20). This implies that the stratigraphic depth of the unconformity decreases, rather than increases, towards the north-west, and/or varies markedly across the outcrop belt, thus contrasting previous models suggested for the Lower Cretaceous depositional system (Fig. 20; e.g. Gjelberg and Steel 1995; Grundvåg and Olaussen 2017; Grundvåg *et al.* 2017, 2019).

Biostratigraphy

Age-diagnostic dinocysts in the Rurikfjellet Formation include *Endoscrinium hauterivianum*, *Gochteodinia villosa* subsp. *villosa*, *Muderongia australis*, *Muderongia tetracantha*, *Nelchinopsis kostromiensis*, *Oligosphaeridium complex*, *Palaecysta palmula*, *Subtilisphaera perlucida* and *Tubotuberella apatela* (Śliwińska *et al.* 2020). Other typical dinocysts in the formation include *Cyclonephelium cuculliforme sensu* Århus *et al.* (1990), *Discorsia nannus*, *Dissiliodinium acmeum*, *Nyktericysta*? *pannosa*, *Oligosphaeridium abaculum*, *Phoberocysta neocomica*, *Pseudoceratium pelliferum*, *Rhynchodiniopsis aptiana*, *Stanfordella fastigiata*, *Stanfordella ordocava* and *Wrevittia perforobtusa*. Based on the last occurrences of *P. palmula* and first occurrence of *O. complex*, Śliwińska *et al.* (2020) dated the base of the formation (i.e. the base of the Myklegardfjellet Bed) to the lower Valanginian in the Myklegardfjellet section, and noted that the first occurrence of *N. kostromiensis* in the lower part of the formation in several sections is also indicative for the lower Valanginian (Figs 4 & 8). The stratigraphic range of *E. hauterivianum* is restricted to the Hauterivian, with its first occurrence demarcating the base of the stage (Figs 4, 8, 11, 12, 14). *N. kostromiensis* has previously been recorded in the: (1) upper Hauterivian–lower Barremian in NE Greenland; upper Valanginian–lower Barremian in the North Sea; and (2) Hauterivian–lower Barremian in the Barents Sea (Århus e*t al.* 1990; Śliwińska *et al.* 2020, and references therein). Consequently, the top of the Rurikfjellet Formation is regarded to be of late Hauterivian–early Barremian age, demarcated by the last occurrence of *N. kostromiensis*, in line with the previous age assessments of Grøsfjeld (1991)

and Midtkandal *et al.* (2016) (Figs 4, 8, 14). The dinocyst age assessment is constrained by: (1) a single *Tollia* (*Neocraspedites*) aff. *subtilis* ammonite of middle early Valanginian age and a single fragmented, large *Simbirskites* (*Speetoniceras*) ex. gr. *inversum* ammonite of middle Hauterivian age observed in the Myklegardfjellet section (Fig. 8; Jelby *et al.* 2020b); and (2) a single *Simbirskites* (*Speetoniceras*) ex. gr. *inversum* ammonite of middle Hauterivian age in the Janusfjellet section (Fig. 5; This study). In addition, a questionable *"Paracraspedites stenomphaloides" sensu* Shulgina (1972) ammonite in the uppermost Agardhfjellet Formation in the DH-5 core is suggestive of an early Ryazanian age for this level (Fig. 4; Jelby *et al.* 2020b).

Carbon-isotope stratigraphy

The uppermost part of the Agardhfjellet Formation (lower upper Ryazanian) is characterized by steady-state $\delta^{13}C_{org}$ conditions (Fig. 21; Jelby *et al.* 2020b). This trend is punctuated by an abrupt and marked positive carbon-isotope excursion (CIE) of up to 5.5‰ in the lower(?) Valanginian, coinciding with the base of the Rurikfjellet Formation (Figs 4, 8, 21; Jelby *et al.* 2020b). The CIE is clearly recognized in both core (DH-5 and DH-6) and outcrop (Myklegardfjellet) sections, where it reaches the in average most positive values (up to –24.2‰) recorded since the Callovian (Middle Jurassic) (Koevoets *et al.* 2016; Jelby *et al.* 2020b). This trend is consistent with the globally recognized Weissert Event (e.g. Lini *et al.* 1992; Weissert *et al.* 1998; Weissert and Erba 2004; Jelby *et al.* 2020b). Following the CIE of the Weissert Event, the $\delta^{13}C_{org}$ values remain relatively high, displaying overall steady-state conditions to a slight increase into the Hauterivian and lower Barremian in the upper part of the Rurikfjellet Formation (Figs 4, 8, 21; Vickers *et al.* 2019, 2023; Jelby *et al.* 2020b). In Svalbard, the Weissert Event appears to occur earlier than in other Boreal, Tethyan, Atlantic and Pacific sites, where the CIE initiation roughly coincides with the lower–upper Valanginian boundary (e.g. Price *et al.* 2016). Specifically, the onset of the Weissert Event in Svalbard is dated to coincide with the base of the Tethyan *T. pertransiens* ammonite zone at the Ryazanian–Valanginian boundary, whereas it roughly correlates with the top of the Tethyan *N. neocomiensiformis* and Sub-Boreal *Polyptychites* ammonite zones in most other sites. Thus, the offset in the initiation of the CIE between the $\delta^{13}C$ records corresponds to the Tethyan *T. pertransiens–N. neocomiensiformis* ammonite zones (Jelby *et al.* 2020b).

Basin configuration and evolution

Depositional model and physiography

The Bohemanneset and Fotografryggen members are interpreted to represent prodelta to delta front and offshore transition to strandplain shoreface environments, respectively. Recently, Nagy and Naoroz (2018) interpreted a reduced foraminiferal alpha diversity in the upper part of the Bohemanneset Member to reflect hyposaline conditions in an interdistributary bay setting, in line with the original interpretation of Edwards (1976) who referred the uppermost Fotografryggen Member to lagoonal and barrier-island systems. As emphasised by Grundvåg and Olaussen (2017), however, no convincing facies-related evidence of such depositional environments have been recorded throughout Spitsbergen. Instead, the facies belts of the Bohemanneset and Fotografryggen members are laterally extensive, and both members are dominated by wave- and storm-generated deposits, including metre-thick tempestites. These deposits are suggestive of a high-fetch (most likely hundreds of kilometres) marine setting capable of generating large storm waves in contrast to

the restricted setting of interdistributary bays. Further, the fourth-order high-frequency sequences and parasequences of the two members never develop into backshore or continental strata in the top, thus being characterized by gentle facies transitions across the inferred flooding surfaces that cap the sequences. This suggests that such deposits were either: (1) eroded due to wave ravinement during intervening transgressions; or (2) not developed due to a low-angle ramp physiography of the basin (Midtkandal and Nystuen 2009). As emphasised by Grundvåg *et al.* (2019), no transgressive lags typical of wave ravinement or evidence of forced regression (e.g. sharp-based shoreface deposits or foreshortened stratigraphy) have been identified throughout the outcrop belt on Spitsbergen. Instead, the stratal architecture of the parasequences probably reflects deposition onto a fully subaqueous, low-gradient ramp (Grundvåg *et al.* 2017, 2019; Jelby *et al.* 2020a; Midtkandal *et al.* 2020). This model is consistent with the notion that no clinoforms have been recognized throughout the outcrop belt, albeit this is strongly dependant on the scale and lateral persistence of the outcrops (Grundvåg *et al.* 2017).

In comparison, the voluminous but laterally restricted succession of mass-transport deposits in the Adventpynten Member is consistent with gravity-derived sediment, shed into a confined sub-basin of much higher accommodation space than the surrounding areas of the ramp. The occurrence of a rafted block of delta-plain deposits and overlying prodeltaic strata in the DH-1 and DH-2 well cores suggest that gravity flows were sourced from a relatively unstable and/or local delta front. The Lower Cretaceous succession of Svalbard has been suggested to represent the proximal part of a prograding shelf-prism-type clinoform system, widely reported on the Barents Shelf (Marin *et al.* 2016; Grundvåg *et al.* 2017; Midtkandal *et al.* 2020). In this scenario, however, the mass-transport deposits observed in the Adventpynten Member would probably form a laterally extensive sheet or lobe, and this model is consequently considered unlikely. Instead, localised accommodation space may have formed from relatively small collapses of the succession and associated subaqueous escarpments, perhaps due to growth-faulting and/or short-lived tectonic pulses of reactivated structural lineaments in eastern Svalbard (Grundvåg *et al.* 2019). This model is supported by the variable parasequence stacking patterns of the Bohemanneset Member in northern Nordenskiöld Land, with local variations in both the thickness and number of parasequences (e.g. wells DH-4 and DH-5, Forkastningsfjellet, Janusfjellet and Mälardalen; Figs 1c, 4, 5, 15b–d, 20c). Considering the low depositional gradient of the Rurikfjellet Formation ramp and that these sections represent deposition more than 50 km from the deltaic shoreline (Jelby *et al.* 2020a), it is deemed unlikely that deltaic processes alone (e.g. avulsion with compensational stacking and/or erosion of lobes; Bhattacharya *et al. (*2019) could have controlled the observed stratigraphic variability in such a distal setting. Instead, it speculated herein that a highly variable basin morphology was inherited following the deposition of the Adventpynten Member, and/or that periodic reactivation of former escarpments could have led to locally increased accommodation space and associated thickening of some parasequences (Figs 15c, d, 20).

Stratigraphic development and palaeogeography

The mudstone-dominated Wimanfjellet Member represents the most distal portion of the Rurikfjellet Formation depositional system, reflecting open-marine conditions well below SWB throughout the Valanginian–early Hauterivian (Grundvåg *et al.* 2019). The long-lived slight upwards-increase in sandstone content recorded in the member is consistent with

shoaling from lower to upper offshore environments through the entirety of the Valanginian, probably due to the gradually approaching shorelines of the Bohemanneset Member from the north-west and Fotografryggen Member from the west. The Adventpynten Member probably records advancement of a rapidly approaching local delta commencing in the late(?) Valanginian before the entire depositional system back-stepped and returned to lower offshore conditions in the early Hauterivian, as indicated by the MFS recorded in the uppermost part of the Wimanfjellet Member (Fig. 20; Grundvåg *et al.* 2019). This retreat of the depositional system was probably relatively short-lived and was immediately followed by successive basinward progradation of the Bohemanneset and Fotografryggen members into the area of the present-day outcrop belt in the early to earliest late Hauterivian (Fig. 20). Due to the stratigraphic position of the Bohemanneset Member above the Adventpynten Member, it may be speculated that the Bohemanneset Member represents the distal portion of the deltaic shoreline that fed the Adventpynten Member at an earlier point.

In the Bohemanneset and Fotografryggen members, the lack of backshore and continental facies in any of the parasequences indicates that the shorelines and source area of the wedges were at all times located beyond the present-day outcrop belt (to the north-west and west, respectively). Grundvåg *et al.* (2017) proposed north-eastern Greenland as a potential source area, due to its proximity to Svalbard in the Early Cretaceous (Fig. 2c), although this assertion is yet to be confirmed from provenance analyses.

The retrogradational parasequence stacking pattern in the upper part of the Bohemanneset and Fotografryggen members indicates that the entire system retreated in the late Hauterivian–early Barremian, and the uppermost mudstone-dominated unit that commonly caps the parasequence set may thus reflect an early Barremian semi-regional flooding (Grundvåg *et al.* 2019). In the Bohemanneset section, the mudstone unit coarsens upwards into a relatively coarse-grained parasequence of proximal delta-front origin in the top of the succession, which represents the most proximal facies recorded in the Bohemanneset Member (Figs 14 & 20c). This parasequence is thus considered to record a final, rapid progradational pulse of the deltaic shoreline in the northern basin reaches and may simultaneously represent the earliest indications of the stepwise forced regression that led to sequential subaerial erosion of the Rurikfjellet Formation ramp and the associated deposition of the Louiseberget Bed and Festningen Member in the early Barremian (Fig. 20; Grundvåg and Olaussen 2017).

It is noteworthy that the second-order R–T supersequence trend recorded through the Rurikfjellet Formation contradicts the long-term global eustatic sea-level curves of Haq

(2014) and Gale *et al.* (2020) (Fig. 3). Specifically, Haq (2014) indicates a relatively prominent sea-level rise through the Valanginian–Hauterivian, whereas this interval is largely regressive in the Rurikfjellet Formation. This could reflect: (1) a regional rift-shoulder uplift related to the opening of the Canada Basin, predating the HALIP (Fig. 2c); or (2) that the thermo-tectonic uplift north of Svalbard, related to formation of the HALIP, may have started as early as the Valanginian and gradually outpaced the rising eustatic sea level prior to peak uplift in the early Barremian. Nevertheless, the Hauterivian–lower Barremian third-order R–T–R stacking pattern recorded in the uppermost Wimanfjellet Member and through the Bohemanneset and Fotografryggen members roughly correlates with the short-term sea-level curve of Haq (2014), including a mid-Hauterivian fall, late Hauterivian rise, and earliest Barremian fall. Significantly, the short-term cycles are of *c.* 1 Myr length (Haq 2014), which is likely to correspond well with the duration of the third-order sequences recorded in the Rurikfjellet Formation (Catuneanu 2019; Jelby *et al.* 2020b). It may thus be speculated that the sequence stratigraphic trends observed in the Rurikfjellet Formation were partly controlled by short-term global eustatic sea level oscillations, superimposed on the regional uplift, in the late Hauterivian–early Barremian. This inference, however, is tentative.

Carbon cycling and climate

The presence of the Weissert Event in the Rurikfjellet Formation confirms previous assertions that this CIE represents a global carbon-cycle perturbation affecting the entire exchangeable carbon reservoir based on its recognition in numerous records retrieved from Tethyan, Boreal, Atlantic and Pacific basins (Figs 2b & 21; e.g. Weissert and Erba 2004; Price *et al.* 2016 and references therein). However, prior to this in the Late Jurassic, a > 4 ‰ negative CIE termed the 'Volgian Isotopic Carbon Excursion' (VOICE; Hammer *et al.* 2012) has been recognized in several disparate regions across the globe, including Argentina (Neuquén Basin), Saudi Arabia, and at localities across the Boreal Realm, all of which are characterized by being restricted settings (Galloway *et al.* 2020; Jelby *et al.* 2020b; Capelli *et al.* 2021; Rodriguez Blanco *et al.* 2022; Weger *et al.* 2022; Vickers *et al.* 2023; Fallatah *et al.* 2024). These records are at odds with global carbonate stable carbon-isotope ($\delta^{13}C_{carb}$) records, which are characterized by a gradual, steady decline in $\delta^{13}C_{carb}$ values across the Jurassic–Cretaceous boundary (Price *et al.* 2016). Changes in relative sea level (linked to the rifting associated with the break-up of Pangaea) causing the partly isolated basin configuration of the regions may have driven the decoupling of the carbon reservoirs at these sites from the global signal, and thereby lead to the subsequent evolution of local carbon-cycle dynamics away from global trends; ultimately resulting in the VOICE. The positive CIE of the Weissert Event represents an important re-equilibration of the carbon cycle where these restricted basins were recoupled with global signals (Galloway *et al.* 2020; Jelby *et al.* 2020b; Weger *et al.* 2022; Vickers *et al.* 2023). The initiation of the Weissert Event is dated to the mid-Valanginian in most records (Price *et al.* 2016), which coincides with a global eustatic sea-level rise (Haq 2014). Recoupling of the carbon cycle was thus probably controlled by re-establishment of ocean connections following a Late Jurassic sea-level lowstand (Galloway *et al.*

2020; Jelby *et al.* 2020b). However, Jelby *et al.* (2020b) recognized that the upper Valanginian–lower Barremian decay of the CIE in Svalbard is negligible compared to most other records, and that the signal remains relatively stable at near-peak values throughout the Rurikfjellet Formation following the positive excursion (Figs 3 and 21). This indicates that the oceanographic reconnection between higher and lower latitudes, and thus ocean ventilation, must have been sufficiently limited to keep some Boreal basins (including Svalbard) somewhat disconnected from prevailing global carbon-cycle dynamics following the isotopic event.

A continued limited connectivity of Boreal basins following the time of the Weissert Event is supported by recent studies suggesting that the isotopic event occurred within a time interval of relatively prolonged cooling of up to ~4°C superimposed on the general Early Cretaceous greenhouse climate (Price and Passey 2013; Meissner *et al.* 2015; Möller *et al.* 2015; Rogov *et al.* 2017; Vickers *et al.* 2019). This model is consistent with sedimentological evidence in the Rurikfjellet Formation and across the Boreal Realm in the form of "cold-water" glendonites (often associated with outsized clasts of possible sea-ice origin), dated from the Berriasian (i.e. upper Volgian–Ryazanian) through to the Hauterivian/Barremian (Figs 4–6a, 8, 12, 15a, d, 16h; Price and Nunn 2010; Rogov *et al.* 2017; Vickers *et al.* 2019; Jelby *et al.* 2020b). Potentially capable of sustaining limited polar ice caps, this cooling may have impeded the eustatic sea-level rise enough to inhibit a full oceanographic reconnection to some Boreal basins, including the Svalbard area (cf. Dypvik and Harris 2001; Galloway *et al.* 2020).

Valanginian disconformity or biostratigraphic diachronism?

The age of the base of the Rurikfjellet Formation, i.e. the Myklegardfjellet Bed, is disputed (e.g. Rakociński *et al.* 2018; Hammer *et al.* 2019). The early Valanginian age assessment of the boundary in this study confirms several previous observations (Pchelina 1965; Harland 1972; Bjærke 1978; Århus 1992; Nagy and Naoroz 2018). Notably, Harland (1972) claimed that the Berriasian (i.e. upper Volgian–Ryazanian) stage is missing in Svalbard, and Dypvik *et al.* (1992) proposed that the Myklegardfjellet Bed followed a depositional break of relatively limited time span, based on foraminiferal assemblage studies from and immediately below the boundary. More recently, Nagy and Naoroz (2018) referred the lower part of the Wimanfjellet Member to the Valanginian *Glomospirella multivoluta* and *Rhizammina brosgei* foraminiferal zones. Wierzbowski *et al.* (2011) reported a relatively rich Ryazanian ammonite fauna related to methane seep mounds in the uppermost Agardhfjellet Formation. A questionable *"Paracraspedites stenomphaloides" sensu* Shulgina (1972) ammonite of early Ryazanian age was found in the uppermost Agardhfjellet Formation in the DH-5 core (Jelby *et al.* 2020b), whereas Koevoets *et al.* (2019a) indicated the entire upper Ryazanian to be absent based on ammonite biostratigraphy. In addition, the presence of glauconite in the Myklegardfjellet Bed is indicative of slow sedimentation rate or sediment starvation in a suboxic environment (Hesselbo and Hugget 2001, and references therein). Collectively, this indicates that the Ryazanian–Valanginian boundary in most of the Svalbard area represents a depositional hiatus, possibly in association with strong stratal condensation of the Myklegardfjellet Bed.

The onset of the Weissert Event coincides with the base of the Rurikfjellet Formation, and the initiation of the CIE is dated to occur earlier (with an offset corresponding to the Tethyan *T. pertransiens–N. neocomiensiformis* ammonite zones) than in most other sites, notably in lower

palaeo-latitudes (Jelby *et al.* 2020b). Yet, the abundant records of the Weissert Event in both high and low palaeo-latitude basins clearly indicates that this carbon-cycle perturbation was of global significance (Weissert and Erba 2004; Price *et al.* 2016). Thus, it is deemed unlikely that the dated offset reflects delayed carbon cycling in lower latitudes compared to the Svalbard area. Instead, the offset probably reflects an inevitable consequence of the well-known Late Jurassic–Early Cretaceous provincialism of biostratigraphically important fossil groups, such as ammonites (e.g. Zakharov and Rogov 2008; Shurygin and Dzyuba 2015), which has yielded different zonal schemes and, notably, prohibited the rectification of a unified global chronostratigraphy (Gale *et al.* 2020; Hesselbo *et al.* 2020). It is therefore speculated herein that: (1) Valanginian dinocyst and ammonite biostratigraphy lack proper calibration and coherence, both in supra-basinal Tethyan–Boreal correlations and intra-basinal Boreal correlations; and (2) most of the lower Valanginian (corresponding the Tethyan *T. pertransiens–N. neocomiensiformis* ammonite zones) is missing in Svalbard or is condensed in the Myklegardfjellet Bed (Fig. 3).

Summary

A holostratigraphic scheme and depositional model is presented for the Lower Cretaceous (Valanginian–lower Barremian) Rurikfjellet Formation in Svalbard. The new stratigraphic framework is based on synthesis of the latest published facies-analytical, wireline-log, sequence stratigraphic, dinocyst and ammonite biostratigraphic, and $\delta^{13}C_{org}$ stratigraphic results from cored onshore wells and outcrop sections distributed across Spitsbergen, combined with new sedimentological data from five measured outcrop sections.

A revised lithostratigraphy for the Rurikfjellet Formation is presented herein, including the definition of three new members. The Wimanfjellet Member (Valanginian–lower Barremian), which comprises the basal glauconitic, plastic clay unit of the Myklegardfjellet Bed, is retained with a redefined type section and introduction of two new reference sections, and forms a relatively homogeneous, mudstone-dominated offshore succession across the entire outcrop belt of the Rurikfjellet Formation. The Adventpynten Member (upper(?) Valanginian–lowermost upper Hauterivian) is formally erected, and forms a *c.* 150 m thick succession of mass-transport deposits identified in two wells near Longyearbyen and in the north-eastern part of the Forkastningsfjellet mountain, northern Nordenskiöld Land. The Kikutodden Member is discarded and replaced by the Hauterivian–lower Barremian Bohemanneset and Fotografryggen members, which form two geographically separate and stratigraphically distinct clastic wedges. The Bohemanneset Member forms a heterogeneous (sandstone and mudstone) succession of storm-dominated and fluvial-influenced prodelta to delta front deposits in the northern basin reaches, from Oscar II Land through Nordenskiöld Land to Heer Land, with its southernmost occurrence at Kvalhovden. The Fotografryggen Member forms a sandstone-dominated succession of wave-dominated strandplain shoreface deposits in the southern basin reaches, from Sørkapp Land to Wedel Jarlsberg Land, with its northernmost occurrence at Langryggsåta. The area between the two clastic wedges constitutes most of Nathorst Land and north-easternmost Wedel Jarlsberg Land and is dominated by mudstones of the Wimanfjellet Member, which in this central part of the basin represents the entire Rurikfjellet Formation.

Deposition of the Rurikfjellet Formation took place on a fully subaqueous, high-fetch and low-gradient ramp, with the shoreline and source area at all times being located north-west and west of

the present-day outcrop belt. The succession forms a large-scale, second-order R–T supersequence, superimposed by two to three third-order R–T sequences, reflecting: (1) Valanginian open-marine conditions that shoaled from lower to upper offshore; (2) earliest Hauterivian local and rapid progradation, followed by transgression and maximum flooding; (3) early to earliest late Hauterivian deltaic and strandplain shoreline progradation towards the SE and E, respectively; (4) late Hauterivian–early Barremian shoreline retreat and semi-regional flooding; and (5) early Barremian rapid progradation. The Rurikfjellet Formation is overlain by local incised valley fill of the Louiseberget Bed and regional fluvial deposits of the Festningen Member, both of the Helvetiafjellet Formation, representing early Barremian stepwise forced regression that led to subaerial exposure and erosion of the Rurikfjellet Formation ramp.

The basal unit of the Rurikfjellet Formation (i.e. the Myklegardfjellet Bed) unconformably overlies the Ryazanian, and incorporates the onset of the globally recognized mid-Valanginian CIE; i.e. the Weissert Event. The initiation of the Weissert Event in Svalbard is dated to occur earlier than in other global records of the CIE, being offset by the Tethyan *T. pertransiens–N. neocomiensiformis* ammonite zones, which may indicate that: (1) Valanginian dinocyst and ammonite biostratigraphy lack Tethyan–Boreal and intra-Boreal calibration and coherence; and (2) most of the lower Valanginian is missing in Svalbard or condensed in the glauconitic clay of the Myklegardfjellet Bed.

Acknowledgements

The drill cores used in the study are managed by UNIS CO_2 Lab AS. UNIS and Lufttransport assisted with field-related logistics and transport. We warmly thank reviewers Gareth Lord and Rhodri Jerrett for critical and constructive comments, which greatly improved the outcome of this paper. Sincere thanks are also extended to the Norwegian Committee on Stratigraphy for reviewing the lithostratigraphic amendment; to William Helland-Hansen for insightful discussions; and to Fredrik Sønderholm, Simon Hansen Serre, Trude Hohle and Trygvi Bech Árting for invaluable assistance and pleasant company in the field.

Funding

This study was funded by the industry-sponsored consortium 'Lower Cretaceous Basin Studies in The Arctic' (LoCrA, https://wp.ux.uis.no/locra), and partly undertaken during a Carlsberg Foundation Internationalisation Fellowship granted to MEJ. MLV was supported by the Research Council of Norway through the Centres of Excellence funding scheme (project no. 332523, PHAB).

References

Ainsworth, R.B., Vakarelov, B.K. and Nanson, R.A. 2011. Dynamic spatial and temporal prediction of changes in depositional processes on clastic shorelines: toward improved subsurface uncertainty reduction and management. *AAPG Bulletin*, **95**, 267–297.

Alsen, P., Jelby, M.E., Mutterlose, J. and Śliwińska, K.K. 2020. An Early Cretaceous stratigraphic marker fossil in the High Arctic: the belemnite *Arctoteuthis bluethgeni*. *Geological Magazine*, **157**, 1715–1725.

Århus, N. 1991. Dinoflagellate cyst stratigraphy of some Aptian and Albian sections from North Greenland, southeastern Spitsbergen and the Barents Sea. *Cretaceous Research*, **12**, 209–225.

Århus, N. 1992. Some dinoflagellate cysts from the Lower Cretaceous of Spitsbergen. *Grana*, **31**, 305–314.

Århus, N., Kelly, S.R.A. Collins, J.S.H. and Sandy, M.R. 1990. Systematic palaeontology and biostratigraphy of two Early Cretaceous condensed sections from the Barents Sea. *Polar Research*, **8**, 165–194.

Bhattacharya, J.P. and MacEachern, J.A. 2009. Hyperpycnal rivers and prodeltaic shelves in the Cretaceous Seaway of North America. *Journal of Sedimentary Research*, **79**, 184–209.

Bhattacharya, J.P., Miall, A.D., Ferron, C., Gabriel, J., Randazzo, N., Kynaston, D., Jicha, B.R. and Singer, B.S. 2019. Time-stratigraphy in point sourced river deltas: Application to sediment budgets, shelf construction, and paleo-storm records. *Earth-Science Reviews*, **199**, 102985.

Birkenmajer, K. 1975. Jurassic and Lower Cretaceous sedimentary formations of SW Torell Land, Spitsbergen. *Studia Geologica Polonica*, **44**, 7–42.

Birkenmajer, K. 1980. Jurassic–Lower Cretaceous succession at Agardhbukta, East Spitsbergen. *Studia Geologica Polonica*, **66**, 35–52.

Birkenmajer, K., Pugaczewska, H. and Wierzbowski, A. 1982. The Janusfjellet Formation (Jurassic-Lower Cretaceous) at Myklegardfjellet, east Spitsbergen. *Palaeontologia Polonica*, **43**, 107–140.

Bjærke, T. 1978. Mesozoic palynology of Svalbard III. Dinoflagellates from the Rurikfjellet Member, Janusfjellet Formation (Lower Cretaceous) of Spitsbergen. *Palinologia, numero extraordin*, **1**, 69–93.

Bodin, S., Meissner, P., Janssen, N.M.M., Steuber, T. and Mutterlose, J. 2015. Large igneous provinces and organic carbon burial: Controls on global temperature and continental weathering during the Early Cretaceous. *Global and Planetary Change*, **133**, 238–253.

Bouma, A.H. 1962. Sedimentology of Some Flysch Deposits: A Graphic Approach to Facies Interpretation. *Elservier, Amsterdam,* 168 pp.

Braathen, A., Bælum, K., Christiansen, H.H., Dahl, T., Eiken, O., Elvebakk, H., Hansen, F., Hanssen, T.H., Jochmann, M., Johansen, T.A., Johnsen, H., Larsen, L., Lie, T., Mertes, J., Mørk, A., Mørk, M.B., Nemec, W., Olaussen, S., Oye, V., Rød, K., Titlestad, G.O., Tveranger, J. and Vagle, K. 2012. The Longyearbyen CO_2 Lab of Svalbard, Norway—initial assessment of the geological conditions for CO_2 sequestration. *Norwegian Journal of Geology*, **92**, 353–376.

Capelli, I.A., Scasso, R.A., Spangenberg, J.E., Kietzmann, D.A., Cravero, F., Duperron, M., and Adatte, T. 2021. Mineralogy and geochemistry of deeply-buried marine sediments of the Vaca Muerta-Quintuco system in the Neuquén Basin (Chacay Melehue section), Argentina: Paleoclimatic and paleoenvironmental implications for the global Tithonian-Valanginian reconstructions. *Journal of South American Earth Sciences*, **107**, 103103.

Catuneanu, O. 2019. Scale in sequence stratigraphy. *Marine and Petroleum Geology*, **106**, 128–159.

Collins, D.S., Johnson, H.D., Allison, P.A., Guilpain, P. and Damit, A.R. 2017. Coupled 'storm-flood' depositional model: Application to the Miocene–Modern Baram Delta Province, north-west Borneo. *Sedimentology*, **64**, 1203–1235.

Corfu, F., Polteau, S., Planke, S., Faleide, J.I., Svensen, H., Zayoncheck, A. and Stolbov, N. 2013. U–Pb geochronology of Cretaceous magmatism on Svalbard and Franz Josef Land, Barents Sea Large Igneous Province. Geological Magazine, **150**, 1127–1135.

Dallmann, W.K., Elvevold, S., Majka, J. and Piepjohn, K. 2015. Tectonics and tectonothermal events. *In:* Dallmann, W.K. (ed.) *Geoscience Atlas of Svalbard. Norsk Polarinstitutt Rapportserie*, **148**, 292 pp.

Dott, R.H., Jr and Bourgeois, J. 1982. Hummocky stratification: Significance of its variable bedding sequences. *GSA Bulletin*, **93**, 663–680.

Dypvik, H. 1980. The sedimentology of the Janusfjellet Formation, Central Spitsbergen (Sassenfjorden and Agardhfjellet areas). *Norsk Polarinstitutt Skrifter*, **172**, 97–134.

Dypvik, H. 1985. Jurassic and Cretaceous black shales of the Janusfjellet Formation, Svalbard, Norway. *Sedimentary Geology*, **41**, 235–248.

Dypvik, H. and Bue, B. 1984. The U, Th and K distribution in black shales of the Janusfjellet Formation, Svalbard, Norway. *Chemical Geology*, **42**, 287–296.

Dypvik, H. and Harris, N. 2001. Geochemical facies analysis of fine-grained siliciclastics using Th/U, Zr/Rb and (Zr + Rb)/Sr ratios. *Chemical Geology*, **181**, 131–146.

Dypvik, H., Nagy, J., Eikeland, T.A., Backer-Owe, K., Andersen, A., Haremo, P., Bjærke, T., Johansen, H. and Elverhøi, A. 1991a. The Janusfjellet Subgroup (Bathonian to Hauterivian) on central Spitsbergen: a revised lithostratigraphy. *Polar Research*, **9**, 21–43.

Dypvik, H., Nagy, J., Eikeland, T.A., Backer-Owe, K. and Johansen, H. 1991b. Depositional conditions of the Bathonian to Hauterivian Janusfjellet Subgroup, Spitsbergen. *Sedimentary Geology*, **72**, 55–78.

Dypvik, H., Nagy, J. and Krinsley, D.H. 1992. Origin of the Myklegardfjellet Bed, a basal Cretaceous marker on Spitsbergen. *Polar Research*, **11**, 21–31.

Dypvik, H., Håkansson, E. and Heinberg, C. 2002. Jurassic and Cretaceous palaeogeography and stratigraphic comparisons in the North Greenland-Svalbard region. *Polar Research*, **21**, 91–108.

Dzyuba, O.S., Izokh, O.P. and Shurygin, B.N. 2013. Carbon isotope excursions in Boreal Jurassic–Cretaceous boundary sections and their correlation potential. *Palaeogeography, Palaeoclimatology, Palaeoecology*, **381–382**, 33–46.

Edwards, M.B. 1976. Depositional environments in Lower Cretaceous regressive sediments, Kikutodden, Sørkapp Land, Svalbard. *Norsk Polarinstitutt Årbok 1974*, 35–50.

Embry, A., Beauchamp, B., Dewing, K. and Harrison, C. 2023. Sverdrup Basin Composite Tectono-Sedimentary Element, Canadian Arctic Islands. *In*: Drachev, S.S., Brekke, H., Henriksen, E. and Moore, T. (eds) *Sedimentary Successions of the Arctic Region and their Hydrocarbon Prospectivity. Geological Society, London, Memoirs*, **57**, https://doi.org/10.1144/M57-2017-11.

Fallatah, M.I., Alnazghah, M., Kerans, C. and Al-Hussaini, A. 2024. Sedimentology and carbon isotope stratigraphy from the Late Jurassic – Early Cretaceous of the Arabian plate: The Weissert event and the VOICE in the Tethys Realm? *Marine and Petroleum Geology*, **161**, 106670.

Föllmi, K.B. 2012. Early Cretaceous life, climate and anoxia. *Cretaceous Research*, **35**, 230–257.

Gale, A.S., Mutterlose, J., Batenburg, S., Gradstein, F.M., Agterberg, F.P., Ogg, J.G. and Petrizzo, M.R. 2020. The Cretaceous Period. *In*: Gradstein, F.M., Ogg, J.G., Schmitz, M.D. and Ogg, G.M. (eds) *Geological Time Scale 2020*. Elsevier, Boston, MA, 1023–1086.

Galloway, J.M., Vickers, M., Price, G.D., Poulton, T., Grasby, S.E., Hadlari, T., Beauchamp, B. and Sulphur, K. 2020. Finding the VOICE: organic carbon isotope chemostratigraphy of Late Jurassic – Early Cretaceous Arctic Canada. Geological Magazine, **157**, 1643–1657.

Gjelberg, J. and Steel, R.J. 1995. Helvetiafjellet Formation (Barremian–Aptian), Spitsbergen: characteristics of a transgressive succession. *In*: Steel, R.J. (ed.) *Sequence Stratigraphy on the Northwest European Margin*. *Norwegian Petroleum Society Special Publications*, **5**, 571–593.

Grantz, A., Hart, P.E. and Childers, V.A. 2011. Geology and tectonic development of the Amerasia and Canada Basins, Arctic Ocean. *In*: Spencer, A.M., Embry, A.F., Gautier, D.L., Stoupakova, A.V., and Sørensen, K. (eds) *Arctic Petroleum Geology*. *Geological Society, London, Memoirs*, **35**, 771–799.

Gröcke, D.R., Price, G.D., Robinson, S.A., Baraboshkin, E.Y., Mutterlose, J. and Ruffell, A.H. 2005. The Upper Valanginian (Early Cretaceous) positive carbon–isotope event recorded in terrestrial plants. *Earth and Planetary Science Letters*, **240**, 495–509.

Grøsfjeld, K. 1991. Palynological age constraints on the base of the Helvetiafjellet Formation (Barremian) on Spitsbergen. *Polar Research*, **11**, 11–19.

Grundvåg, S.-A. and Olaussen, S. 2017. Sedimentology of the Lower Cretaceous at Kikutodden and Keilhaufjellet, southern Spitsbergen: implications for an onshore–offshore link. *Polar Research*, **36**, 1302124.

Grundvåg, S.-A., Marin, D., Kairanov, B., Śliwińska, K.K., Nøhr-Hansen, H., Jelby, M.E., Escalona, A. and Olaussen, S. 2017 The Lower Cretaceous succession of the northwestern Barents Shelf: Onshore and offshore correlations. *Marine and Petroleum Geology*, **86**, 834–857.

Grundvåg, S.-A., Jelby, M.E., Śliwińska, K.K., Nøhr-Hansen, H., Aadland, T., Sandvik, S.E., Tennvassås, T. and Olaussen, S. 2019. Sedimentology and palynology of the Lower Cretaceous succession of central Spitsbergen: integration of subsurface and outcrop data. *Norwegian Journal of Geology*, **99**, 253–284.

Grundvåg, S.-A., Jelby, M.E., Olaussen, S. and Śliwińska, K.K. 2021. The role of shelf morphology on storm-bed variability and stratigraphic architecture, Lower Cretaceous, Svalbard. *Sedimentology*, **68**, 196–237.

Hammer, Ø., Collignon, M. and Nakrem, H.A. 2012. Organic carbon isotope chemostratigraphy and cyclostratigraphy in the Volgian of Svalbard. *Norwegian Journal of Geology*, **92**, 103–112.

Hammer, Ø., Alsen, P., Grundvåg, S.-A., Jelby, M.E., Nøhr-Hansen, H., Olaussen, S., Senger, K., Śliwińska, K.K. and Smelror, M. 2019. Comment on 'Redox conditions, productivity, and volcanic input during deposition of uppermost Jurassic and Lower Cretaceous organic-rich siltstones in Spitsbergen, Norway' by Rakociński et al. (2018). *Cretaceous Research*, **96**, 241–243.

Haq, B.U. 2014. Cretaceous eustasy revisited. *Global and Planetary Change*, **113**, 44–58.

Harland, W.B. 1972. Mesozoic geology of Svalbard. *In:* Pitcher, M.G. (ed.) *Arctic Geology – Proceedings of the Second International Symposium on Arctic Geology. American Association of Petroleum Geologists Memoir*, **19**, 135–148.

Héquette, A. and Hill, P.R. 1993. Storm-generated currents and offshore sediment transport on a sandy shoreface, Tibjak Beach, Canadian Beaufort Sea. *Marine Geology*, **113**, 283–304.

Héquette, A. and Hill, P.R. 1995. Response of the seabed to storm-generated combined flows on a sandy Arctic shoreface, Canadian Beaufort Sea. *Journal of Sedimentary Research*, **65**, 461–471.

Hesselbo, S.P. and Hugget, J.M. 2001. Glaucony in ocean-margin sequence stratigraphy (Oligocene-Pliocene, Offshore New Jersey, U.S.A.; ODP Leg 174A). *Journal of Sedimentary Research*, **71**, 599–607.

Hesselbo, S.P., Ogg, J.G., Ruhl, M., Hinnov, L.A. and Huang, C.J. 2020. The Jurassic Period. *In*: Gradstein, F.M., Ogg, J.G., Schmitz, M.D. and Ogg, G.M. (eds) *Geological Time Scale 2020*. Elsevier, Boston, MA, 955–1021.

Jelby, M.E., Grundvåg, S.-A., Helland-Hansen, W., Olaussen, S. and Stemmerik, L., 2020a. Tempestite facies variability and storm-depositional processes across a wide ramp: Towards a polygenetic model for hummocky cross-stratification. *Sedimentology*, **67**, 742–781.

Jelby, M.E., Śliwińska, K.K., Koevoets, M.J., Alsen, P., Vickers, M.L., Olaussen, S. and Stemmerik, L. 2020b. Arctic reappraisal of global carbon-cycle dynamics across the Jurassic–Cretaceous boundary and Valanginian Weissert Event. *Palaeogeography, Palaeoclimatology, Palaeoecology*, **555**, 109847.

Jelby, M.E., Ineson, J.R., Sheldon, E. and Anderskouv, K. 2024. Old chalk, new tricks: revisiting the Lower Cretaceous carbonates of the Danish Central Graben. *In:* Hart, M.B., Batenburg, S.J., Huber, B.T., Price, G.D., Thibault, N., Wagreich, M. and Walaszczyk, I. (eds) *Cretaceous Project 200 Volume 2: Regional Studies. Geological Society, London, Special Publications*, **545**, https://doi.org/10.1144/SP545-2023-134.

Knaust, D. 2019. The enigmatic trace fossil *Tisoa* de Serres, 1840. *Earth-Science Reviews*, **188**, 123–147.

Kneller, B.C. and Branney, M.J. 1995. Sustained high-density turbidity currents and the deposition of thick massive sands. *Sedimentology*, **42**, 607–616.

Koevoets, M.J., Abay, T.B., Hammer, Ø. and Olaussen, S. 2016. High-resolution organic carbon–isotope stratigraphy of the Middle Jurassic–Lower Cretaceous Agardhfjellet Formation of central Spitsbergen, Svalbard. *Palaeogeography, Palaeoclimatology, Palaeoecology*, **449**, 266–274.

Koevoets, M.J., Hammer, Ø. and Little, C.T.S. 2019a. Palaeoecology and palaeoenvironments of the Middle Jurassic to lowermost Cretaceous Agardhfjellet Formation (Bathonian–Ryazanian), Spitsbergen, Svalbard. *Norwegian Journal of Geology*, **99**, 17–40.

Koevoets, M.J., Hammer, Ø, Olaussen, S., Senger, K. and Smelror, M. 2019b. Integrating subsurface and outcrop data of the Middle Jurassic to Lower Cretaceous Agardhfjellet Formation in central Spitsbergen. *Norwegian Journal of Geology*, **99**, 213–246.

Kuhn, D., Redfield, T.F., Hermanns, R.L., Fuchs, M., Torizin, J. and Balzer, D. 2019. Anatomy of a mega-rock slide at Forkastningsfjellet, Spitsbergen and its implications for landslide hazard and risk considerations. *Norwegian Journal of Geology*, **99**, 41–61.

Lini, A., Weissert, H. and Erba, E. 1992. The Valanginian carbon isotope event: a first episode of greenhouse climate conditions during the Cretaceous. *Terra Nova*, **4**, 374–384.

Lowe, D.R. 1982. Sediment gravity flows: II. Depositional models with special reference to the deposits of high-density turbidity currents. *Journal of Sedimentary Petrology*, **52**, 279–297.

Lundin, E.R. and Doré, A.G. 1997. A tectonic model for the Norwegian passive margin with implications for the NE Atlantic: Early Cretaceous to break-up. *Journal of the Geological Society, London*, **154**, 545–550.

MacEachern, J.A., Bann, K.L., Pemberton, S.G. and Gingras, M.K. 2007. The ichnofacies paradigm: high-resolution paleoenvironmental interpretation of the rock record. *In:* MacEachern, J.A., Bann, K.L., Gingras, M.K. and Pemberton, S.G. (eds) *Applied Ichnology. SEPM Short Course Notes*, **52**, https://doi.org/10.2110/pec.07.52.0027.

MacEachern, J.A. and Bann, K.L. 2020. The *Phycosiphon* Ichnofacies and the *Rosselia* Ichnofacies: two new ichnofacies for marine deltaic environments. *Journal of Sedimentary Research*, **90**, 855–886.

MacEachern, J.A. and Bann, K.L. 2023. Departures from the archetypal deltaic ichnofacies. *In:* Cónsole-Gonella, C., de Valais, S., Díaz-Martínez, I., Citton, P., Verde, M. and McIlroy, D. (eds) *Ichnologi in Shallow-marine and Transitional Environments*. *Geological Society, London, Special Publications*, **522**, 175–213.

Macquaker, J.H.S., Bentley, S.J. and Bohacs, K.M. 2010. Wave-enhanced sediment-gravity flows and mud dispersal across continental shelves: Reappraising sediment transport processes operating in ancient mudstone successions. *Geology*, **38**, 947–950.

Maher, H.D. 2001. Manifestations of the Cretaceous High Arctic Large Igneous Province in Svalbard. *The Journal of Geology*, **109**, 91–104.

Marin, D., Escalona, A., Śliwińska, K.K., Nøhr-Hansen, H. and Mordasova, A. 2016. Sequence stratigraphy and lateral variability of Lower Cretaceous clinoforms in the southwestern Barents Sea. *AAPG Bulletin*, **101**, 1487–1517.

Meissner, P., Mutterlose, J. and Bodin, S. 2015. Latitudinal temperature trends in the northern hemisphere during the Early Cretaceous (Valanginian–Hauterivian). *Palaeogeography, Palaeoclimatology, Palaeoecology*, **424**, 17–39.

Midtkandal, I. and Nystuen, J.P. 2009. Depositional architecture of a low-gradient ramp shelf in an epicontinental sea: the lower Cretaceous of Svalbard. *Basin Research*, **21**, 655–675.

Midtkandal, I., Nystuen, J.P. and Nagy, J. 2007. Paralic sedimentation on an epicontinental ramp shelf during a full cycle of relative sea-level fluctuation; the Helvetiafjellet Formation in Nordenskiöld Land, Spitsbergen. *Norwegian Journal of Geology*, **87**, 343–359.

Midtkandal, I., Nystuen, J.P., Nagy, J. and Mørk, A. 2008. Lower Cretaceous lithostratigraphy across a regional subaerial unconformity in Spitsbergen: the Rurikfjellet and Helvetiafjellet formations. *Norwegian Journal of Geology*, **88**, 287–304.

Midtkandal, I., Svensen, H.H., Planke, S., Corfu, F., Polteau, S., Torsvik, T.H., Faleide, J.I., Grundvåg, S.-A., Selnes, H., Kürschner, W. and Olaussen, S. 2016. The Aptian (Early Cretaceous) oceanic anoxic event (OAE1a) in Svalbard, Barents Sea, and the absolute age of the Barremian-Aptian boundary. *Palaeogeography, Palaeoclimatology, Palaeoecology*, **463**, 126–135.

Midtkandal, I., Faleide, J.I., Faleide, T.S., Serck, C.S., Planke, S., Corseri, R., Dimitriou, M. and Nystuen, J.P. 2020. Lower Cretaceous Barents Sea strata: epicontinental basin configuration, timing, correlation and depositional dynamics. *Geological Magazine*, **157**, 458–476.

Mozely, P.S. 1989. Relation between depositional environment and the elemental composition of early diagenetic siderite. *Geology*, **17**, 704–706.

Möller, C., Mutterlose, J. and Alsen, P. 2015. Integrated stratigraphy of Lower Cretaceous sediments (Ryazanian–Hauterivian) from North-East Greenland. *Palaeogeography, Palaeoclimatology, Palaeoecology*, **437**, 85–97.

Mørk, A. 1978. Observations on the stratigraphy and structure of the inner Hornsund area. *Norsk Polarinstitutt Årbok 1977*, 61–70.

Mørk, A., Dallmann, W.K., Dypvik, H., Johannessen, E.P., Larssen, G.B., Nagy, J., Nøttvedt, A., Olaussen, S., Pčelina, T.M. and Worsley, D. 1999. Mesozoic lithostratigraphy. *In*: Dallmann, W.K. (ed.) *Lithostratigraphic Lexicon of Svalbard – Review and Recommendations for Nomenclature use; Upper Palaeozoic to Quaternary bedrock*. Norsk Polarinstitutt, Tromsø, 127–214.

Myrow, P.M. 1992. Bypass-zone tempestite facies model and proximality trends for an ancient muddy shoreline and shelf. *Journal of Sedimentary Petrology*, **62**, 99–115.

Myrow, P.M. and Southard, J.B. 1996. Tempestite deposition. *Journal of Sedimentary Research*, **66**, 875–887.

Myrow, P.M., Fischer, W. and Goodge, J.W. 2002. Wave-modified turbidites: combined-flow shoreline and shelf deposits, Cambrian, Antarctica. *Journal of Sedimentary Research*, **72**, 641–656.

Nagy, J. and Naoroz, M. 2018. Changing depositional environments reflected by foraminifera in a transgressive–regressive sequence of the Lower Cretaceous on Spitsbergen. *Palaeogeography, Palaeoclimatology, Palaeoecology*, **511**, 144–167.

Nagy, J., Løfaldi, M., Bäckström, S.A. and Johansen, H. 1990. Agglutinated foraminiferal stratigraphy of Middle Jurassic to basal Cretaceous shales, central Spitsbergen. *In:* Hemleben, C., Kaminski, M.A., Kuhnt, W. and Scott, D.B. (eds) *Paleoecology, Biostratigraphy, Paleoceanography and Taxonomy of Agglutinated Foraminifera*. *NATO Science Series C*, **327**, 969–1015.

Nalnyaeva, T.I., Basov, N.A. and Meledina, S.V. 2011. Jurassic and Lower Cretaceous stratigraphy and belemnites of western Spitsbergen (Svalbard). *News of Palaeontology and Stratigraphy*, **16–17**, 109–129. [In Russian.]

Nystuen, J.P. 1989. Rules and recommendations for naming geological units in Norway – by the Norwegian Committee on Stratigraphy. *Norsk Geologisk Tidsskrift*, **69**, 119 pp.

Olaussen, S., Larssen, G.B., Helland-Hansen, W., Johannessen, E.P., Nøttvedt, A., Riis, F., Rismyhr, B., Smelror, M. and Worsley, D. 2018. Mesozoic strata of Kong Karls Land, Svalbard, Norway; a link to the northern Barents Sea basins and platforms. *Norwegian Journal of Geology*, **98**, 1–69.

Olaussen, S., Grundvåg, S.-A., Senger, K., Anell, I., Betlem, P., Birchall, T., Braathen, A., Dallmann, W., Jochmann, M., Johannessen, E.P., Lord, G., Mørk, A., Osmundsen, P.T., Smyrak-Sikora, A. and Stemmerik, L. 2023. Svalbard Composite Tectono-Sedimentary Element, Barents Sea. *In:* Drachev, S.S., Brekke, H., Henriksen, E. and Moore, T. (eds) *Sedimentary Successions of the*

Arctic Region and their Hydrocarbon Prospectivity. *Geological Society, London, Memoirs*, **57**, https://doi.org/10.1144/M57-2021-36.

Parker, J.R. 1967. The Jurassic and Cretaceous sequence in Spitsbergen. *Geological Magazine*, **104**, 487–505.

Parsons, J.D., Bush, J.W.M. and Syvitski, J.P.M. 2001. Hyperpycnal plume formation from riverine outflows with small sediment concentrations. *Sedimentology*, **48**, 465–478.

Pchelina. T. M. 1965a. Stratigraphy and composition of the Mesozoic deposits in central Vestspitsbergen. *In:* Sokolov. V.N. (ed.) *Geology of Spitsbergen*, 131–154. In Russian; English translation by National Lending Library, Boston, Spa, 1970.

Pcelina, T.M. 1965b. Mesozoic deposits around Vand Keulenfjord, Vestspitsbergen. *In:* Sokolov. V.N. (ed.) *Geology of Spitsbergen*, 155–181. In Russian; English translation by National Lending Library, Boston, Spa, 1970.

Price, G.D. 1999. The evidence and implications of polar ice during the Mesozoic. *Earth-Science Reviews*, **48**, 183–210.

Price, G.D. and Nunn, E.V. 2010. Valanginian isotope variation in glendonites and belemnites from Arctic Svalbard: Transient glacial temperatures during the Cretaceous greenhouse. *Geology*, **38**, 251–254.

Price, G.D. and Passey, B.H. 2013. Dynamic polar climates in a greenhouse world: Evidence from clumped isotope thermometry of Early Cretaceous belemnites. *Geology*, **41**, 923–926.

Price, G.D., Főzy, I. and Pálfy, J. 2016. Carbon cycle history through the Jurassic–Cretaceous boundary: A new global $\delta^{13}C$ stack. *Palaeogeography, Palaeoclimatology, Palaeoecology*, **451**, 46–61.

Price, G.D., Janssen, N.M.M., Martinez, M., Company, M., Vandevelde, J.H. and Grimes, S.T. 2018. A high-resolution belemnite geochemical analysis of Early Cretaceous (Valanginian-Hauterivian) environmental and climatic perturbations. *Geochemistry, Geophysics, Geosystems*, **19**, 3832–3843.

Rakociński, M., Zatoń, M., Marynowski, L., Gedl, P. and Lehmann, J. 2018. Redox conditions, productivity, and volcanic input during deposition of uppermost Jurassic and Lower Cretaceous organic-rich siltstones in Spitsbergen, Norway. *Cretaceous Research*, **89**, 126–147.

Rodriguez Blanco, L., Swart, P.K., Eberli, G.P. and Weger, R.J. 2022. Negative $\delta^{13}C_{carb}$ values at the Jurassic-Cretaceous boundary – Vaca Muerta Formation, Neuquén Basin, Argentina. *Palaeogeography, Palaeoclimatology, Palaeoecology*, **603**, 111208.

Rogov, M.A., Ershova, V.B., Shchepetova, E.V., Zakharov, V.A., Pokrovsky, B.G. and Khudoley, A.K. 2017. Earliest Cretaceous (late Berriasian) glendonites from Northeast Siberia revise the timing of initiation of transient Early Cretaceous cooling in the high latitudes. *Cretaceous Research*, **71**, 102–112.

Rozycki, S.Z. 1959. Geology of the north-western part of Torell Land, Vestspitsbergen. *Studia Geologica Polonica*, **2**, 1–98.

Senger, K., Tveranger, J., Ogata, K., Braathen, A. and Planke, S. 2014. Late Mesozoic magmatism in Svalbard: A review. *Earth-Science Reviews*, **139**, 123–144.

Senger, K., Brugmans, P., Grundvåg, S.-A., Jochmann, M., Nøttvedt, A., Olaussen, S., Skotte, A. and Smyrak-Sikora, A. 2019. Petroleum, coal and research drilling onshore Svalbard: a historical perspective. *Norwegian Journal of Geology*, **99**, 377–407.

Shanmugam, G. 1996. High-density turbidity currents; are they sandy debris flows? *Journal of Sedimentary Research*, **66**, 2–10.

Shephard, G.E., Müller, R.D. and Seton, M. 2013. The tectonic evolution of the Arctic since Pangea breakup: Integrating constraints from surface geology and geophysics with mantle structure. *Earth-Science Reviews*, **124**, 148–183.

Shulgina, N.I. 1972. Ammonites from the North of Middle Siberia. *In:* Sachs, V.N. (ed.) *Jurassic–Cretaceous boundary and Berriasian Stage in Boreal Realm.* Novosibirsk, Nauka, 137–175. (In Russian)

Shurygin, B.N. and Dzyuba, O.S. 2015. The Jurassic/Cretaceous boundary in northern Siberia and Boreal–Tethyan correlation of the boundary beds. *Russian Geology and Geophysics*, **56**, 652–662.

Śliwińska, K.K., Jelby, M.E., Grundvåg, S.-A., Nøhr-Hansen, H., Alsen, P. and Olaussen, S. 2020. Dinocyst stratigraphy of the Valanginian–Aptian Rurikfjellet and Helvetiafjellet formations on Spitsbergen, Arctic Norway. *Geological Magazine*, **157**, 1693–1714.

Sømme, T.O., Doré, A.G., Lundin, E.R. and Tørudbakken, B.O. 2018. Triassic–Paleogene paleogeography of the Arctic: Implications for sediment routing and basin fill. *AAPG Bulletin*, **102**, 2481–2517.

Steel, R. and Worsley, D. 1984. Svalbard's post-Caledonian strata – an atlas of sedimentational patterns and palaeogeographic evolution. *In*: Spencer, A.M. (ed.) *Petroleum Geology of the North European Margin*. Norwegian Petroleum Society, Graham & Trotman Limited, London, 109–135.

Taylor, A.M. and Goldring, R. 1993. Description and analysis of bioturbation and ichnofabric. *Journal of the Geological Society, London*, **150**, 141–148.

Torsvik, T.H., Carlos, D., Mosar, J., Cocks, L.R.M. and Malme, T.N. 2002. Global reconstructions and North Atlantic paleogeography 440 Ma to Recent. In: Eide, E.A. (ed.) *BATLAS – Mid Norway plate reconstruction atlas with global and Atlantic perspectives*. Geological Survey of Norway, Trondheim, 18–39.

Van Wagoner, J.C., Mitchum, R.M., Campion, K.M. and Rahmanian, V.D. 1990. Siliciclastic sequence stratigraphy in well logs, cores, and outcrops: concepts for high-resolution correlation of time and facies. *AAPG Methods in Exploration Series*, **7**, 55 pp.

Vickers, M., Watkinson, M., Price, G.D. and Jerrett, R. 2018. An improved model for the ikaite - glendonite transformation: evidence from the Lower Cretaceous of Spitsbergen, Svalbard. *Norwegian Journal of Geology*, **98**, 1–15.

Vickers, M.L., Price, G.D., Jerrett, R.M., Sutton, P., Watkinson, M.P., FitzPatrick, M. 2019. The duration and magnitude of Cretaceous cool events: Evidence from the northern high latitudes. *GSA Bulletin*, **131**, 1979–1994.

Vickers, M.L., Hougård, I.W., Alsen, P., Ullmann, C.V., Jelby, M.E., Bedington, M. and Korte, C. 2022. Middle to Late Jurassic palaeoclimatic and palaeoceanographic trends in the Euro-Boreal region: Geochemical insights from East Greenland belemnites. *Palaeogeography, Palaeoclimatology, Palaeoecology*, **597**, 111014.

Vickers, M.L., Jelby, M.E., Śliwińska, K.K., Percival, L.M.E., Wang, F., Sanei, H., Price, G.D., Ullmann, C.V., Grasby, S.E., Reinhard, L., Mather, T.A., Frieling, J., Korte, C., Jerrett, R.M., Jones, M.T., Midtkandal, I. and Galloway, J.M. 2023. Volcanism and carbon cycle perturbations in the High Arctic during the Late Jurassic – Early Cretaceous. *Palaeogeography, Palaeoclimatology, Palaeoecology*, **613**, 111412.

Wang, Y., Huang, C., Sun, B., Quan, C., Wu, J. and Lin, Z. 2014. Paleo-CO_2 variation trends and the Cretaceous greenhouse climate. *Earth-Science Reviews*, **129**, 136–147.

Weger, R.J., Eberli, G.P., Blanco, L.R., Tenaglia, M. and Swart, P.K. 2023. Finding a VOICE in the Southern Hemisphere: A new record of global organic carbon? *GSA Bulletin*, **135**, 2107–2120.

Weissert, H. and Erba, E. 2004. Volcanism, CO_2 and palaeoclimate: a Late Jurassic–Early Cretaceous carbon and oxygen isotope record. *Journal of the Geological Society, London*, **161**, 695–702.

Weissert, H., Lini, A., Föllmi, K.B. and Kuhn, O. 1998. Correlation of Early Cretaceous carbon isotope stratigraphy and platform drowning events: a possible link? *Palaeogeography, Palaeoclimatology, Palaeoecology*, **137**, 189–203.

Wierzbowski, A., Hryniewicz, K., Hammer, Ø., Nakrem, H.A., Little, C.T.S. 2011. Ammonites from hydrocarbon seep carbonate bodies from the uppermost Jurassic – lowermost Cretaceous of Spitsbergen and their biostratigraphic importance. *Neues Jahrbuch für Geologie und Paläontologie Abhandlungen*, **262**, 267–288.

Zakharov, V.A. and Rogov, M.A. 2008. Let the Volgian stage stay in the Jurassic. *Russian Geology and Geophysics*, **49**, 408–412.

Žák, K., Košťák, M., Otakar, M., Zakharov, V.A., Rogov, M.A., Pruner, P., Rohovec, J., Dzyuba, O.S. and Mazuch, M., 2011. Comparison of carbonate C and O stable isotope records across the Jurassic/Cretaceous boundary in the Tethyan and Boreal Realms. *Palaeogeography, Palaeoclimatology, Palaeoecology*, **299**, 83–96.

Figure Captions

Fig. 1. Maps of the geological setting of the Lower Cretaceous succession in Svalbard, and location of measured sections from this (Festningen, Fotografryggen, Oppdalssåta, Romnæstoppen and Slottsmøya) and previous studies, including the type and reference sections of the Rurikfjellet Formation as defined herein, and other sections of lithostratigraphic significance. (a) Present-day location of Svalbard representing the north-western corner of the Barents Shelf. (b) Geological map of central to southern Spitsbergen (modified from Dallmann *et al.* 2015), highlighting the distribution of the Adventdalen Group. The rose diagrams represent palaeocurrent measurements of unidirectional sedimentary structures in the Bohemanneset (Jelby *et al.* 2020a) and Fotografryggen (Grundvåg and Olaussen 2017) members, indicating a dominantly eastwards shore-normal and southwards shore-parallel transport direction, respectively. BFZ, Billefjorden Fault Zone, LFZ, Lomfjorden Fault Zone; WSFTB, West Spitsbergen Fold and Thrust Belt. (c) Terrain model (modified from the Norwegian Polar Institute, https://geodata.npolar.no) of the area in the vicinity of Longyearbyen, northern Nordenskiöld Land, showing the position of outcrop logs and the cored wells DH-1 to DH-7 at Adventpynten and in Adventdalen. White, semi-transparent areas are glaciers.

Fig. 2. Palaeogeographic reconstructions of the Boreal Realm and Svalbard in the Early Cretaceous. (a) Global reconstruction of the super-continent Pangaea at 130 Ma (modified from Deep Time Maps™, https://deeptimemaps.com), corresponding to the late Hauterivian (Gale *et al.* 2020). (b) Inset map of the northern hemisphere in (a) indicating how Svalbard formed part of widespread epeiric seas in the Boreal Realm with a relatively restricted connection to the southern Tethyan Realm. (c) Simplified configuration of Svalbard and adjacent Boreal basins during the earliest Cretaceous, including main structural elements. The reconstruction is based on Steel and Worsley (1984), Dypvik *et al.* (2002) and Torsvik *et al.* (2002), and modified from Grundvåg *et al.* (2017, 2019). The Viking Corridor between Greenland and Baltica most likely acted as the main conduit for exchange of waters between the Boreal and Tethyan realms in the Late Jurassic–Early Cretaceous (Vickers *et al.* 2022). BFZ, Billefjorden Fault Zone; KKL, Kong Karls Land; LFZ, Lomfjorden Fault Zone. (d) Simplified evolution of the Svalbard area during deposition of the Rurikfjellet Formation in the Valanginian–early Barremian, including the gross progradational nature of the depositional system, from open-marine ramp conditions of the Wimanfjellet Member, to deltaic and strandplain shoreface (i.e. non-deltaic) environments of the northern Bohemanneset and southern Fotografryggen members, respectively. The reconstruction is based on Grundvåg and Olaussen (2017), Grundvåg *et al.* (2017, 2019) and Jelby *et al.* (2020a).

Fig. 3. Stratigraphic summary chart of the Middle Jurassic–Lower Cretaceous Adventdalen Group on Spitsbergen, showing the gross relative lateral distribution, thickness, first- and second-order regressive–transgressive (R–T) sequences, and organic stable carbon-isotope ($\delta^{13}C_{org}$) stratigraphy of the succession in a NW–SE-oriented cross-section. The chart is compiled from Parker (1967), Steel and Worsley (1984), Dypvik *et al.* (1991a), Gjelberg and Steel (1995), Grundvåg and Olaussen (2017), Grundvåg *et al.* (2019), Koevoets *et al.* (2019a), Jelby *et al.* (2020a, b), Śliwińska *et al.* (2020), and Vickers *et al.* (2023), and annotated according to the lithostratigraphic nomenclature defined in this

study. Numerical ages, chronostratigraphy, continuous $\delta^{13}C$ stratigraphy and events, and sea-level curve are compiled from the Geological Time Scale 2020 (GTS2020) of Gale *et al.* (2020) and Hesselbo *et al.* (2020). CIE, carbon-isotope excursion; OAE, Oceanic Anoxic Event; SU, subaerial unconformity; VOICE, Volgian Isotopic Carbon Excursion.

Fig. 4. General stratigraphy of the Rurikfjellet Formation exemplified by the cored DH-5 well (northern Nordenskiöld Land; see Fig. 1c for location), including: chronostratigraphy, lithostratigraphy, third- and fourth-order regressive–transgressive sequences with maximum regressive (MRS) and maximum flooding (MFS) surfaces, petrophysical gamma-ray (GR) log, sedimentological log, ammonite and dinocyst biostratigraphy, and organic stable carbon-isotope ($\delta^{13}C_{org}$) and total organic carbon (TOC) curves (partly adopted from Jelby *et al.* 2020b and Śliwińska *et al.* 2020). The accompanying legend is also applicable to Figs 5, 6, 8, 9, 11, 12, 14, 15, 17, 18, 20 and 21. uH–lB, upper Hauterivian–lower Barremian.

Fig. 5. Stratigraphy of the Rurikfjellet Formation type section (Janusfjellet, northern Nordenskiöld Land; see Fig. 1c for location), including: chronostratigraphy, lithostratigraphy, third- to fifth-order regressive–transgressive sequences with maximum regressive (MRS) and maximum flooding (MFS) surfaces, sedimentological log, a new finding of an age-diagnostic ammonite, and Bioturbation Index of Taylor and Goldring (1993). uH–lB, upper Hauterivian–lower Barremian.

Fig. 6. Stratigraphy of the Rurikfjellet Formation reference sections (see Fig. 1b, c for locations), including: chronostratigraphy, lithostratigraphy, third- and fourth-order regressive–transgressive sequences with maximum regressive (MRS) and maximum flooding (MFS) surfaces, petrophysical gamma-ray (GR) logs, sedimentological logs, and Bioturbation Index of Taylor and Goldring (1993). (a) Festningen, north-western Nordenskiöld Land. (b) Keilhaufjellet, southern Sørkapp Land. (c) Cored well DH-1, northern Nordenskiöld Land. (d) Cored well DH-4, northern Nordenskiöld Land. uH–lB, upper Hauterivian–lower Barremian.

Fig. 7. Representative photographs of the Rurikfjellet Formation (see Fig. 1b, c for locations). (a) SW-oriented helicopter view of the name-giving Rurikfjellet mountain, southern Sabine Land. (b) Type section of the Rurikfjellet Formation at Janusfjellet, northern Nordenskiöld Land. Note the overall regressive development of the succession, with the mudstone-dominated Wimanfjellet Member coarsening upwards into the sandstone-rich Bohemanneset Member. (c) Detail of the Bohemanneset Member at Janusfjellet, indicating the third-order regressive–transgressive sequence development, superimposed by fourth-order high-frequency sequences or parasequences and fifth-order bed-sets (see Fig. 5 for an integrated stratigraphy and sedimentological log of the section). MRS, Maximum regressive surface. (d) S-oriented view from Fotografryggen in eastern Wedel Jarlsberg Land, showing the Rurikfjellet Formation and overlying Helvetiafjellet Formation at Polakkfjellet. Note the relatively thin sandstone unit of the Fotografryggen Member in the top of the Rurikfjellet Formation, immediately below the regional Barremian subaerial unconformity.

Fig. 8. Stratigraphy of the Wimanfjellet Member and Myklegardfjellet Bed type section (Myklegardfjellet, south-eastern Sabine Land; see Fig. 1b for location), including: chronostratigraphy, lithostratigraphy, third- and fourth-order regressive–transgressive sequences with maximum regressive (MRS) and maximum flooding (MFS) surfaces, sedimentological log, Bioturbation Index of Taylor and Goldring (1993), ammonite and dinocyst biostratigraphy, and organic stable carbon-isotope ($\delta^{13}C_{org}$) and total organic carbon (TOC) curves (partly adopted from Jelby *et al.* 2020b and Śliwińska *et al.* 2020). uH–lB, upper Hauterivian–lower Barremian.

Fig. 9. Stratigraphy of the Wimanfjellet Member reference sections (see Fig. 1b for locations), including: chronostratigraphy, lithostratigraphy, third- and fourth-order regressive–transgressive sequences with maximum regressive (MRS) and maximum flooding (MFS) surfaces, sedimentological logs, and Bioturbation Index of Taylor and Goldring (1993). (a) Oppdalssåta, southern Sabine Land. uH–lB, upper Hauterivian–lower Barremian. (b) Baronfjella, south-eastern Heer Land.

Fig. 10. Representative photographs of the Wimanfjellet Member (see Fig. 1b for locations, and Figs 9 & 10 for integrated stratigraphies and sedimentological logs). (a) Reference section of the Wimanfjellet Member at Baronfjella, south-eastern Heer Land. The member is dominated by dark mudstones intersected by numerous siderite concretions (strata-bound bands in the photograph). (b) Detail of the basal part of the Baronfjella section at terrain (beach) level, exposing homogenous, relatively fissile mudstone intersected by a strata-bound siderite band (rifle for scale in lower left corner of photograph). (c) Exposure of the Myklegardfjellet Bed type section at Myklegardfjellet, south-eastern Sabine Land. Note the relatively marked facies transition between the dark-grey mudstones of the Agardhfjellet Formation below and the green to yellow and rust-coloured clay of the Myklegardfjellet Bed. (d) Conspicuous boundary between the gently sloping, black mudstones of the Wimanfjellet Member and cliff-forming yellow sandstones of the Louiseberget Bed of the Festningen Member at Ullaberget, southern Nathorst Land.

Fig. 11. Stratigraphy of the Adventpynten Member type section (cored well DH-1, northern Nordenskiöld Land; see Fig. 1c for location), including: chronostratigraphy, lithostratigraphy, third- and fourth-order regressive–transgressive sequences with maximum regressive (MRS) and maximum flooding (MFS) surfaces, petrophysical gamma-ray (GR) log, sedimentological log, and dinocyst biostratigraphy (partly adopted from Grundvåg *et al.* 2019 and Śliwińska *et al.* 2020).

Fig. 12. Stratigraphy of the Adventpynten Member reference section (cored well DH-2, northern Nordenskiöld Land; see Fig. 1c for location), including: chronostratigraphy, lithostratigraphy, third- and fourth-order regressive–transgressive sequences with maximum regressive (MRS) and maximum flooding (MFS) surfaces, petrophysical gamma-ray (GR) log, sedimentological log, and dinocyst biostratigraphy (partly adopted from Grundvåg *et al.* 2019 and Śliwińska *et al.* 2020).

Fig. 13. Representative photographs of the Adventpynten Member (see Fig. 1c for locations, and Figs 11 & 12 for integrated stratigraphies and sedimentological logs). (a) S-oriented view of the only known outcrop of the member, located in the north-eastern part of Forkastningsfjellet, displaying a markedly wedge-shaped architecture of diamictites. Note that the indicated faults are related to present-day slope failures typical for this site (Kuhn *et al.* 2019). (b) Coarse-tail graded, sandy mudstone diamictites overlain by a soft-sediment-deformed sandstone division (DH-1 well core, *c.* 377 m depth). (c) Poorly sorted, sandy mudstone diamictites, with a large rafted intra-clast of

bioturbated mudstone in the basal part (DH-2 well core, *c.* 325 m depth). (d) Folded and faulted heterolithic division (DH-1 well core, *c.* 344 m depth).

Fig. 14. Stratigraphy of the Bohemanneset Member type section (Bohemanneset, south-eastern Oscar II Land; see Fig. 1b for location), including: chronostratigraphy, lithostratigraphy, third- to fourth-order regressive–transgressive sequences with maximum regressive (MRS) and maximum flooding (MFS) surfaces, sedimentological log, Bioturbation Index of Taylor and Goldring (1993), and dinocyst biostratigraphy (partly adopted from Jelby *et al.* 2020a, b and Śliwińska *et al.* 2020). Note the rich assemblage of the belemnite *Arctoteuthis bluethgeni* in the basal part of the succession (see Alsen *et al.* 2020).

Fig. 15. Stratigraphy of the Bohemanneset Member reference sections (see Fig. 1b, c for locations), including: chronostratigraphy, lithostratigraphy, third- to sixth-order regressive–transgressive sequences with maximum regressive (MRS) and maximum flooding (MFS) surfaces, sedimentological logs, and Bioturbation Index of Taylor and Goldring (1993). (a) Festningen, north-western Nordenskiöld Land. (b) Cored well DH-4, northern Nordenskiöld Land. (c) Forkastningsfjellet, northern Nordenskiöld Land. (d) Mälardalen, northern Nordenskiöld Land.

Fig. 16. Representative photographs of the Bohemanneset Member (see Fig. 1b, c for locations, and Figs 14 & 15 for integrated stratigraphies and sedimentological logs). (a) The typical regressive–transgressive sequence stacking of the member exposed at Ramfjellet, south-eastern Oscar II Land. (b) Large-scale HCS sandstone bed (i.e. tempestite) intersecting dark-grey, lenticular mudstone in the uppermost parasequence of the member at Bohemanneset, south-eastern Oscar II Land (rifle for scale). (c) Typical facies expression of interbedded HCS sandstone beds (i.e. tempestites) and bioturbated mudstone beds (i.e. fair-weather deposits) at Bohemanneset. (d) Detail of intercalated HCS sandstone beds and lenticular mudstone in the uppermost parasequence of the member at Bohemanneset. (e) Transgressive third-order sequence development demarcated by a retrogradational stacking of fourth-order parasequences in Mälardalen, northern Nordenskiöld Land. Person (encircled) for scale. (f) Regressive–transgressive stacking of frequently interbedded HCS sandstone beds (i.e. tempestites) and bioturbated mudstone beds (i.e. fair-weather deposits) at Romnæstoppen, western Nordenskiöld Land. (g) Typical trace-fossil assemblage of the *Rosselia* Ichnofacies (MacEachern and Bann 2020, 2023), including *Rosselia* (*Ro*) that vertically penetrates through a HCS sandstone bed (i.e. tempestite) and an underlying mudstone bed (i.e. fair-weather deposit) with *Chondrites* (*Ch*) and *Phycosiphon* (*Py*), and displaying an internal biomottling representing exploitation of the shaft by *Asterosoma* (*As*), *Helminthopsis* (*He*), *Nereites missouriensis* (*Ne*) and partly *Planolites* (*Pl*) (DH-4 well core, *c.* 204 m depth). (h) Glendonite in a sandy mudstone matrix at Janusfjellet. MRS, Maximum regressive surface.

Fig. 17. Stratigraphy of the Fotografryggen Member type section (Keilhaufjellet, southern Sørkapp Land; see Fig. 1b for location), including: chronostratigraphy, lithostratigraphy, third- to sixth-order regressive–transgressive sequences with maximum regressive (MRS) and flooding (FS) surfaces, sedimentological log, Bioturbation Index of Taylor and Goldring (1993), and indication of depositional sub-environments (partly adopted from Grundvåg and Olaussen 2017). uH–lB, upper Hauterivian–lower Barremian.

Fig. 18. Stratigraphy of the Fotografryggen Member reference sections (see Fig. 1b for locations), including: chronostratigraphy, lithostratigraphy, third- and fourth-order regressive–transgressive sequences with maximum regressive surfaces (MRS), sedimentological logs, and Bioturbation Index of Taylor and Goldring (1993). (a) Strykejernet, southernmost Wedel Jarlsberg Land (log is modified from Mørk 1978). uH–lB, upper Hauterivian–lower Barremian. (b) Fotografryggen, eastern Wedel Jarlsberg Land.

Fig. 19. Representative photographs of the Fotografryggen Member (see Fig. 1b for locations, and Figs 17 & 18 for integrated stratigraphies and sedimentological logs). (a) Overview of the type section at Keilhaufjellet, southern Sørkapp Land. (b) Detail of the progradationally stacked, coarsening-upwards, thickening-upwards sandstone-dominated parasequences at Keilhaufjellet, which are capped by a transgressive unit of mudstone immediately below the regional unconformity at the base of the Festningen Member of the Helvetiafjellet Formation. MRS, Maximum regressive surface. (c) Bioturbated 'pipe-rock' with abundant *Skolithos* (*Sk*) penetrating trough cross-stratified sandstone at Keilhaufjellet. (d) N-oriented view of the Fotografryggen Member at Fotografryggen, eastern Wedel Jarlsberg Land, with the three northernmost sections of the member seen in the distance (i.e. Skiferkammen, Einvola and Langryggsåta). (e) Trough cross-bedded sandstone, representing a lower shoreface depositional environment, in the top of the Fotografryggen Member at Fotografryggen immediately below the Festningen Member of the Helvetiafellet Formation. (f) Bioturbated sandstone and lenticular mudstone intersected by an amalgamated hummocky cross-stratified (HCS) sandstone bed, representing an upper offshore transition zone depositional environment, in the lower part of the Fotografryggen Member at Fotografryggen.

Fig. 20. Regional sequence stratigraphic correlations of the Rurikfjellet Formation. (a) Map showing the correlation transects through selected sites (see Fig. 1 for a map legend). (b) N–S-oriented correlation flattened on the upper maximum regressive surface (MRS) as correlation datum, showing the gross and markedly different stratigraphic architectures of the Adventpynten, Bohemanneset and Fotografryggen members, and how the latter two are inferred to pinch out in a, respectively, southwards direction north of Nathorst Land, and in a northwards direction between Langryggsåta and Zillerberget in eastern Wedel Jarlsberg Land (Strykejernet and Louiseberget logs are modified from Mørk 1978 and Grundvåg *et al.* 2017, respectively). (c) W–E-oriented correlation, showing the regressive–transgressive (i.e. progradational–retrogradational) stacking of the third-order sequences and fourth-order high-frequency sequences and parasequences in the Bohemanneset Member. Section abbreviations refer to: Bo, Bohemanneset; Fe, Festningen; For, Forkastningsfjellet; Fot, Fotografryggen; Ja, Janusfjellet; Ke, Keilhaufjellet; La, Langryggsåta; Lo, Louiseberget; Mä, Mälardalen; My, Myklegardfjellet; Op, Oppdalssåta; Ro, Romnæstoppen; St, Strykejernet; Zi, Zillerberget. FS, Flooding surface; uH–lB, upper Hauterivian–lower Barremian.

Fig. 21. Correlation of organic stable carbon-isotope ($\delta^{13}C_{org}$) stratigraphy between the cored wells DH-2, DH-5 and DH-6 and the Myklegardfjellet outcrop section (see Fig. 1b, c for locations), calibrated by total organic carbon (TOC) trends, and dinocyst and ammonite biostratigraphy (modified from Jelby *et al.* 2020b). The boundary between the Agardhfjellet and Rurikfjellet formations (conforming to a base-Valanginian unconformity and demarcated by a marked drop in TOC values) is used as correlation datum. Note the clear expression of the Weissert Event and 'Volgian Isotopic Carbon Excursion' (VOICE) in the different sections. uH–lB, upper Hauterivian–lower Barremian.

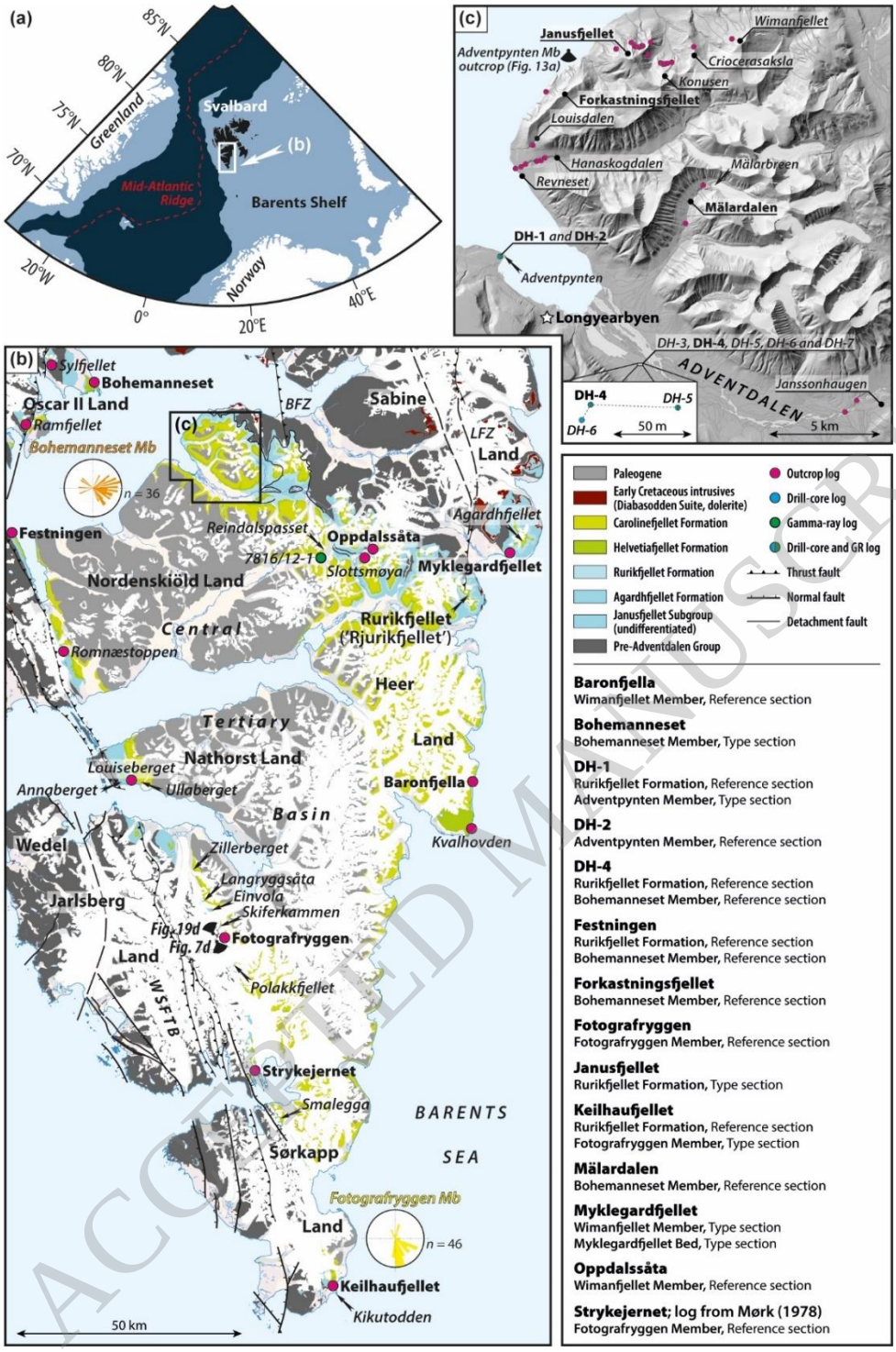

Figure 1

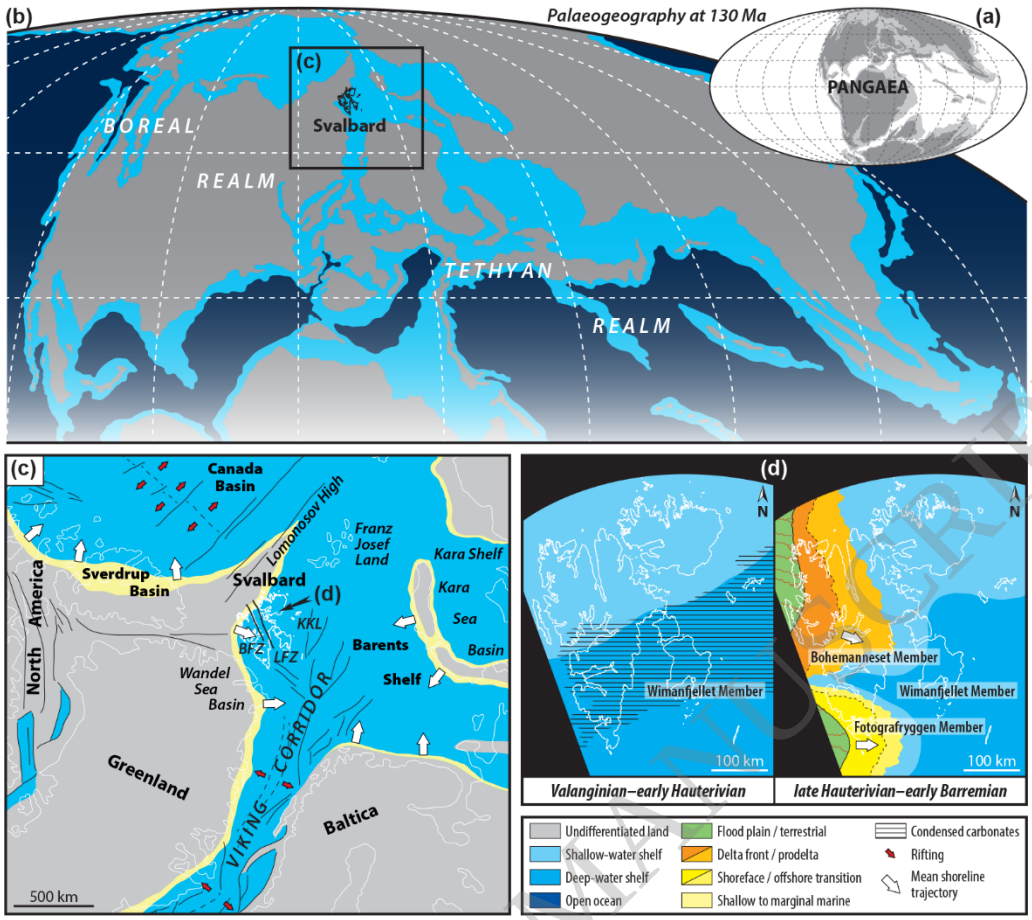

Figure 2

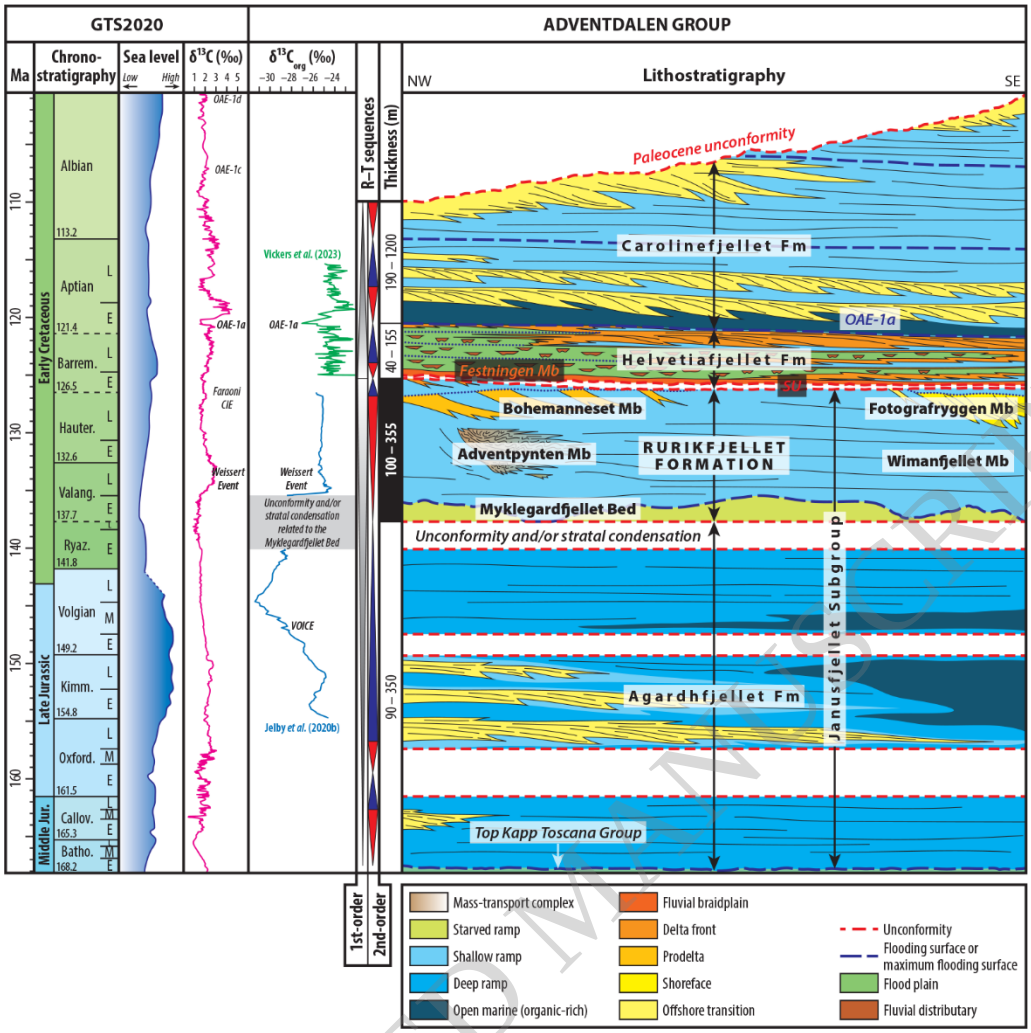

Figure 3

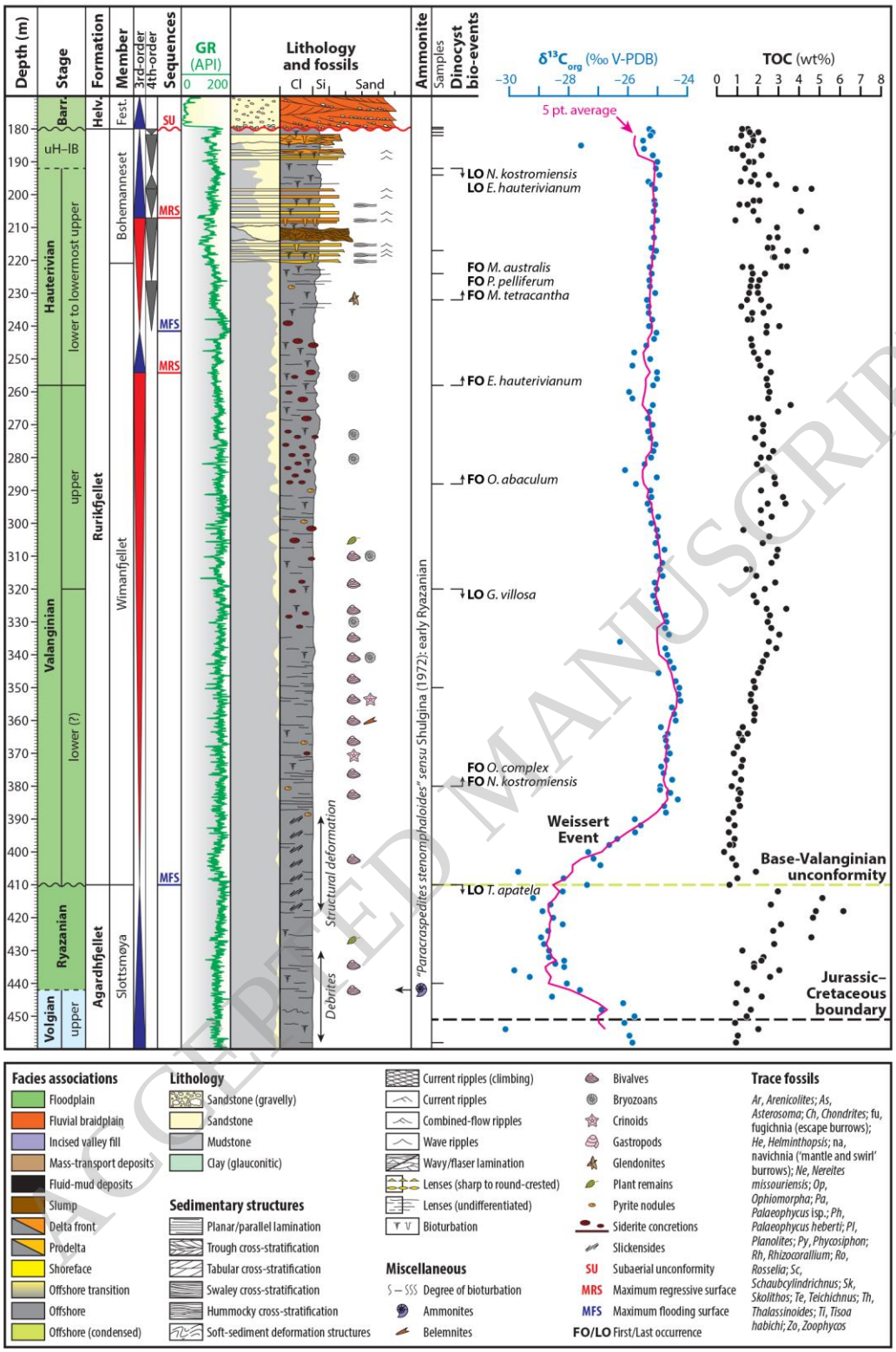

Figure 4

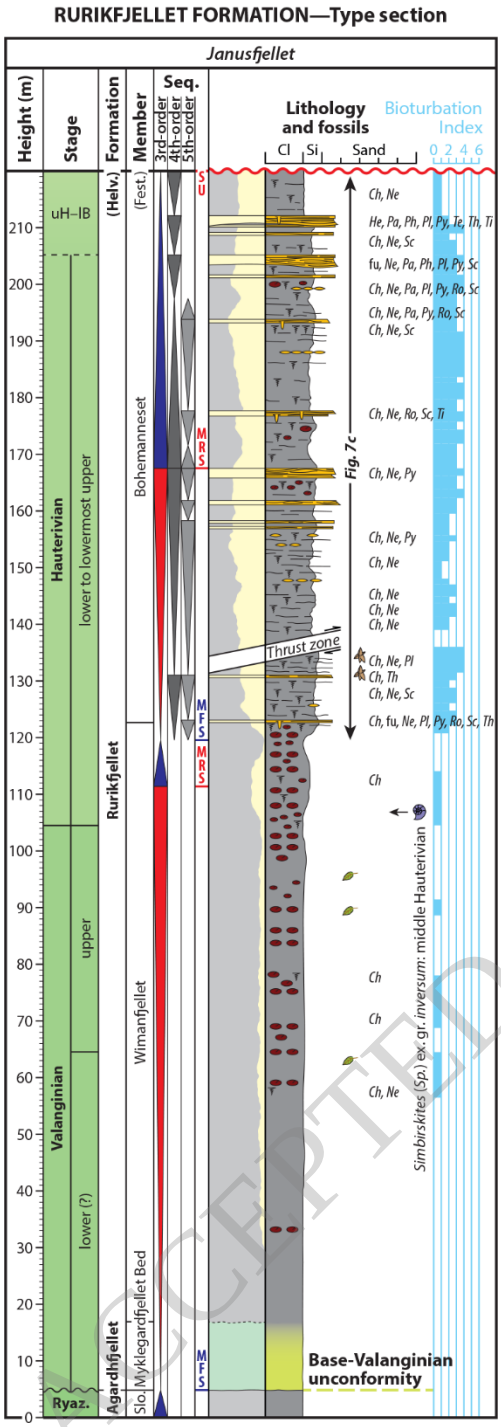

Figure 5

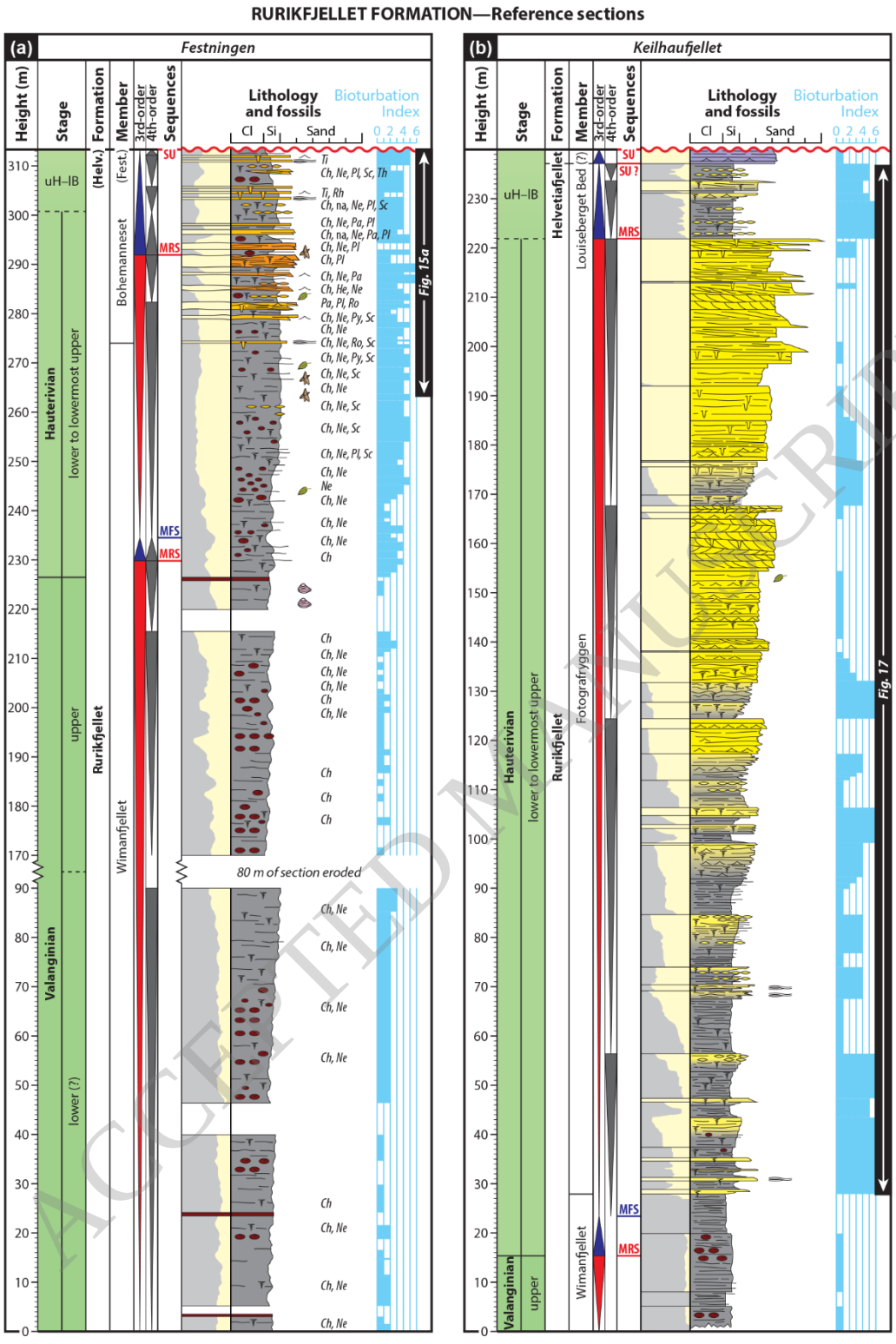

Figure 6 a,b

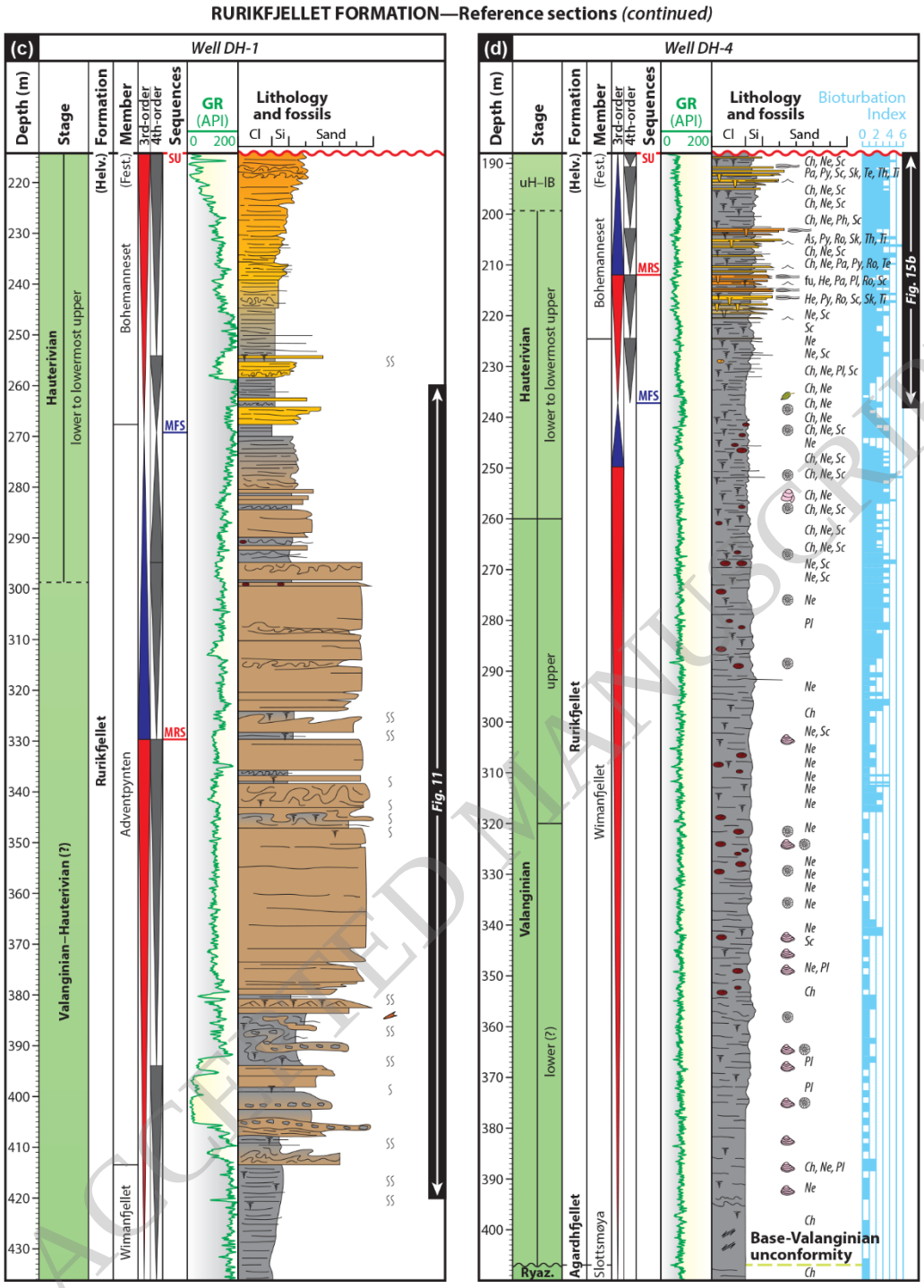

Figure 6 c,d

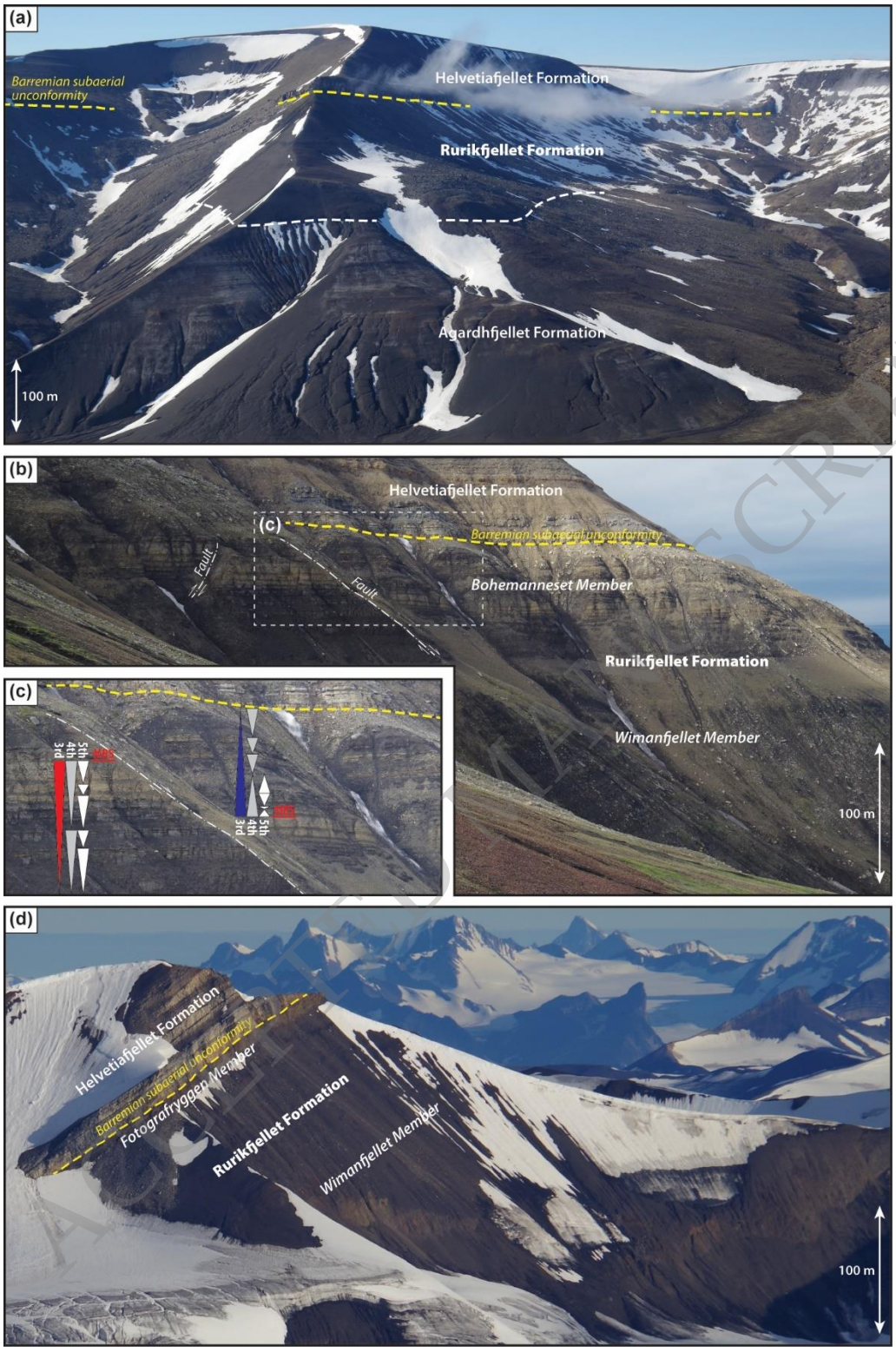
(a)
Barremian subaerial unconformity
Helvetiafjellet Formation
Rurikfjellet Formation
Agardhfjellet Formation
100 m
(b)
Helvetiafjellet Formation
(c)
Barremian subaerial unconformity
Fault
Fault
Bohemanneset Member
Rurikfjellet Formation
Wimanfjellet Member
100 m
(c)
3rd
4th
5th
3rd
4th
5th
(d)
Helvetiafjellet Formation
Barremian subaerial unconformity
Fotografryggen Member
Rurikfjellet Formation
Wimanfjellet Member
100 m

Figure 7

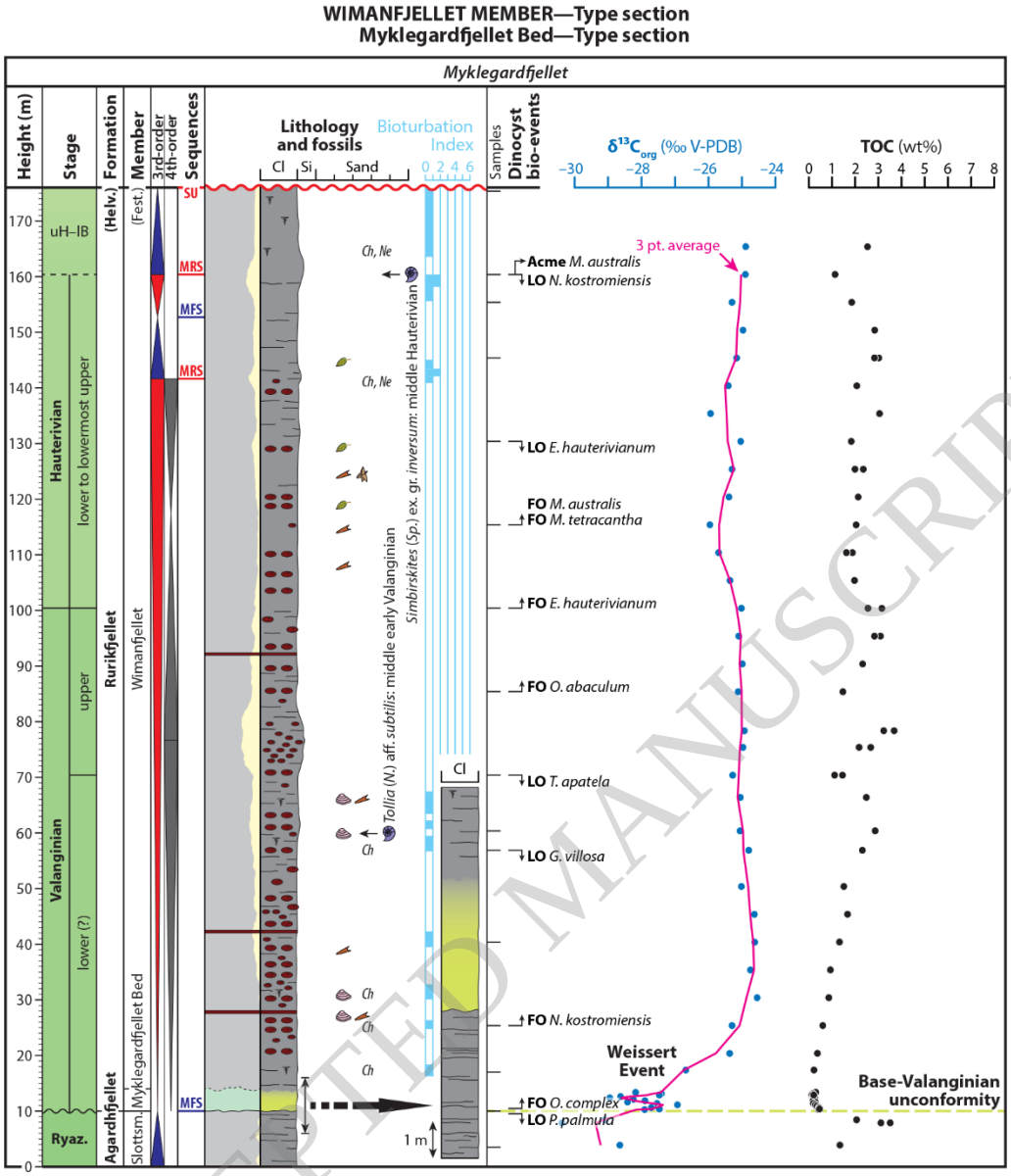

Figure 8

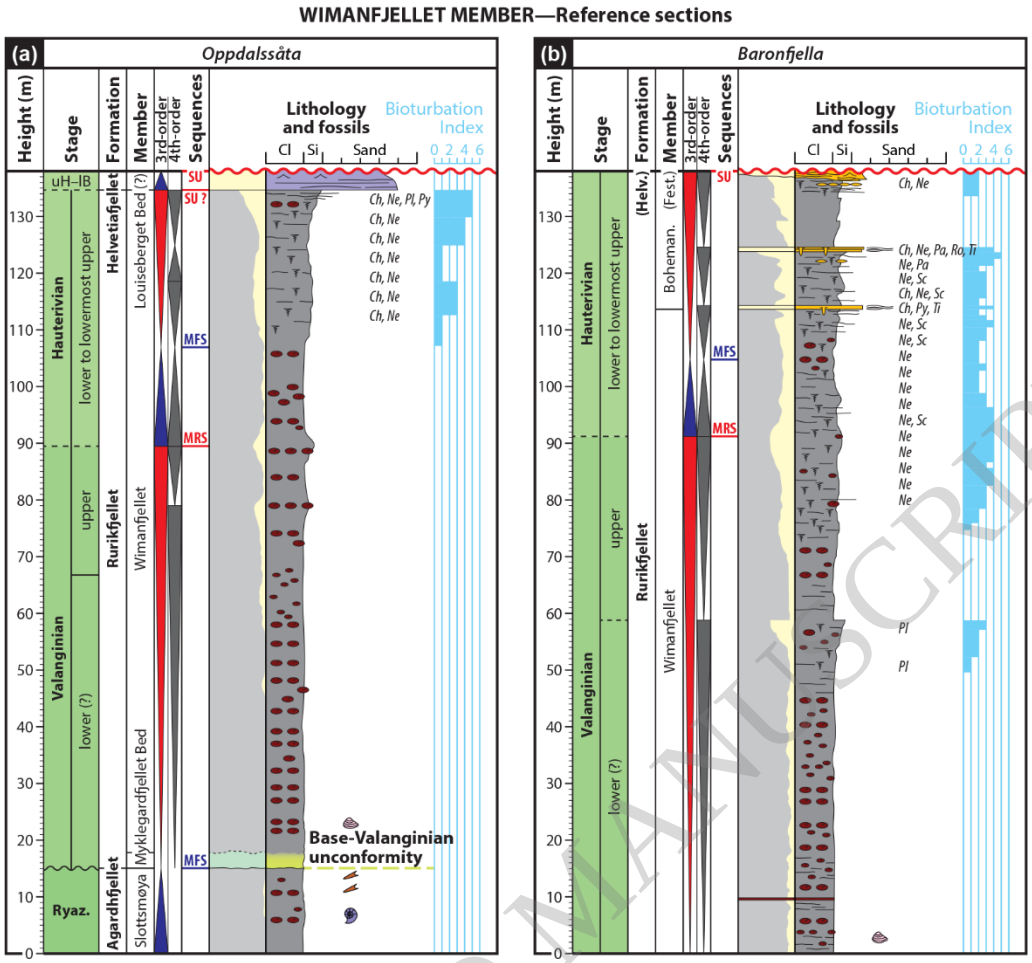

Figure 9

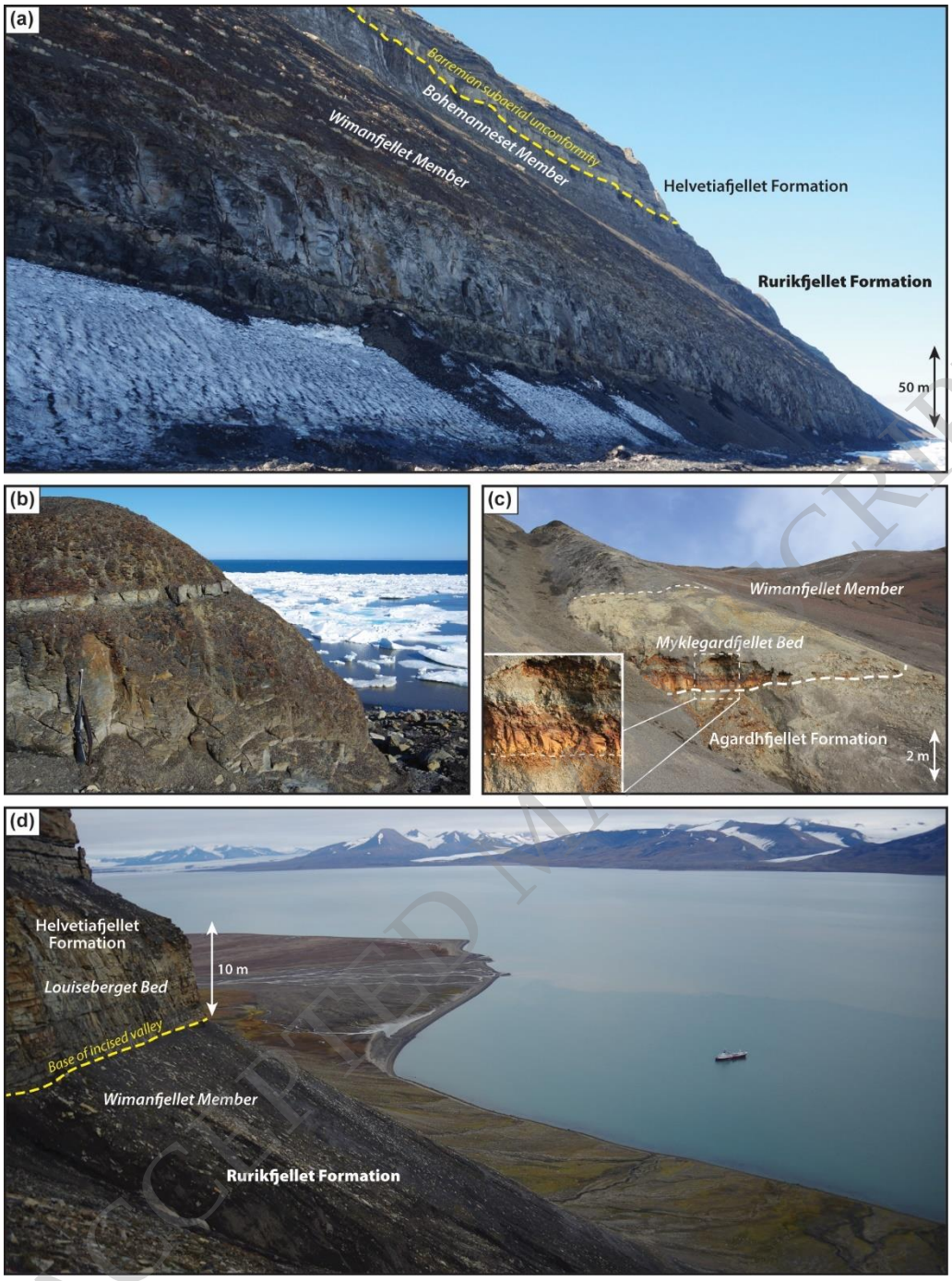

Figure 10

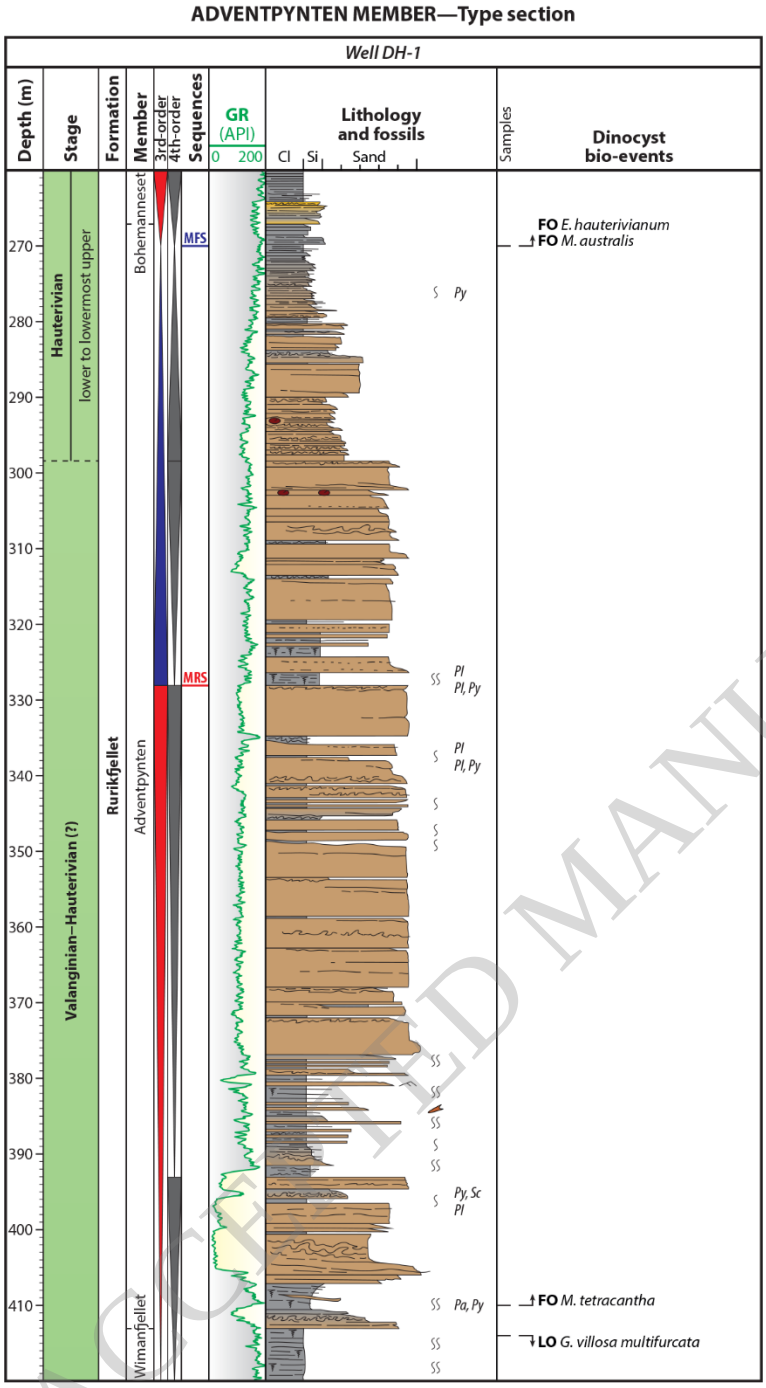

Figure 11

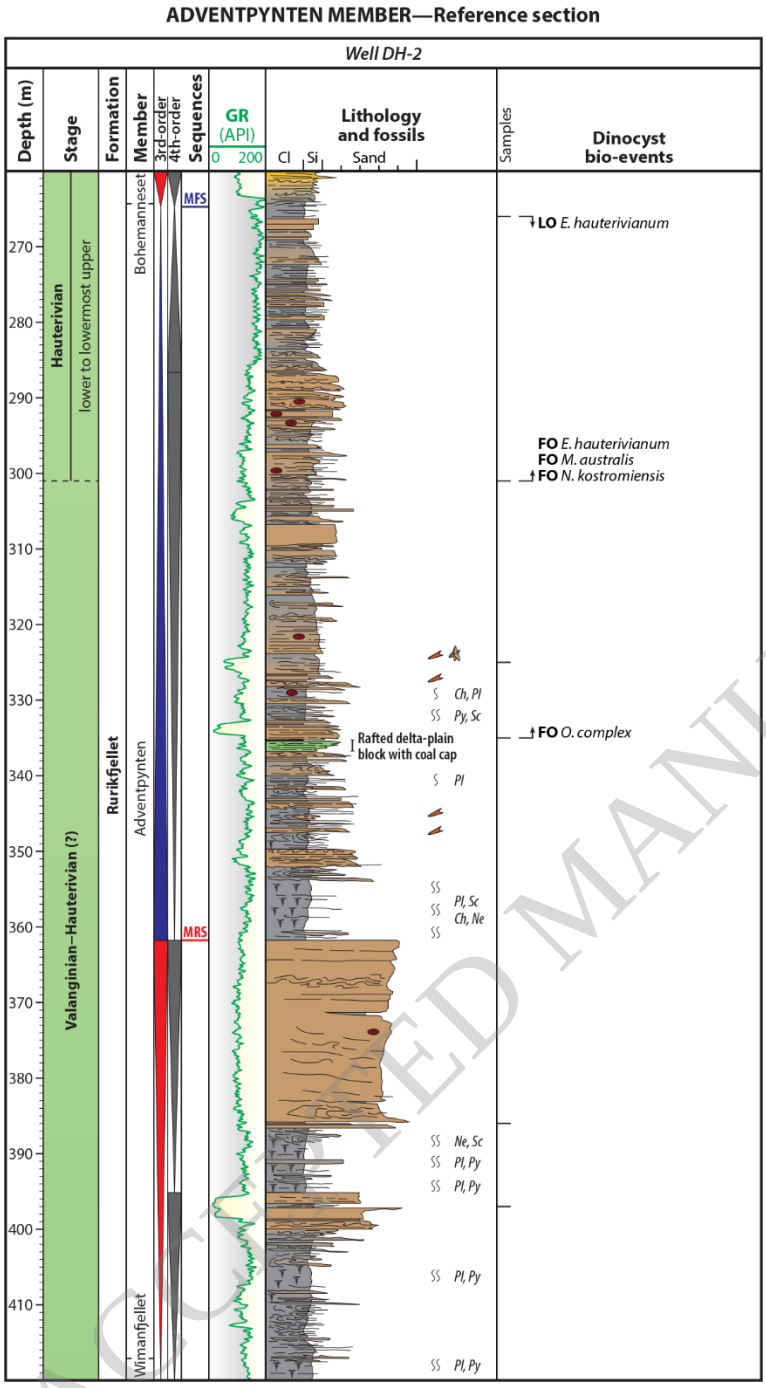

Figure 12

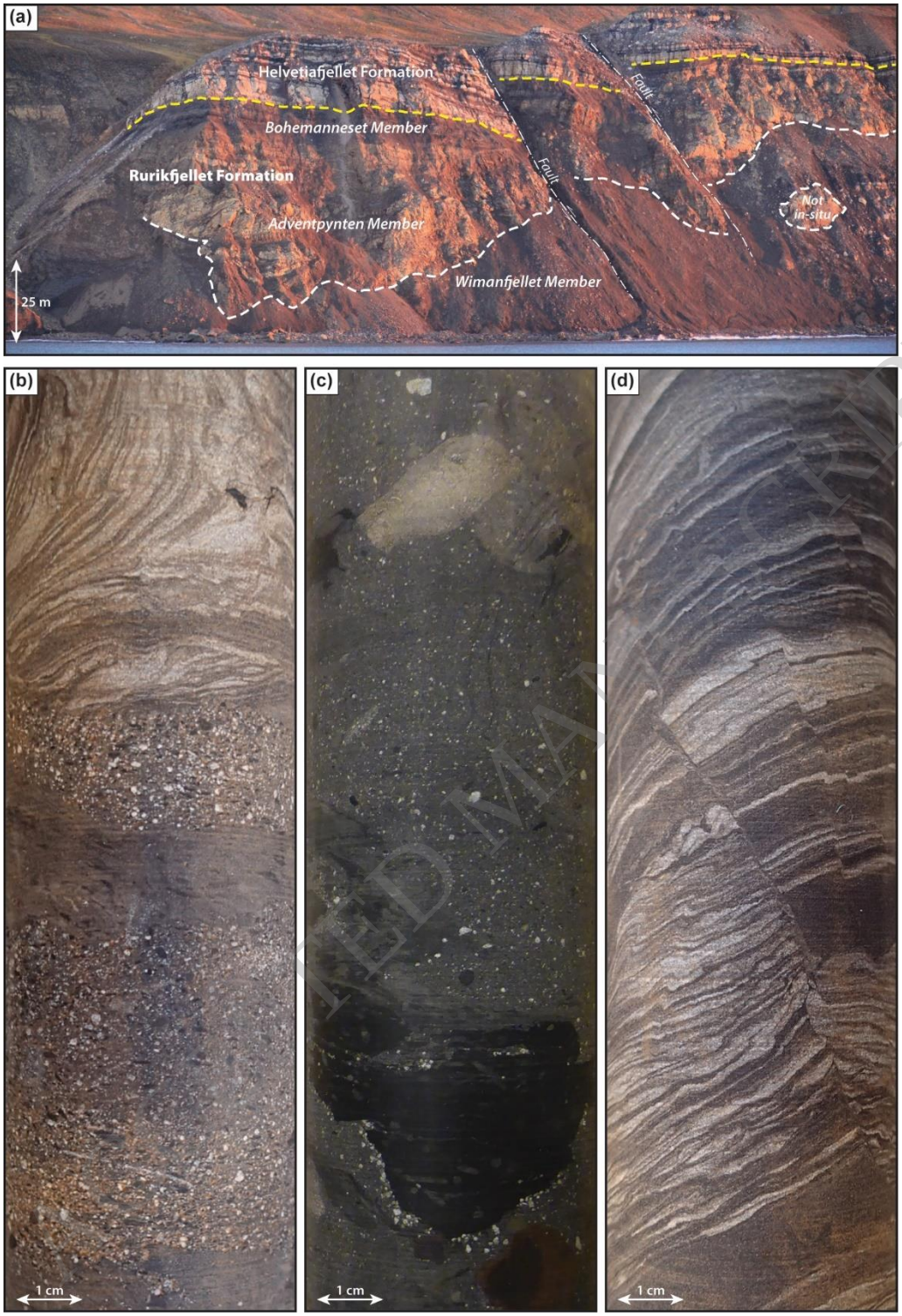

Figure 13

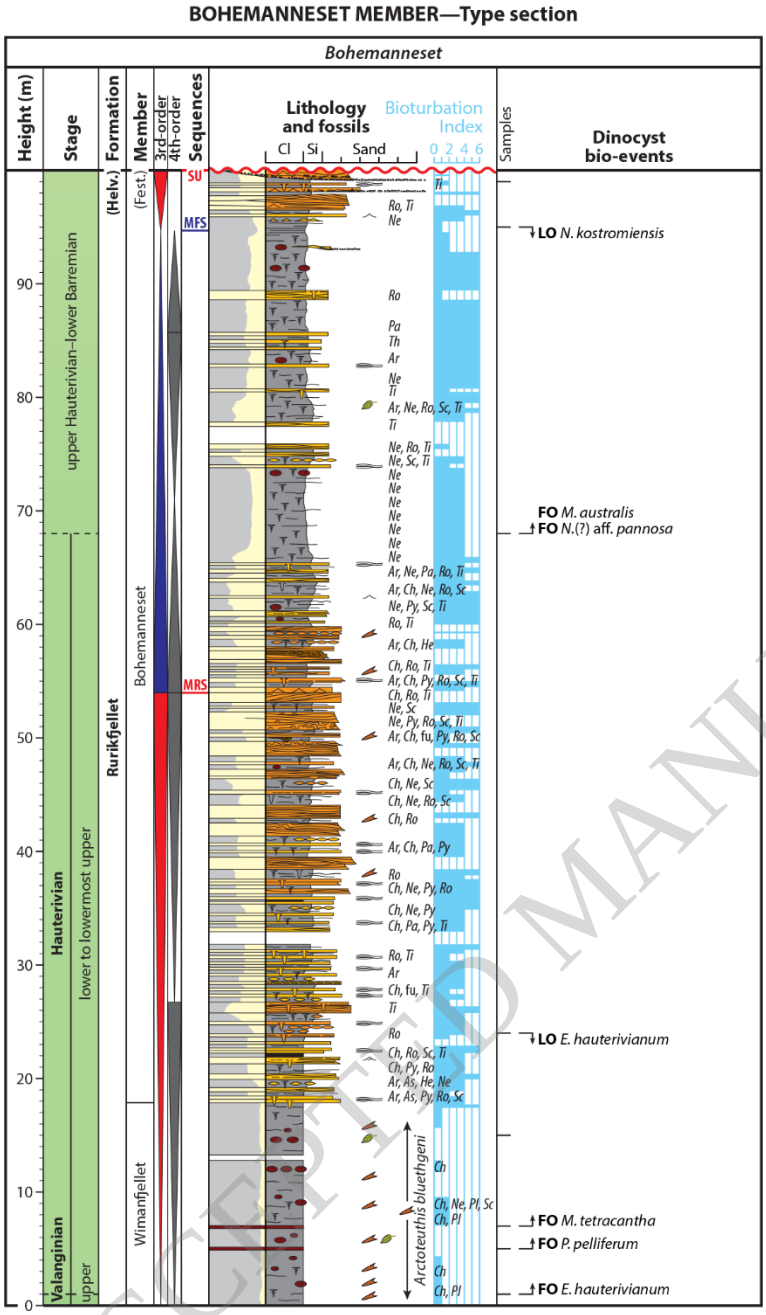

Figure 14

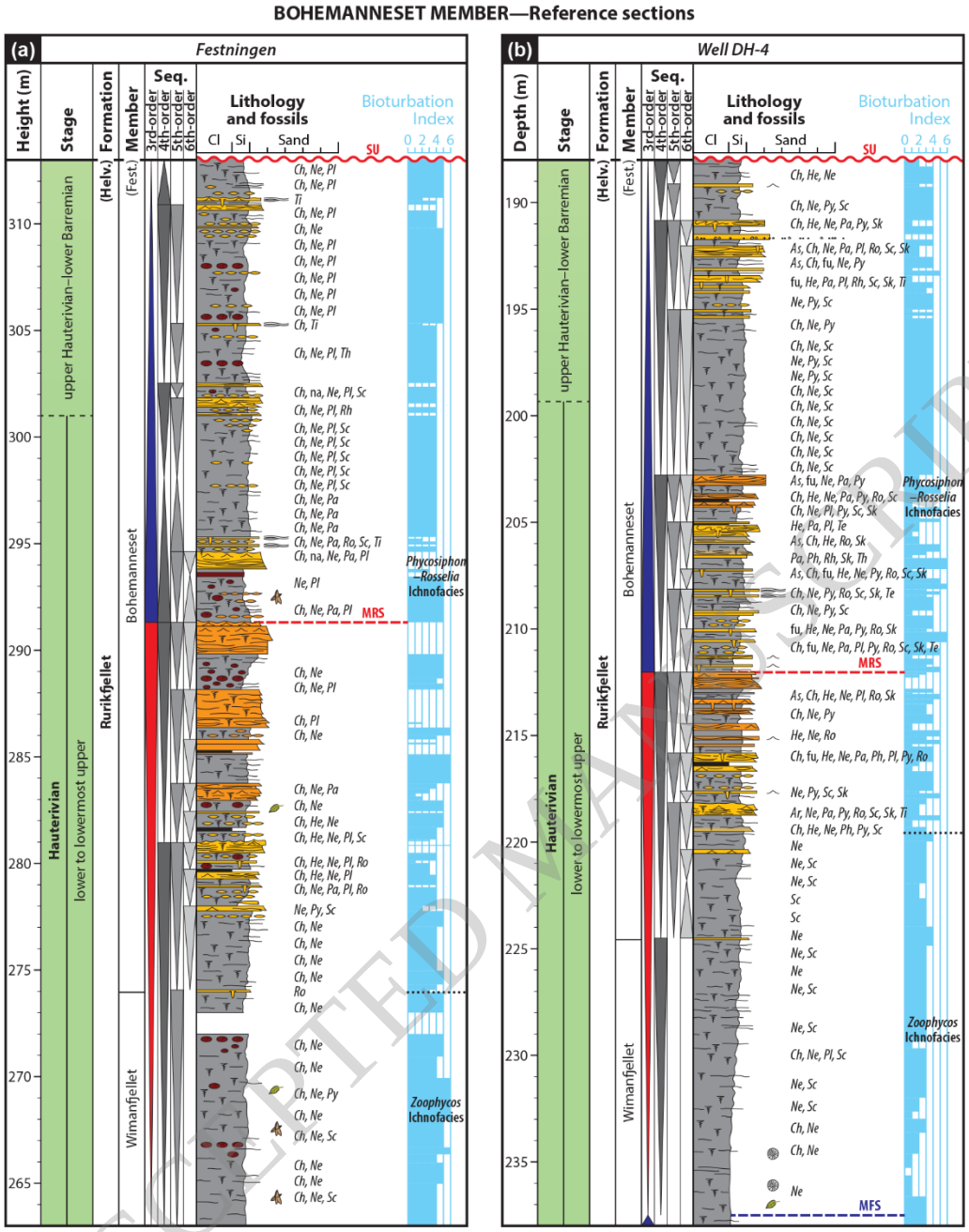

Figure 15 a,b

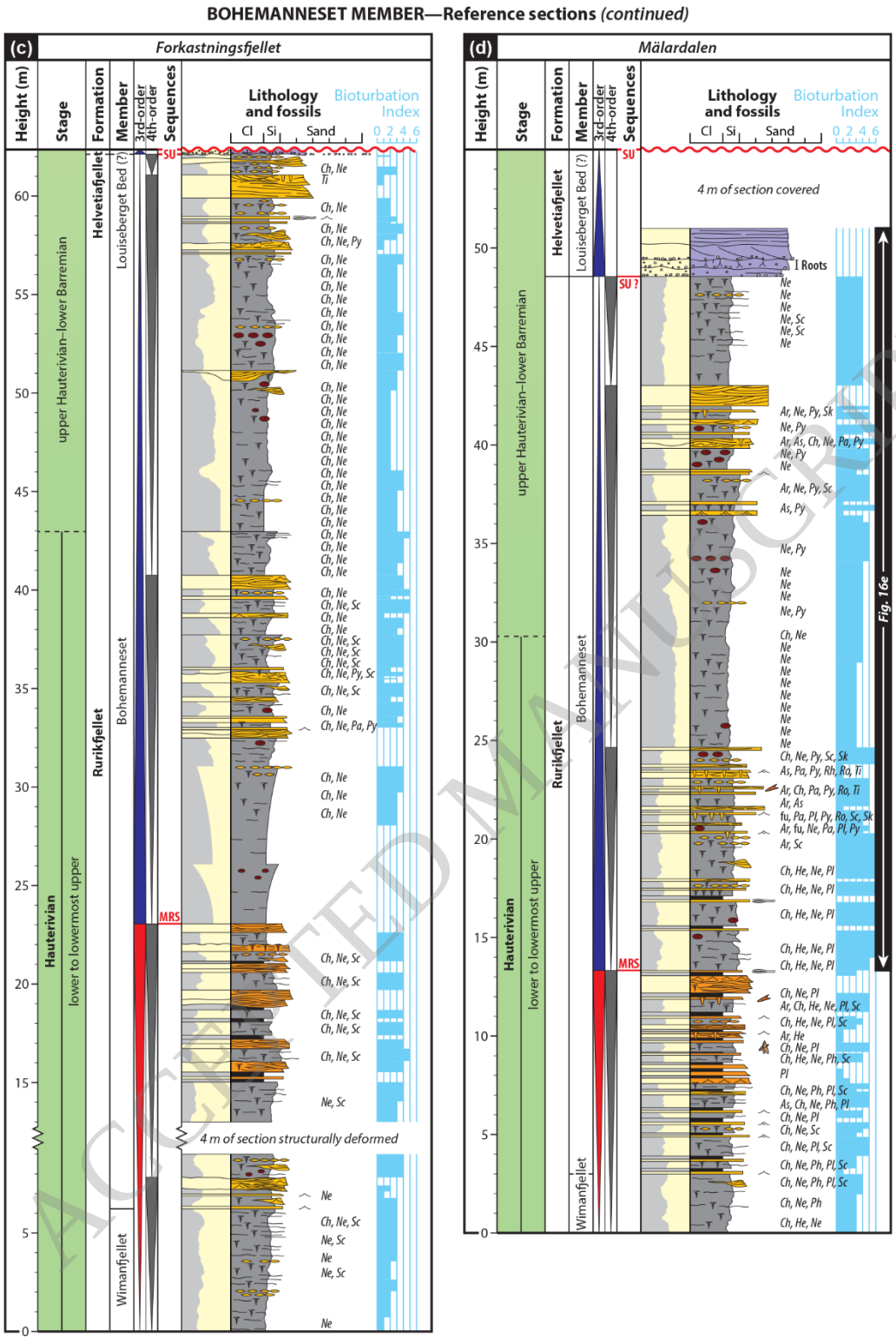

Figure 15 c,d

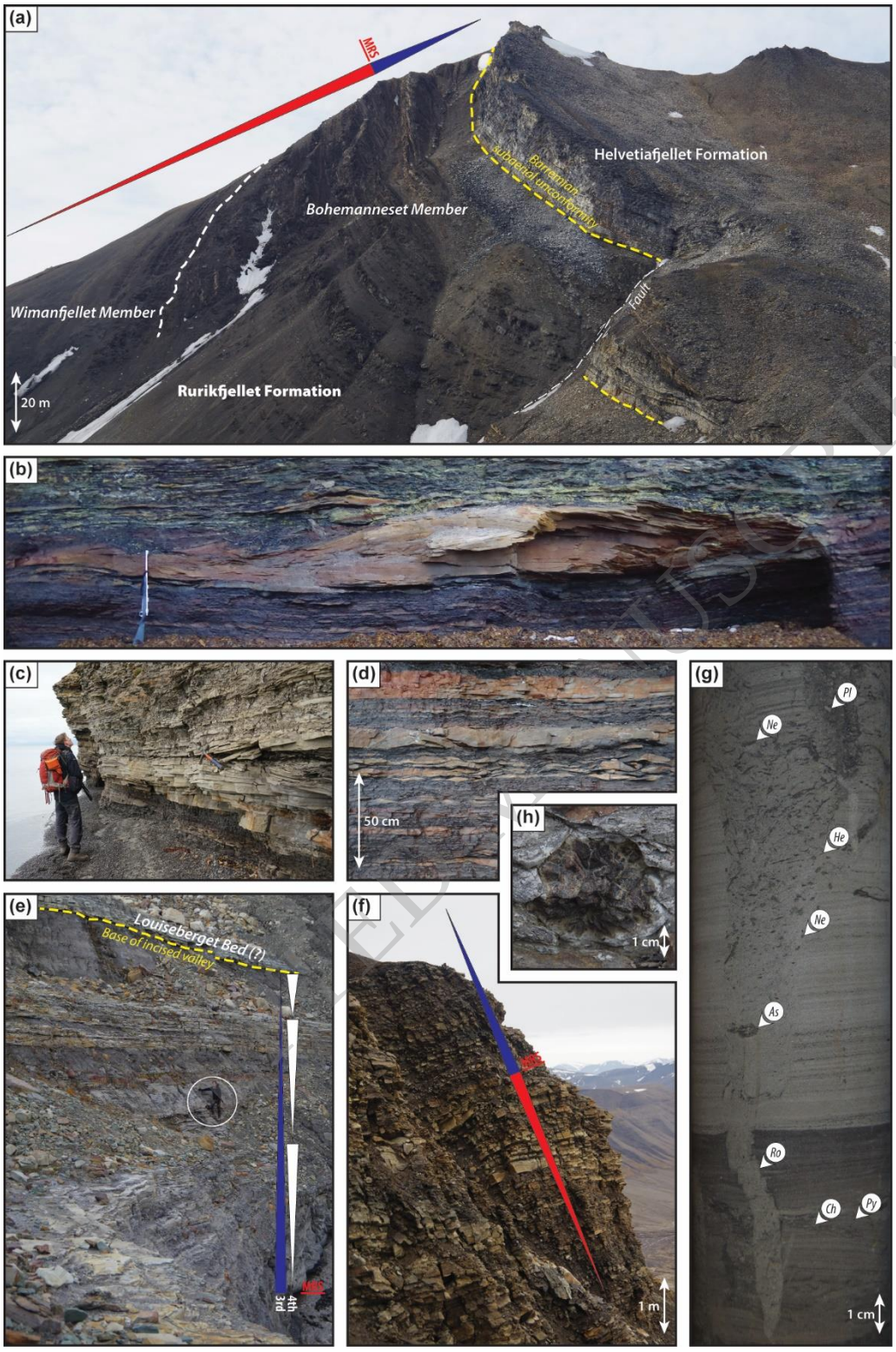
(a)
MRS
Helvetiafjellet Formation
Barremian subaerial unconformity
Bohemanneset Member
Fault
Wimanfjellet Member
20 m
Rurikfjellet Formation
(b)
(c)
(d)
50 cm
(h)
1 cm
(g)
Pl
Ne
He
Ne
As
Ro
Ch
Py
1 cm
(e)
Louiseberget Bed (?)
Base of incised valley
MRS
4th
3rd
(f)
MRS
1 m

Figure 16

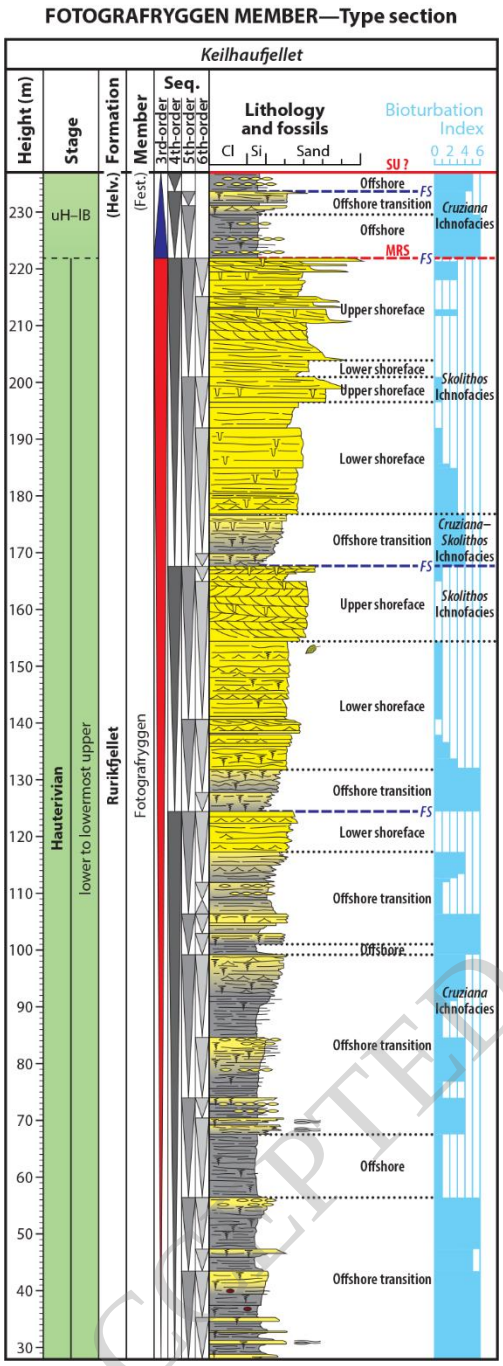

Figure 17

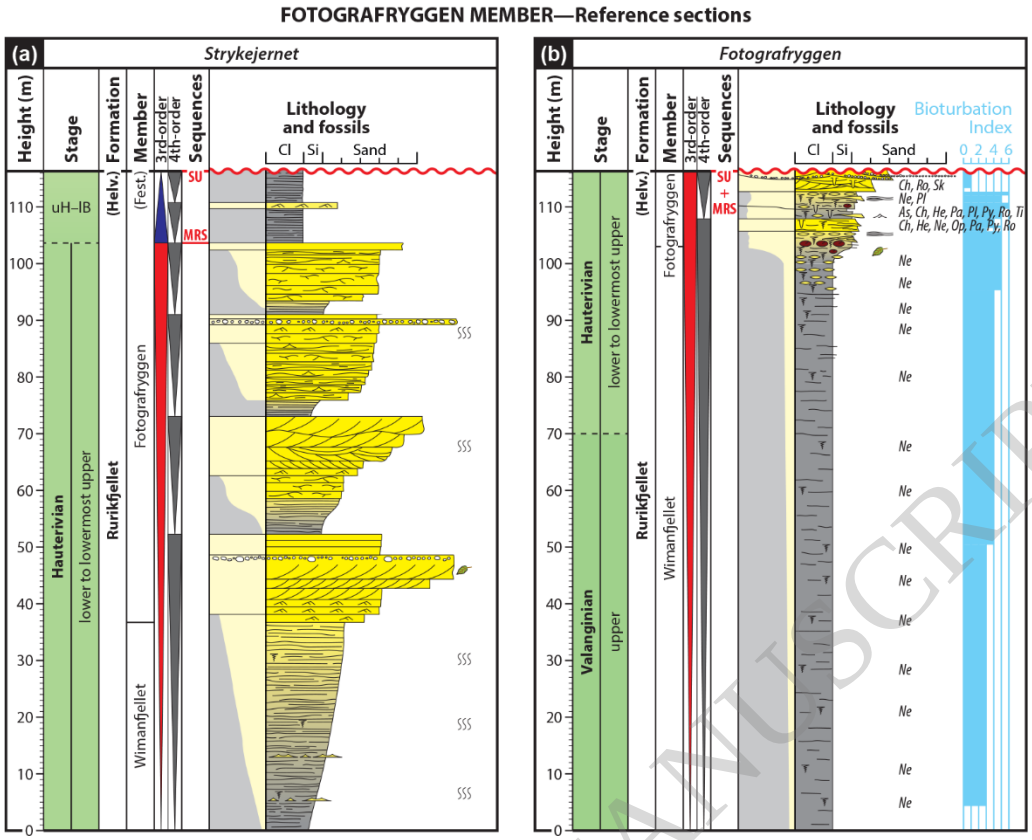

Figure 18

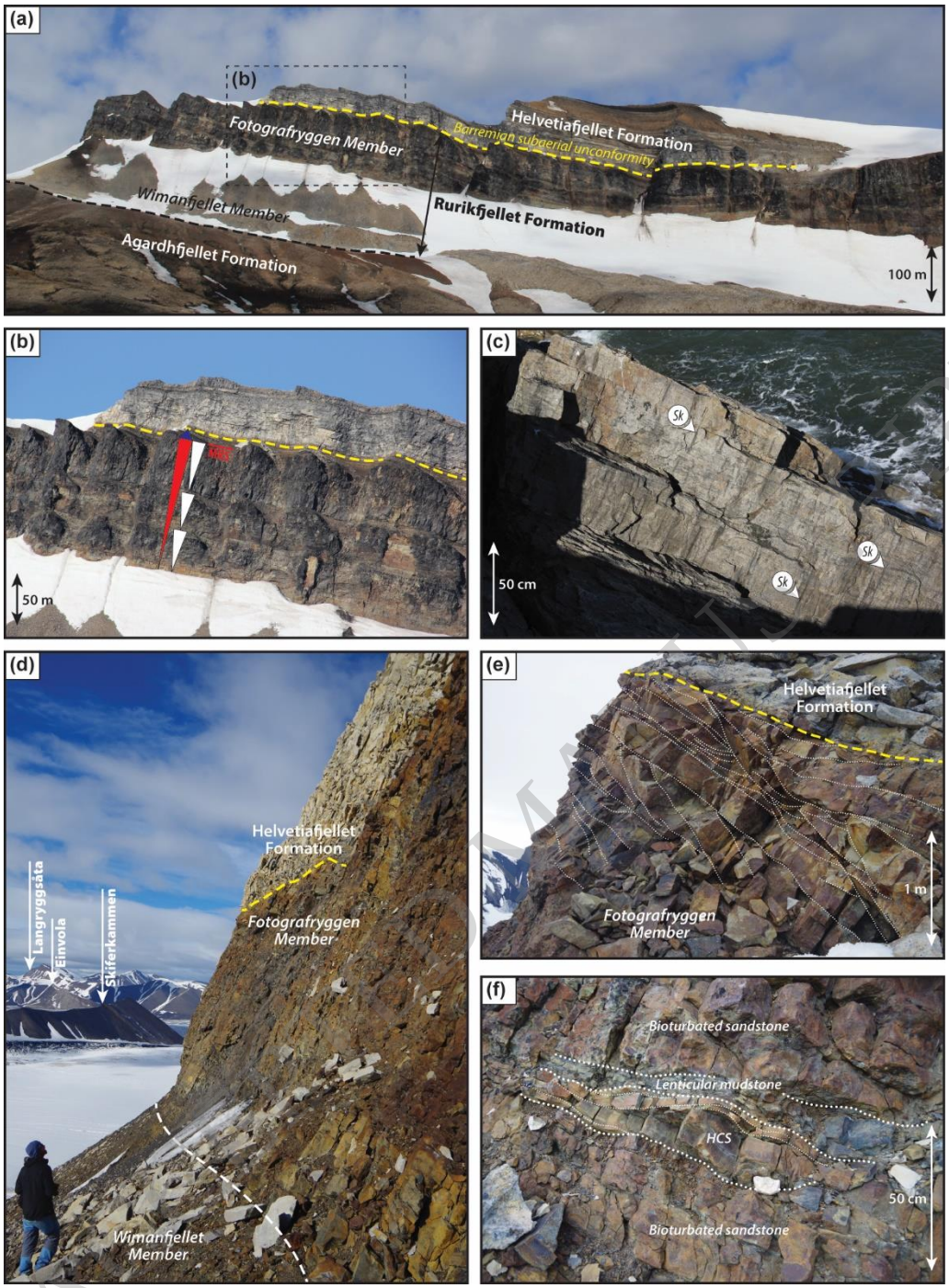
(a)
(b)
Fotografryggen Member
Barremian subaerial unconformity
Helvetiafjellet Formation
Wimanfjellet Member
Rurikfjellet Formation
Agardhfjellet Formation
100 m
(b)
MBF
50 m
(c)
Sk
Sk
Sk
50 cm
(d)
Helvetiafjellet Formation
Langryggsåta
Einvola
Skiferkammen
Fotografryggen Member
Wimanfjellet Member
(e)
Helvetiafjellet Formation
1 m
Fotografryggen Member
(f)
Bioturbated sandstone
Lenticular mudstone
HCS
50 cm
Bioturbated sandstone

Figure 19

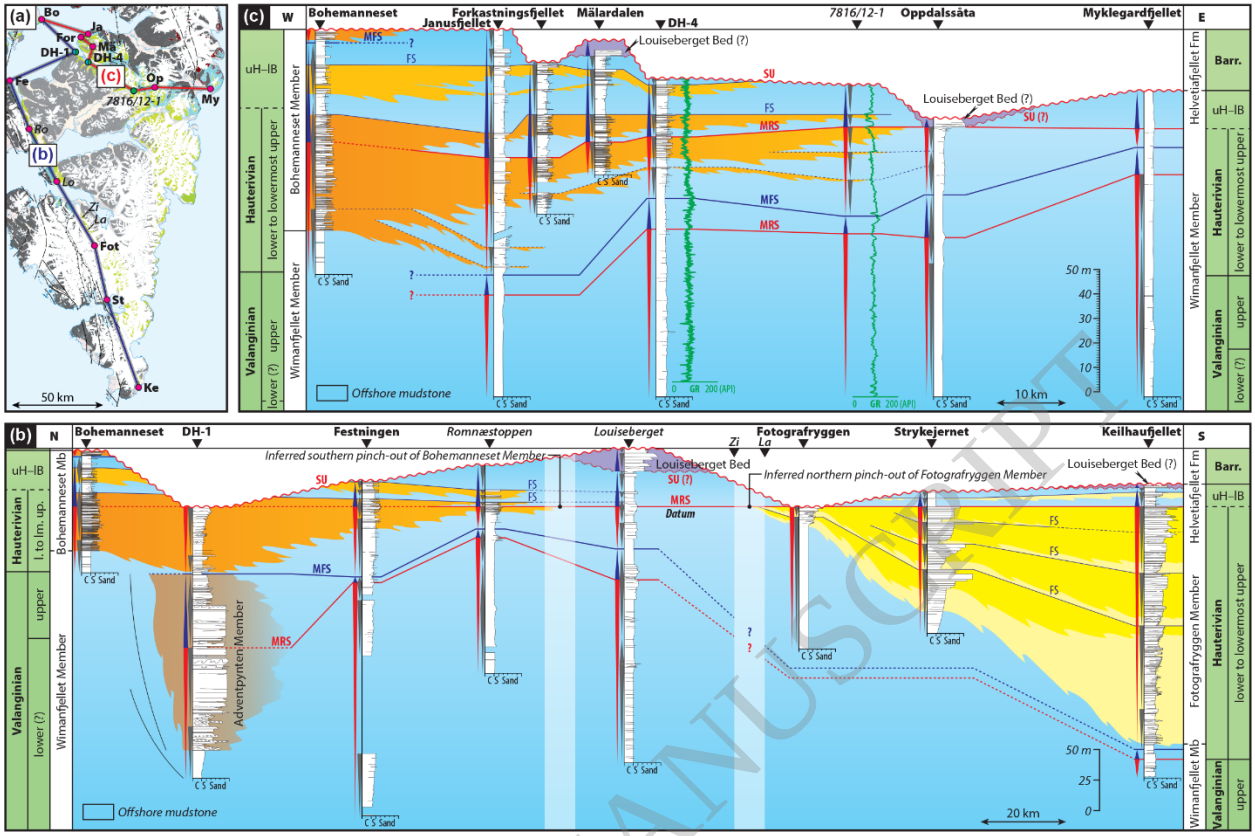

Figure 20

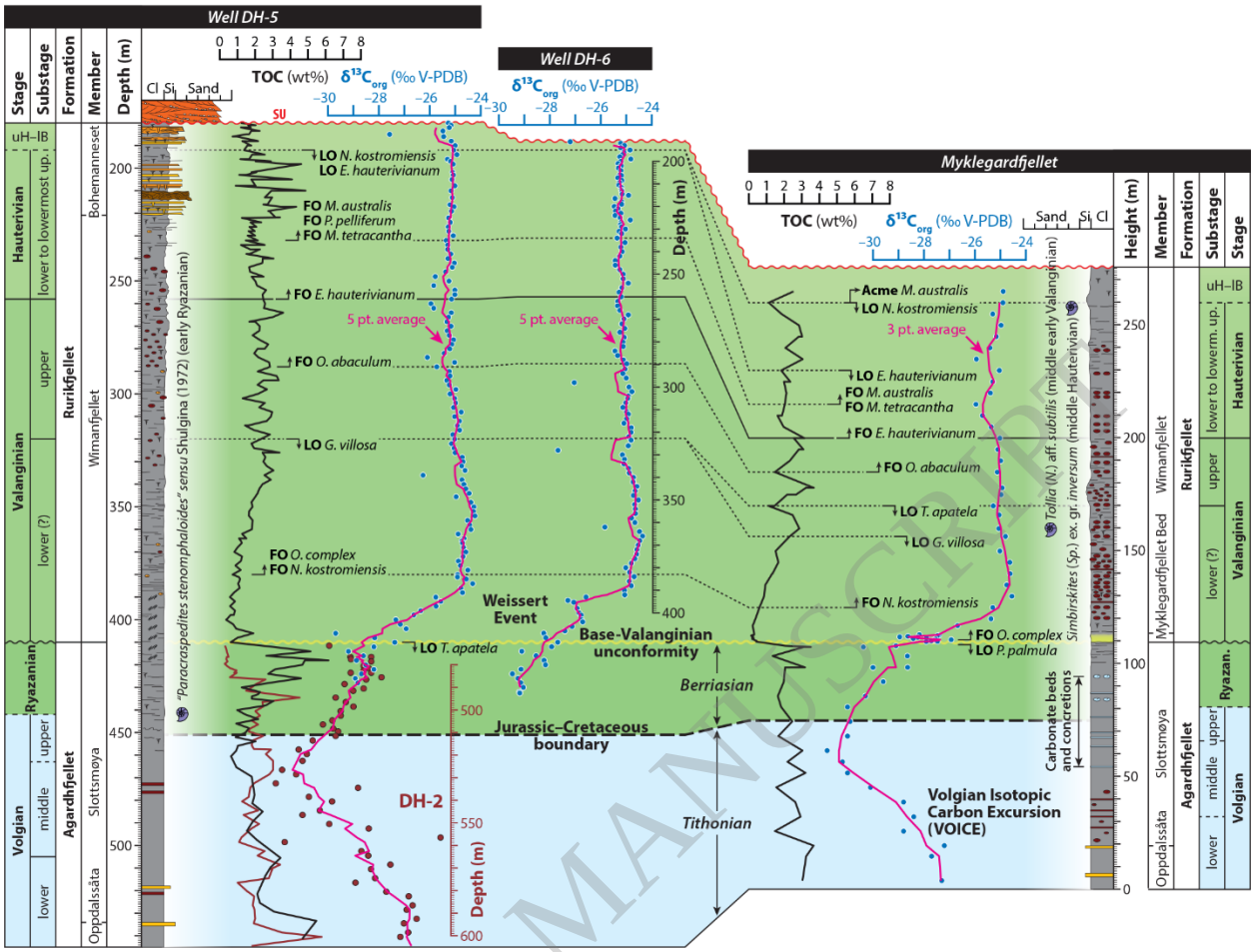

Figure 21